Investigating Inactive Conformations of Protein Kinases

Sanjay B. Hari

A dissertation
submitted in partial fulfillment of the
requirements for the degree of

Doctor of Philosophy

University of Washington

2013

Reading Committee:

Dustin Maly, Chair

Michael Gelb

Ethan Merritt

Program authorized to offer degree:

Department of Chemistry

University of Washington

Abstract

Investigating Inactive Conformations of Protein Kinases

Sanjay B. Hari

Chair of Supervisory Committee:
Associate Professor Dustin J. Maly
Department of Chemistry

Protein kinases comprise a substantial fraction of the human genome and constitute a wide array of cell signaling pathways that control countless cellular processes. Improper kinase regulation has been implicated in a number of grievous diseases; hence, these enzymes have become prominent therapeutic targets. The crux of kinase regulation lies in the ability of these proteins to switch between catalytically active and inactive conformations. The latter have recently gained prominence as drug targets in an effort to achieve selectivity in a family of more than 500 members with very similar active sites. However, despite the pharmacological significance of inactive conformations, neither their biophysical properties nor their potential roles in kinase regulation have been thoroughly investigated.

The first two chapters of this work explore the determinants of a specific inactive kinase conformation, its potential physiological consequences, and how it can be used to study noncatalytic kinase functions. The final chapter examines how kinase inhibitor potency is

affected by specific architectural motifs within kinases. It is expected that insight gained from this work will aid kinase drug development and enhance our knowledge of kinase regulation.

TABLE OF CONTENTS

LIST OF ABBREVIATIONS

3D	Three-domain
4-MUP	4-methylumbelliferyl phosphate
Abl	Ableson protein tyrosine kinase
ASK1	Apoptosis signal-regulating kinase 1
Asp	Aspartate
ATP	Adenosine-5'-triphosphate
BCR	Breakpoint cluster region
B-factor	Temperature factor
BODIPY	Boron-dipyrromethene
BSA	Bovine serum albumin
CDK6	Cyclin-dependent kinase 6
Cys	Cysteine
DMSO	Dimethyl sulfoxide
DNA	Deoxyribonucleic acid
DTT	Dithiothreitol
DUSP	Dual-specificity phosphatase
EC_{50}	Half maximal effector concentration
EDTA	Ethylenediaminetetraacetic acid
EGF	Epidermal growth factor
EGFR	Epidermal growth factor receptor
EGTA	Ethylene glycol tetraacetic acid
ELISA	Enzyme-linked immunosorbent assay
Erk1/2	Extracellular signal-regulated kinase 1/2
Ex/Em	Excitation/emission
Flt3	FMS-like tyrosine kinase 3
GFP	Green fluorescent protein
Glu	Glutamate
Gly	Glycine
GST	Glutathione S-transferase
Hck	Hematopoietic cell kinase
HEK	Human embryonic kidney
HEPES	(4-(2-hydroxyethyl)-1-piperazineethanesulfonic acid)
His_6	Hexahistidine
HPLC	High performance liquid chromatography
HRP	Horseradish peroxidase
HX	Hydrogen-deuterium exchange
I.D.	Inner diameter
I/σ(I)	Intensity over error

IC_{50}	Half maximal inhibitory concentration
ICAT	Isotope-coded affinity tagging
IPTG	Isopropyl β-D-1-thiogalactopyranoside
IRK	Insulin-receptor kinase
Jnk3	c-Jun N-terminal kinase 3
k_{cat}	Catalytic turnover
K_d	Dissociation constant
KD	Kinase domain
K_i	Substrate-independent half-maximal inhibitory concentration
K_m	Michaelis constant
LB	Lysogeny broth
LC/MS	Liquid chromatography / Mass spectrometry
Lck	Lymphocyte-specific protein tyrosine kinase
LCQ	Liquid chromatography quadrupole
LIC	Ligation-independent cloning
m/z	Charge-to-mass ratio
Map3k1	MAPK kinase kinase 1
MAPK	Mitogen-activated protein kinase
MD	Molecular dynamics
MEK	Mitogen-activated protein kinase kinase
MKK	Mitogen-activated protein kinase kinase
MOPS	3-(N-morpholino)propanesulfonic acid
MS	Mass spectrometry
NEt_3	Triethylamine
NMR	Nuclear magnetic resonance
NTA	Nitrilotriacetic acid
OD	Optical density
PAGE	Polyacrylamide gel electrophoresis
PDB	Protein Data Bank
PEG	Polyethylene glycol
Phe	Phenylalanine
P-loop	Phosphate-binding loop
R_{free}	Free residual factor
RMSD	Root-mean-square deviation
R_{pim}	Precision-indicating merging residual factor
R_{work}	Residual factor
S/T	Serine/threonine
SDS	Sodium dodecyl sulfate
SFK	Src-family kinase

SH	Src homology
STE	Yeast sterile
$t_{1/2}$	Dissociative half-life
TCEP	Tris (2-carboxyethyl) phosphine hydrochloride
TEV	Tobacco etch virus
TEY	Threonine-glutamate-tyrosine
TFA	Trifluoroacetic acid
TGY	Threonine-glycine-tyrosine
Thr	Threonine
TLS	Translation/libration/screw
TPCK	L-(tosylamido-2-phenyl) ethyl chloromethyl ketone
Tris	Tris(hydroxymethyl)aminomethane
TxY	Threonine-any residue-tyrosine
Tyr	Tyrosine
UV	Ultraviolet
V_{max}	Maximum velocity
XIC	Extracted ion chromatrograph

Units

°	Degree
µ	Micro
Å	Angstrom
C	Celsius
Ci	Curie
g	Gram
h	Hour
L	Liter
m	Milli; meter
M	Molar
min	Minute
mol	Mole
n	Nano
p	Pico
s	Second

NMR

d	Doublet
dd	Doublet of doublets
Hz	Hertz
J	Coupling constant in Hz

m	Multiplet
MHz	Megahertz
ppm	Parts per million
s	Singlet
t	Triplet
δ	Chemical shift in parts per million

LIST OF FIGURES

LIST OF TABLES

ACKNOWLEDGEMENTS

The work presented here was made possible by the support of many individuals. First, I would like to thank my advisor Dustin Maly, who not only provided expert technical guidance, but also kicked my butt into gear whenever I had lost the motivation to do research. The entire Maly lab has provided countless hours of entertainment and camaraderie even when my temper was short and the science was slow. In particular, Gayani Perera and Pratistha Ranjitkar made the majority of the small molecules that I used for these studies, and both were extremely generous in sharing them.

I would also like to thank Ethan Merritt for patiently teaching me how to process crystallography data into protein structures. Stewart Turley was incredibly helpful on the experimental side for data collection.

It is impossible to count how many times I have asked Martin Sadilek for mass spectrometry assistance. He is a priceless resource in the Department of Chemistry.

Looking further back, I would like to thank my undergraduate advisor Tom Magliery at Ohio State for introducing me to research and for his continued mentorship through graduate school.

On the funding side, I graciously acknowledge the National Institutes of Health and the American Heart Association for their financial support.

Finally, I thank my family for their unyielding encouragement of my personal and professional goals. My parents, brother, and sister-in-law have been champions of my endeavors. My wife Jenny has put up with several years of the ups and downs that come with graduate school, and words alone cannot express how grateful I am for her love and support.

DEDICATION

To Jenny: my wife, colleague, and best friend.

VITA

2004.....Lakota East High School, Liberty Township, OH

2008.....B.S. Biochemistry, Ohio State University, Columbus, OH

2008 – present.....Graduate student, University of Washington, Seattle, WA

Publications (in reverse chronological order):

- **Hari, S.B.**; Merritt, E.A.; Maly, D.J. (2013) "Sequence Determinants of a Specific Inactive Protein Kinase Conformation." *Chem. Biol*. **20**: 806-815 **DOI:** 10.1016/j.chembiol.2013.05.005
- PDB ID: 4I5H. **Hari, S.B.**; Merritt, E.A.; Maly, D.J. (2013) "Crystal Structure of a Double Mutant Rat Erk2 Complexed With a Type II Quinazoline Inhibitor."
- Ranjitkar, P.; Perera, B.G.; Swaney, D.L.; **Hari, S.B.**; Larson, E.T.; Krishnamurty, R.; Merritt, E.A.; Villén, J.; Maly, D.J. (2012) "Affinity-based probes based on type II kinase inhibitors." *J. Am. Chem. Soc.* **134**: 19017-25 **DOI:** 10.1021/ja306035v
- Wang, L.; Perera, B.G., **Hari, S.B.**; Bhhatarai, B.; Backes, B.J.; Seeliger, M.A.,;Schurer, S.C.; Oakes, S.A.; Papa, F.R.; Maly, D.J. (2012) Divergent allosteric control of the IRE1alpha endoribonuclease using kinase inhibitors. *Nat. Chem. Biol.* **8**: 982-989 **DOI:** 10.1038/nchembio.1094
- **Hari, S.B.**; Ranjitkar, P.; Maly, D.J. (2012) "Determination of the kinetics and thermodynamics of ligand binding to a specific inactive conformation in protein kinases." *Methods Mol Biol.* **928**: 153-159 **DOI:** 10.1007/978-1-62703-008-3_12
- Althoff, E. A.; Wang, L.; Jiang, L.; Giger, L.; Lassila, J. K.; Wang, Z.; Smith, M.; **Hari, S.**; Kast, P.; Herschlag, D.; Hilvert, D.; Baker, D. (2012) "Robust design and optimization of retroaldol enzymes." *Protein Sci.* **21**: 717–726 **DOI:**10.1002/pro.2059
- **Hari, S.B.**; Lau, H.; Razinkov, V.I.; Chen, S.; Latypov, R.F. (2010) "Acid-induced aggregation of human monoclonal IgG1 and IgG2: molecular mechanism and the effect of solution composition." *Biochemistry* **49**: 9328-9338 **DOI:** 10.1021/bi100841u
- **Hari, S.B.**; Byeon, C.; Lavinder, J.J.; Magliery, T.J. (2010) "Cysteine-free Rop: a four-helix bundle core mutant has wild-type stability and structure but dramatically different unfolding kinetics." *Protein Sci.* **19**: 670-679 **DOI:** 10.1002/pro.342
- PDB ID: 3K79. **Hari, S.B.**; Magliery, T.J. "C38A C52V Cysteine-Free Variant of Rop (Rom)."
- Lavinder, J.J.; **Hari, S.B.**; Sullivan, B.J.; Magliery, T.J. (2009) "High-throughput thermal scanning: a general, rapid dye-binding thermal shift screen for protein engineering," *J. Am. Chem. Soc.* **131**: 3794-3795 **DOI:** 10.1021/ja8049063

Introduction

The interior of a living cell teems with activity. In order to survive, cells must take information they receive about their surroundings and act appropriately. To do so, cells use complex signaling cascades that involve enzymes, scaffolding proteins, metabolic substrates, and other molecules. These cascades faithfully convert external stimuli into phenotypic responses.

Protein kinases comprise many of these signaling cascades. These enzymes transfer the γ-phosphate of adenosine-5'-triphosphate (ATP) to a protein substrate, typically on a tyrosine, serine, threonine, or, more rarely, histidine residue (1). The structural and functional responses elicited by phosphorylation are highly dependent on the identity of the protein substrate and even the specific phosphorylation site (2). The canonical outcome of phosphorylation is catalytic activation; in a signaling context, one kinase can be activated after another, thus amplifying a signal which is eventually carried to downstream effector proteins (3, 4).

More than 500 protein kinases are known to exist in humans, which is a fairly large number for any single enzyme family (5). The reason behind this abundance is that kinases play roles in countless signaling pathways: they control, among other activities, cell growth, differentiation, and death (6); inflammation (7); metabolism (8); and protein synthesis (9). Intraspecies kinase diversity appears to have increased over time; indeed, *Saccharomyces cerevisiae* has approximately one-fourth as many total kinases as humans and no tyrosine kinases at all (10). On the other hand, the number of kinases encoded in the *Caenorhabditis elegans* genome is almost 500 (11), rivaling that of humans. Therefore, kinase signaling pathways have likely evolved moreso in complexity than simply increased in number.

Because protein kinases are involved in so many intracellular signaling events, a host of diseases are known to be caused by misregulated kinase activity. Unchecked kinase activity can

lead to uncontrolled cell growth, which in turn can become cancerous (12). For example, specific leukemias, carcinomas, and blastomas are directly caused by improper kinase regulation (13). Hence, these enzymes have become attractive targets for therapeutic development. In fact, according to one source, "…50–70% of current cancer drug discovery programmes are focused on protein kinase inhibitors (14)."

Although kinase drug development is a worthwhile endeavor, it is impeded by the structural homogeneity of kinases across the family. Protein kinases are well-conserved in tertiary structure. Their catalytic domains are composed of a larger, mainly α-helical C-terminal lobe and a smaller N-terminal lobe composed mainly of β-strands (Figure I-1). The active site is located in a cleft between these two lobes. A flexible polypeptide called the activation loop resides on the outer edge of the active site and often contains serine, threonine, or tyrosine residues that can be phosphorylated (4, 15). Activation loop phosphorylation often results in a dramatic increase in a kinase's catalytic activity (16, 17). The activation loop also contains a highly-conserved Asp-Phe-Gly (DFG) motif near its base.

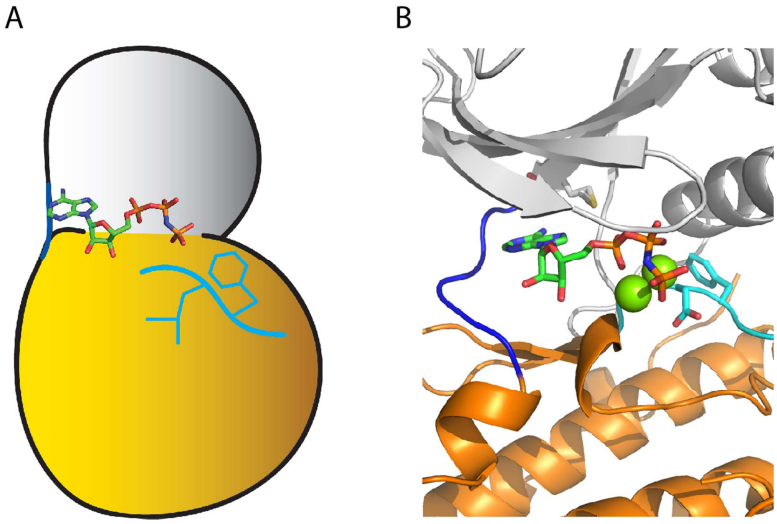

Figure I-1. A. General protein kinase structure with N-lobe (gray), C-lobe (orange), ATP analogue, and activation loop (cyan with DFG motif in sticks). B. Kinase active site. Coloring is the same as in A.

The first generation of kinase inhibitors (type I) were solely ATP-competitive and occupied only the adenosine pocket of the active site (18). These inhibitors are said to target the "active" conformation since no catalytic residues are perturbed upon binding. Additionally, since the phenylalanine residue of the DFG motif points into the active site, this conformation is also called "DFG-in (19)."

The first "inactive" protein kinase conformation was discovered in part by serendipity through the development of an inhibitor for the tyrosine kinase Abl. A specific chromosomal translocation produces a fusion gene product that is a combination of the *bcr* and *abl* genes. The protein product of this gene fusion (BCR-ABL) is a constitutively active form of Abl, which is the cause of almost all cases of chronic myeloid leukemia (20). A phenylamino-pyrimidine-based compound (type II) was developed that showed potent inhibition of Abl (21). This molecule, which later became the blockbuster drug imatinib (Gleevec), had entered clinical trials when the crystal structure of an analogue of it bound to Abl was reported (22).

Surprisingly, imatinib stabilized Abl in a specific inactive conformation that, with the exception of *apo* insulin-receptor kinase (IRK) (23), had not been observed before. The distinguishing feature of this conformation was the position of its activation loop, which had translocated several angstroms from its location in the active conformation. Notably, the phenylalanine of the DFG motif was flipped out and away from the active site, which led to this conformation being named "DFG-out." The movement of this residue revealed a hydrophobic pocket that became occupied by the methylpiperazine moiety of imatinib (Figure I-2).

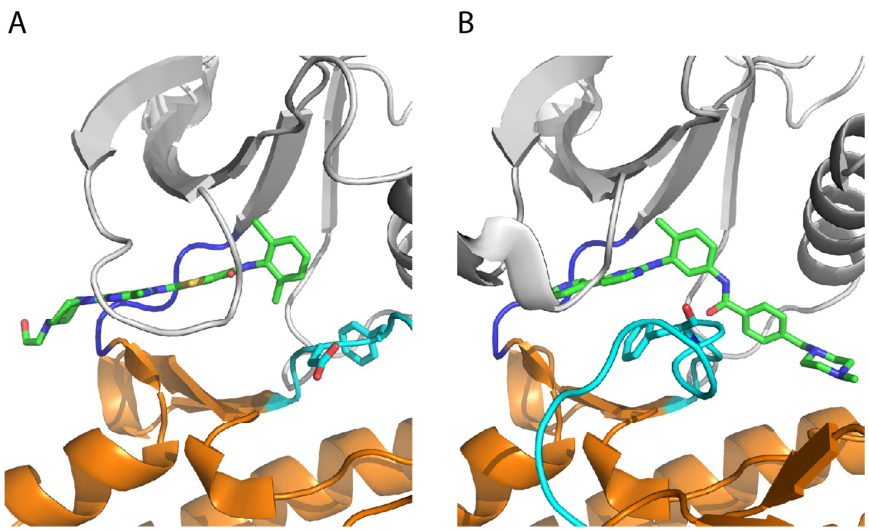

Figure I-2. A. Abl stabilized in the DFG-in conformation by the type I inhibitor dasatinib (PDB ID: 2GQG). B. Abl stabilized in the DFG-out conformation by imatinib (PDB ID: 1IEP). The ligands in both panels are shown in green, and the DFG motifs in cyan.

The revelation that imatinib stabilized the DFG-out conformation led to a new hypothesis to explain the exquisite selectivity of Abl over other closely-related tyrosine kinases such as Src (21): the energetics of Abl allow it to sample a distinct inactive conformation that is inaccessible to other kinases (24). This suggestion was attractive from a drug development standpoint because it offered new hope for attaining kinase selectivity. If only a subset of the kinome could adopt the DFG-out conformation, then the selectivity problem would become significantly more tractable.

This hypothesis remained unchallenged for years (and persists even today) until a few critical discoveries were made. First, a crystal structure of Src in complex with imatinib revealed the kinase was stabilized in the DFG-out conformation (25), thus dispelling the idea that Src could not adopt this specific conformation. Next, two groups (including the present) reported the development of type II inhibitors with equal potency towards Abl and Src (26, 27), thereby demonstrating that no energetic penalty exists for Src to adopt the DFG-out conformation.

While highly illuminating, these studies further complicated the matter of imatinib selectivity and, more generally, kinase plasticity. Two competing hypotheses now predominate: 1) Given

the development of equipotent Src/Abl inhibitors, it is reasonable to suggest that all kinases can adopt the DFG-out conformation given the proper ligand; and 2) While the DFG-out conformation is likely more abundant among the kinase family than previously thought, it is still determined by fundamental properties of a kinase's architecture and is completely inaccessible to many other kinases. Insight into this topic would help guide kinase drug development, specifically if and how the DFG-out conformation can be used for potency and selectivity.

The most straightforward approach to study this issue is through sequence analysis; kinome-wide inhibitor profiling has been performed for many ligands, including those that stabilize the DFG-out conformation (28). Comparing the sequences of kinases that are sensitive to type II inhibitors against those that are not would ideally reveal information on a primary structure level about the specific determinants of the DFG-out conformation. However, despite extensive structural homology among kinases, they are disparate enough in sequence to make pinpointing specific residues very challenging. Therefore, a more controlled (albeit less assured) method would be to find a kinase that is insensitive to multiple type II ligands and use site-directed mutagenesis to attempt to confer sensitivity to them. The dynamics of this kinase pair could then be studied to determine if they can access the same range of conformations or are fundamentally different from each other.

Knowledge of the sequence determinants of specific inactive conformations could also be useful from a chemical genetic standpoint. A very popular method for quickly developing a selective kinase inhibitor involves carving out extra space in the active site via mutagenesis and using a general inhibitor that occupies this space ("bump-hole") (29, 30). It may be possible to extend this approach by using type II inhibitor-sensitized kinase mutants to study noncatalytic functions (31), including scaffolding (32), DNA binding (33), and binding partner activation

(34). Perhaps stabilizing the DFG-out conformation is sufficient to disrupt these noncovalent interactions.

Returning to the tyrosine kinase Abl, much remains to be explained regarding its sensitivity to imatinib. What makes this ligand different from those that inhibit Src and Abl equipotently? Can only imatinib discriminate between the two kinases? Further, imatinib potency has been shown to be abrogated by activation loop phosphorylation (35) as well as clinically-relevant mutations in the glycine-rich phosphate-binding loop (p-loop) (25, 36). Are these effects specific to imatinib or do they apply more broadly to other ligands?

In this work, I explore the determinants, properties, and uses of a specific inactive protein kinase conformation by using small molecule inhibitors, enzymology, mass spectrometry, and x-ray crystallography. It is my hope that the insight gained from the following experiments and analyses will benefit kinase drug development and further improve our understanding of kinase regulation. Chapter one of this text presents a general strategy for sensitizing kinases to type II inhibitors. Chapter two follows this work by using sensitized kinases to study signaling pathways and noncatalyic functions. Finally, chapter three examines how architectural motifs in Abl affect its potency to different inhibitors.

Chapter 1: Sequence Determinants of a Specific Inactive Protein Kinase Conformation[*]

I. Introduction

Protein kinases represent approximately 2% of all human genes (5), a testament to the vast number of kinase-mediated signal transduction pathways. Immunity, cell cycle regulation, and morphogenesis are only a few of the processes controlled by protein kinases (10). Aberrant kinase activity can lead to diseases such as cancer and inflammation (12); thus, normal cell function is reliant on precise kinase regulation, the basis of which lies in the interconversion between active and inactive catalytic states.

Catalytically active kinase conformations are highly conserved, owing to the evolutionary pressure of functional preservation. Inactive conformations, however, lack this pressure and are more varied across the kinase family. While the exact number of discrete inactive conformations is not known (although believed to be limited (37)), only a few have been observed crystallographically in multiple kinases. Small molecule kinase inhibitors have played a large role in determining active site conformational accessibility by stabilizing specific active site conformations. For example, structural characterization of the drug imatinib bound to its target kinase Abl (21, 22) revealed that this inhibitor stabilizes a specific inactive conformation that is characterized by the unique orientation of the highly conserved Asp-Phe-Gly (DFG) motif at the base of Abl's activation loop. In Abl's active conformation (DFG-in), the aspartate side chain of the DFG motif faces into the active site to facilitate catalysis. Additionally, its neighboring

---

[*]This chapter is reprinted with permission from Hari SB, Merritt EA, & Maly DJ (2013) Sequence determinants of a specific inactive protein kinase conformation. *Chem. Biol.* 20(6):806-815.

phenylalanine residue occupies a hydrophobic pocket adjacent to the ATP-binding site. In contrast, the activation loop of the observed inactive form (DFG-out) undergoes a significant translocation that moves the catalytic aspartate out of the active site and the phenylalanine away from the hydrophobic pocket. Since the initial observation that imatinib stabilizes the DFG-out conformation of Abl, a number of ATP-competitive ligands that stabilize this conformation in other protein kinases have been identified (28, 38).

Although the overall topologies of kinase active sites are well-conserved across this enzyme family, less than 10% have been observed in the DFG-out conformation (19), and most examples are tyrosine kinases (22, 39-42) despite serine/threonine (S/T) kinases constituting a majority of the human kinome (5). Furthermore, the few S/T kinases that have been shown to adopt this conformation appear to be outliers in their own subfamilies. For example, the mitogen-activated protein kinase (MAPK) p38α was one of the first kinases to be characterized in the DFG-out conformation, and numerous structures of this kinase bound to conformation-specific ligands that stabilize this inactive form have been reported (43, 44). However, p38δ, which is in the same MAPK subfamily and more than 61% identical in sequence (45), is insensitive to ligands that selectively recognize this conformation (46). Furthermore, there is no experimental evidence that other closely-related MAPKs, such as extracellular signal-regulated kinase 1/2 (Erk1/2) and c-Jun N-terminal kinase 3 (Jnk3), possess the ability to adopt the DFG-out conformation (47-49).

Based on the information above, two main questions arise. First, can p38α adopt the DFG-out inactive conformation because of only a few sequence differences from the other MAPKs, or is this ability due to more global determinants in kinase tertiary structure? Second, how do sequence differences contribute to ligand binding? That is, can all kinases adopt the DFG-out inactive conformation given the appropriate ligand, and simply the energetics of known ligands

that stabilize the DFG-out conformation cause them to prefer p38α; or can p38α access a distinct conformational space that is somehow productive towards ligand binding? Unfortunately, structural studies provide no information about the dynamics or plasticity of kinases. To wit, a reported crystal structure of the *apo* form of inactive p38α adopts the DFG-*in* conformation (50), giving no indication of its ability to adopt the DFG-out conformation. Further confounding is that *apo* forms do exist of other kinases in the DFG-*out* conformation (23, 51).

Here we report the identification of two specific residues that allow MAPKs to adopt the DFG-out inactive conformation. We show that mutagenesis at these positions yields kinases that are sensitive to general ligands that stabilize this inactive conformation. Additionally, we provide structural evidence that an inhibitor-sensitive mutant of Erk2 can adopt the DFG-out inactive conformation. Next, using isotope-coded affinity tagging (ICAT) experiments we show that these mutations change the dynamics of the segment of the activation loop next to the DFG motif. Finally, we extend our observations to the distantly related yeast sterile (STE) group kinase apoptosis signal-regulating kinase 1 (ASK1) to demonstrate that these two residues are relevant to S/T kinases outside the MAPK family. This sensitization strategy may be used to study the effects of inactive conformations in various noncatalytic roles of protein kinases, including scaffolding complexes (32) and binding partner interactions (31).

II. Results and Discussion

A. A small molecule probe reveals binding preference among MAPKs.

ATP-competitive inhibitors have proven to be invaluable reagents for studying the conformational accessibility of protein kinase active sites. Most of these ligands, known as “type I” inhibitors, are able to bind to the active form of kinase ATP-binding sites, where all conserved

catalytic residues are in the proper orientation for catalysis. However, a growing number of ligands have been identified that selectively stabilize ATP-binding site conformations that are not compatible with catalysis. These ligands occupy regions within the kinase that are only accessible through the displacement of conserved catalytic residues. For example, inhibitors that stabilize the helix αC-out inactive conformation induce a rotation of helix αC that disrupts the catalytically important salt bridge between a glutamate residue on helix αC and a lysine residue on the N-lobe beta sheet (52, 53).

Another, more commonly observed inactive conformation is the "DFG-out" inactive conformation described earlier. Ligands that stabilize this conformation (type II) have substituents that extend into a hydrophobic pocket (Figure 1-1A) normally occupied by the conserved phenylalanine of the DFG motif when kinases are in an active conformation. The translocation of the phenylalanine residue perturbs the position of the neighboring catalytic aspartate of the DFG motif. Type II ligands also contain a linkage that connects the substituents that occupy the adenosine and DFG-out pockets, which makes two additional hydrogen bonds with a backbone residue in the DFG motif (Asp) and a conserved glutamate residue located in helix αC. Only in the DFG-out inactive conformation, whereby the DFG motif phenylalanine is removed from the DFG-out pocket, can a kinase active site make the interactions described above with a type II inhibitor.

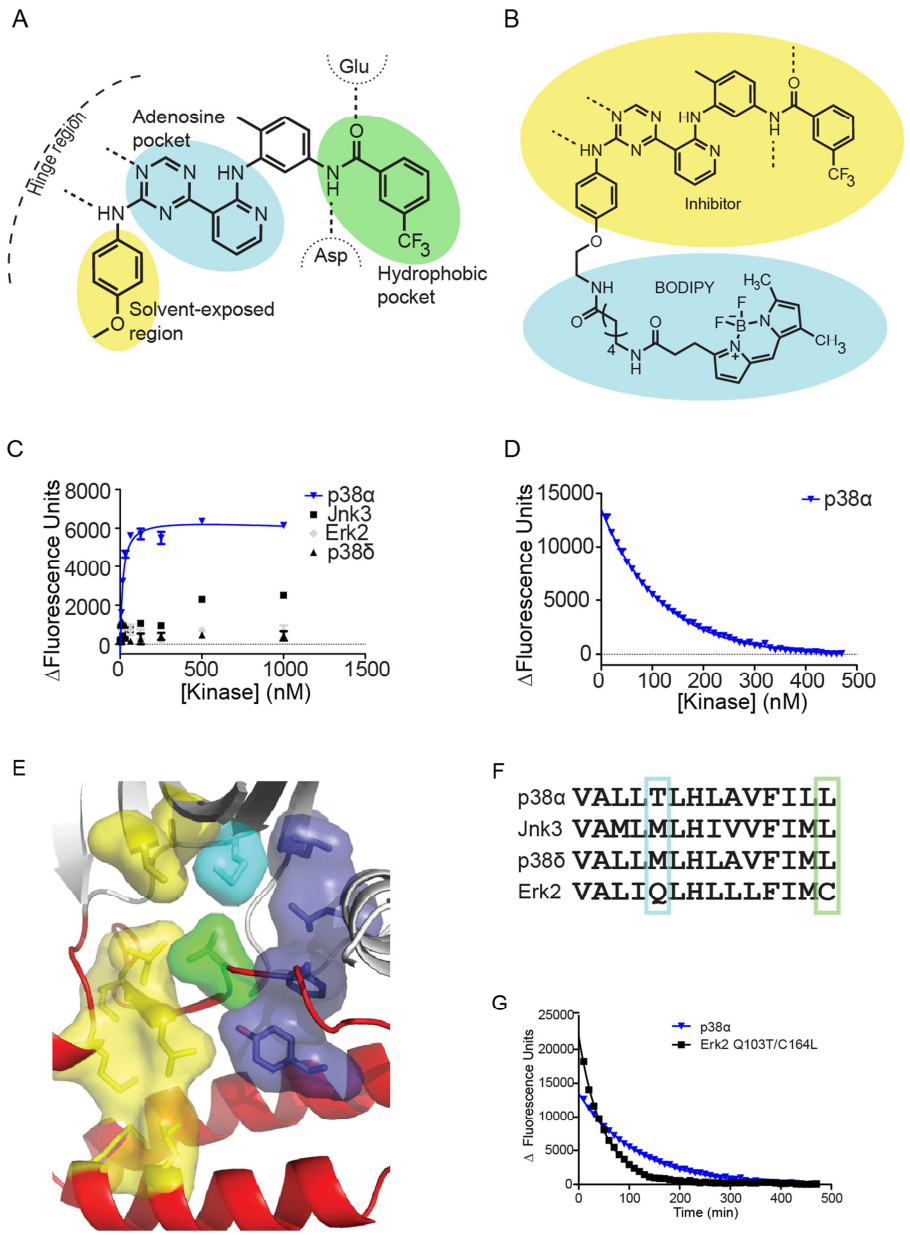

Figure 1-1. A. General properties of a type II ligand, which spans a kinase active site from beyond the adenosine pocket through a hydrophobic pocket that would otherwise be occupied by the DFG motif phenylalanine. B. Structure of probe **F**. C. Titration of MAPKs in the presence of probe **F** shows the most change in fluorescence for p38α (blue triangles, K_d = 15 nM). D. Active site dissociation of probe **F** from p38α. The slow dissociation rate ($t_{1/2}$ = 80 min) is indicative of the large conformational change required to accommodate a type II inhibitor. E. The hydrophobic spines of protein kinase A (C-spine: yellow; N-spine: blue), connected by the gatekeeper (cyan) and xDFG (green) residues (PDB ID: 1ATP). F. Sequence alignments of MAPK hydrophobic spines shows that most of the residues are conserved within the MAPK family. The gatekeeper (cyan boxed) and xDFG (green boxed) residues are the only positions with significant variability. G. Active site dissociation of probe **F** from MAPKs. A gatekeeper/xDFG double mutant of Erk2 (Q103T/C164L, black squares) dissociates from probe **F** at a similar rate to p38α (blue triangles).

The reasons for the far fewer examples of S/T kinases in the DFG-out inactive conformation, relative to tyrosine kinases, are not known. We felt that the high sequence homology of the

MAPKs, and the general availability of diverse ligands that stabilize the DFG-out conformation of p38α, made this kinase group ideal for probing the sequence and structural determinants of ATP-binding site conformational accessibility. First, we confirmed biophysically that MAPKs other than p38α are not sensitive to type II inhibitors, and thus are most likely unable to adopt the DFG-out inactive conformation, with a fluorescently-labeled affinity reagent **F** that we have previously described (Figure 1-1B) (54). This reagent consists of a general ligand for the DFG-out conformation linked to a BODIPY fluorophore. Upon binding to kinases that are able to adopt the DFG-out conformation, this probe demonstrates a significant increase in fluorescence. Direct measurement of binding affinity rather than enzymatic inhibition allows kinase conformational accessibility to be determined independent of enzyme activity or phosphorylation state. Because specific phosphorylation events have been shown to affect the conformational equilibrium of some kinases, this assay simplifies biochemical analysis (25). The binding affinities of the unphosphorylated forms of the MAPKs p38α, p38δ, Jnk3, and Erk2 were determined for BODIPY-conjugated probe **F** (Figure 1-1C and Table 1-1). Consistent with previous structural studies and inhibitor screens, only p38α bound tightly (K_d = 15 nM) to the probe.

Kinase	Probe K_d (nM)	Dissociative $t_{1/2}$ (min)
p38α wt	15 ± 2	79.6 ± 0.2
p38α T106Q	>1000	n/d[a]
Jnk3 wt	n/c[b]	n/d[a]
Jnk3 M146I	10 ± 2	51.8 ± 0.2
Erk2 wt	>1000	n/d[a]
Erk2 Q103T	n/c[b]	n/d[a]
Erk2 Q103A	n/c[b]	n/d[a]
Erk2 Q103T/C164L	40 ± 10	33 ± 1
Erk2	13 ± 7	27.8 ± 1.0

Q103A/C164L		
p38δ wt	>1000	n/d[a]
p38δ M107T	38 ± 5	26.3 ± 0.4

Table 1-1. [a]Not determined. [b]Data were not convergent to a plateau and thus could not be accurately fit to a curve.

One distinguishing characteristic of type II inhibitors is that they display slow association and dissociation kinetics when interacting with the ATP-binding sites of protein kinases (43, 55). This rate is slower than that of type I inhibitors, owing to the significant conformational change that must occur in order to accommodate type II ligands. By monitoring the loss of fluorescent signal of kinase-bound **F** in the presence of a nonfluorescent competitor, the dissociative half-life ($t_{1/2}$) of p38α was determined. Probe **F** dissociates slowly from the active site of p38α (Figure 1-1D and Table 1-1), comparable to studies with other type II ligands (43, 46, 55).

B. Two active site residues affect MAPK sensitivity to type II inhibitors.

Given that closely-related kinases greatly differ in their sensitivities to a general type II ligand, we sought to determine the sequence basis for this disparity. We confined our search to a series of hydrophobic residues that form two spatially conserved hydrophobic spines in kinases that are in the active conformation (56-58) (Figure 1-1E). While almost all of the residues in the hydrophobic spines of p38α, p38δ, Jnk3, and Erk2 are identical, one residue that connects these spines is more varied (Fig. 1F). This position, known as the "gatekeeper" residue, blocks access to a hydrophobic pocket adjacent to the site of ATP binding. The gatekeeper residue has been the subject of considerable study. A number of drug-resistant kinase mutants with altered gatekeeper residues have been identified in the clinic, including BCR-Abl T315I (59), EGFR T790M (60), and KIT T670I (61). Furthermore, conversion of the gatekeeper from a larger to a smaller alanine or glycine residue has been used to confer sensitivity to a series of orthogonal kinase inhibitors (29). Finally, a regulatory role has been suggested for this position based upon the discovery of gatekeeper mutants of Src, Abl, and Erk2 kinases that promote auto-activation (62,

63).

Gatekeeper mutants of p38α, p38δ, Jnk3, and Erk2 differ markedly from their wild-type counterparts in their affinities for fluorescent probe **F** (Table 1-1). Specifically, the p38δ M107T and Jnk3 M146I gatekeeper mutants exhibited low nanomolar affinities for the probe. Conversely, the T106Q gatekeeper mutant of p38α abrogated binding to this probe (K_d >1000 nM). Curiously, the Erk2 Q103T and Q103A gatekeeper mutants showed increased binding to the fluorescent probe, but not to the extent demonstrated by the p38δ or Jnk3 gatekeeper mutants. Therefore, we looked for other positions that differ between Erk2 and the other MAPKs tested. Our attention was drawn to the residue immediately preceding the DFG motif (xDFG), which, like the gatekeeper residue, connects the two hydrophobic spines. The identity of this residue is cysteine in Erk2, but leucine in p38α, p38δ, and Jnk3. Mutating the xDFG position to leucine (C164L) in Erk2 Q103T and Q103A produced Erk2 variants (Q103T/C164L and Q103A/C164L) with increased affinities for probe **F** (K_d = 40 nM and 13 nM, respectively). Further, probe **F** demonstrated slow dissociative half-lives for all of these sensitized variants (Figure 1-1G and Table 1-1). Thus, it appears that the identities of the two residues that connect the hydrophobic spines of MAPKs determine their sensitivities to type II inhibitors and may influence their abilities to adopt the DFG-out conformation.

Having determined MAPK residues that modulate probe **F** binding, we were curious to know whether these positions affected only the pharmacophore of this fluorescent ligand or corresponded more broadly to other ligands that stabilize the DFG-out inactive conformation. Therefore, we tested their enzymatic inhibition by a series of diverse type II ligands. In order to do so, it was necessary to activate the MAPKs with their respective MEKs. All MAPK variants were significantly activated by their upstream MEKs, and Michaelis constants (K_m[ATP]) of the

activated MAPKs were not dramatically different between wild-type and mutant kinases (Table 1-2).

Kinase	K_m(ATP) (μM)	K_i (nM)			
		L1	**L2**	**L3**	**L4**
p38α wt	229 ± 16	8.1 ± 0.2	< 2[a]	8.0 ± 0.4	6.4 ± 1.6
p38α T106Q	>1000[b]	3700 ± 400	1120 ± 20	>10000	55 ± 4
Erk2 wt	120 ± 10	>10000	>10000	>10000	>10000
Erk2 Q103T	83 ± 5	>10000	10.8 ± 0.8	310 ± 20	>10000
Erk2 Q103T/C164L	180 ± 20	4200 ± 600	4.7 ± 0.3	28.4 ± 1.7	6600 ± 700
Erk2 Q103A/C164L	137 ± 6	1490 ± 50	< 2[a]	36 ± 4	1100 ± 300
Jnk3 wt	8.3 ± 0.6	1300 ± 300	106 ± 9	101.6 ± 1.6	660 ± 90
Jnk3 M146I	66 ± 3	67 ± 3	1.65 ± 0.05	5.9 ± 0.5	155 ± 9
p38δ wt	91 ± 6	5800 ± 400	>10000	>10000	>10000
p38δ M107T	380 ± 40	54 ± 5	3.62 ± 0.18	26 ± 2	37.5 ± 0.6

Table 1-2. [a]Assay was performed with 2 nM kinase. [b]Rate of reaction maintained linearity as high as 1000 μM ATP.

A structurally diverse panel of type II inhibitors that are potent inhibitors of p38α with varied structures but all of the features of a general ligand for the DFG-out conformation (Figure 1-2) were tested in activity assays: Iclusig (**L1**) is an inhibitor of wild-type and drug-resistant forms of the oncogenic tyrosine kinase BCR-Abl (64). **L2** is derived from a series of aminoquinazoline inhibitors that target the Src-family kinase Lck (40). The ATP-competitive pharmacophore (**L3**) component of fluorescent probe **F** was also tested. Finally, we included a pyrazolourea (**L4**) inhibitor of p38α that only occupies the hydrophobic binding pocket created by the movement of the DFG motif to an inactive conformation (65). Even with the structural diversity of this ligand set, it is possible that some kinases that are able to adopt the DFG-out conformation will not be sensitive to these inhibitors. Consistent with the binding studies using probe **F**, only p38α was potently inhibited by all of the type II inhibitors tested (Table 1-2). Hence, ligands that stabilize the DFG-out inactive conformation appear to be ineffective towards the other MAPKs despite

extensive structural and sequence homology. However, the probe-sensitized kinase mutants of p38δ, Jnk3, and Erk2 were inhibited by low nanomolar concentrations of virtually all of the inhibitors in our panel. Thus, the gatekeeper and xDFG positions appear to control the sensitivity of MAPKs to pharmacophores that stabilize the DFG-out inactive conformation.

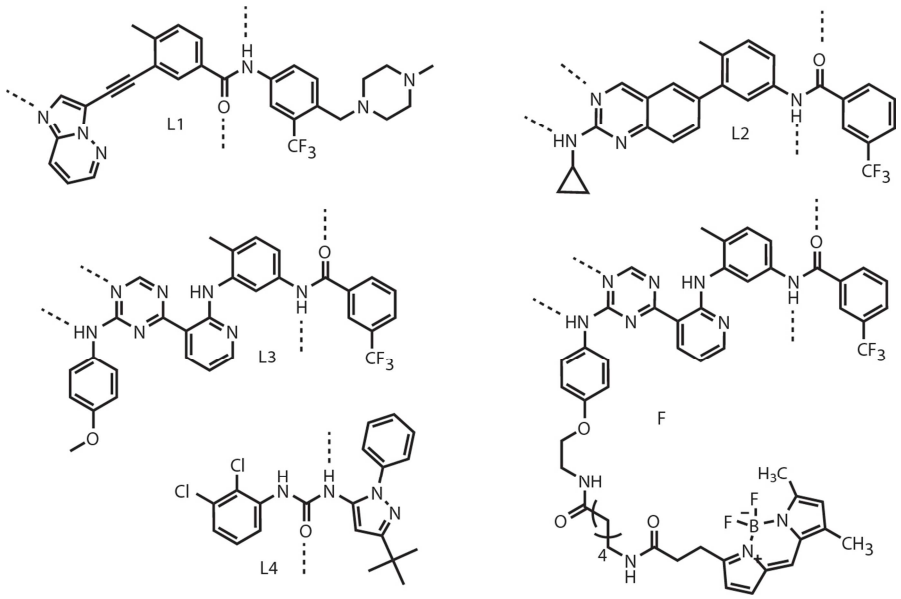

Figure 1-2. Despite varied structures, all of these inhibitors stabilize the DFG-out inactive conformation. Polar contacts are shown with dotted lines.

It is important to note that alanine, glycine, and isoleucine gatekeeper mutants of Jnk3 all have high affinities for probe **F** (Figure 1-3A). An isoleucine side-chain is larger than threonine and in fact occupies almost the same volume as methionine (66); therefore the presence of a small residue at the gatekeeper position is not mandatory for type II inhibitor sensitivity. Nonetheless, both isoleucine and threonine are branched at their β-carbon positions, so we speculated that they may be similar enough to be equally tolerated at the gatekeeper position in other MAPKs. Indeed, p38α T106I binds equipotently to probe **F** as the wild-type (Figure 1-3B), and while p38δ M107I is not as sensitive to inhibitors **L1**-**L4** as M107T, it is notably more so than the wild-type (Figure 1-3C). Positional comparisons among the few S/T kinases that have been characterized to adopt the DFG-out conformation reveal several gatekeeper residues,

including a phenylalanine in CDK6 (Figure 1-3D). This diversity further illustrates that threonine is not the only gatekeeper residue that permits type II inhibitor sensitivity. However, it appears that methionine and glutamine at this position strongly disfavor type II ligand inhibition, which is noteworthy as these two residues combined represent almost half of all gatekeeper residues in human kinases (67).

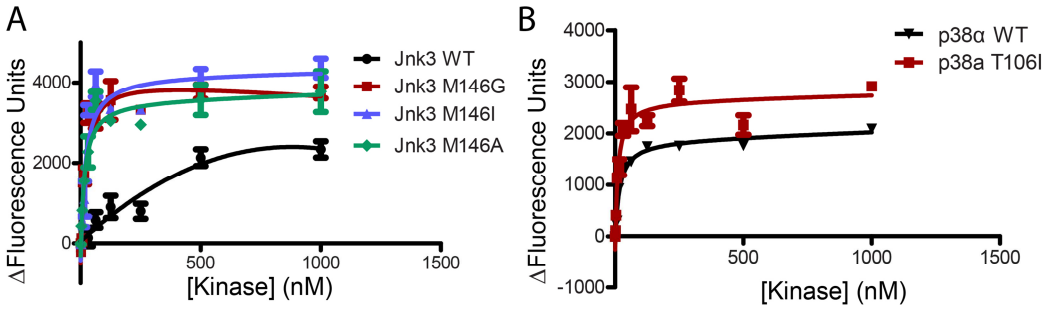

C

	IC_{50} (nM)		
	L1	**L2**	**L4**
p38δ M107I	307 ± 7	220 ± 90	24 ± 2

D

	Gatekeeper	xDFG
Aurora	L210	A273
CDK6	F98	A162
p38β	T106	L167
stk10	I110	A174

Figure 1-3. A. Binding affinities of different gatekeeper mutants of Jnk3 against probe F. Glycine, alanine, and isoleucine appear to be tolerated. B. Binding affinities of p38α wild-type and T106I gatekeeper mutant against probe F. The isoleucine gatekeeper mutant binds with equal potency. C. Inhibition of p38δ M107I by three different ligands. D. Gatekeeper and xDFG residues for four S/T kinases.

C. Structural evidence for DFG-out conformational accessibility.

L1-L4 are conformation-selective inhibitors in that the ATP-binding sites of protein kinases most likely need to adopt the DFG-out conformation in order to accommodate these ligands. To ensure that this is the case, we determined the crystal structure of Erk2 Q103A/C164L bound to the type II ligand **L2** (Table 1-3). Consistent with the increased sensitivity of this kinase mutant to type II inhibitors, the refined structure shows that the phenylalanine residue in the DFG motif (Phe-166) undergoes a large translocation; displacing the catalytic Asp from an orientation that is competent for catalysis (Figure 1-4A). Also, as expected, **L2** is buried within the ATP-binding cleft of this Erk2 mutant and makes all of the characteristic contacts of a type II inhibitor (Figure

1-4B). The 2-aminoquinazoline scaffold makes similar hydrophobic contacts as the adenine ring of ATP and forms two hydrogen bonds with the hinge region. The 3-trifluoromethylphenyl moiety of **L2** occupies the hydrophobic pocket created by movement of the DFG motif phenylalanine side chain, and the amide linker forms hydrogen bonds with the backbone of Asp-165 in the DFG motif and the side chain of Glu-69 in helix αC.

Data collection[a]	
Space group	P 3_1 2 1
Unit cell dimensions	a = b = 77.24 Å, c = 121.79 Å α = β = 90°, γ = 120°
Wavelength (Å)	1.5418
Resolution (Å)	15.46 – 1.90 (2.00 – 1.90)
Unique reflections	33356 (4496)
R_{pim}	0.032 (0.763)
Mean I/σ(I)	12.7 (0.8)
Completeness	98.7 (92.8)
Multiplicity	9.0 (3.8)
Refinement	
Resolution (Å)	1.90
Reflections (working set)	31632
Reflections (test set)	1684
R_{work} / R_{free}	0.218 / 0.256
Wilson B-factor (Å^2)	31
Protein atoms	2735
Inhibitor atoms	34
Water molecules	134
Other atoms	0
TLS groups	9-76, 77-187, 188-248, 249-268, 269-328, 335-356
RMSD bond length (Å)	0.012
RMSD bond angles (°)	1.487
Ramachandran statistics	
In prefered regions	95.4%
In allowed regions	4.6%
Outliers	0%

Table 1-3. [a]Values in parentheses are for highest resolution shell.

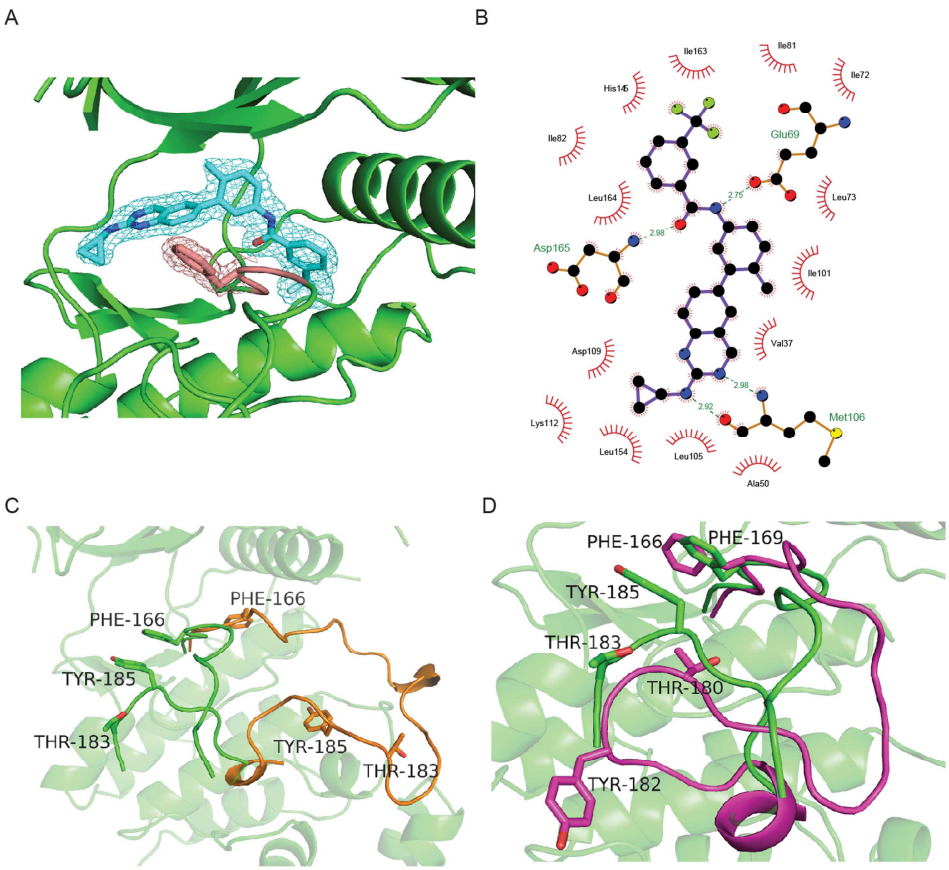

Figure 1-4. A. Erk2 Q103A/C164L with **L2** (cyan) and Phe-166 (salmon) contoured at 1.0σ. Part of the N-lobe beta sheet is hidden for clarity. B. Interaction map of **L2** in the active site of Erk2 Q103A/C164L. Map generated by LigPlot^{+} (68). C. Superimposition of **L2**-bound Erk2 Q103A/C164L (green) with *apo* inactive Erk2 (orange, activation loop shown only) (PDB ID: 1ERK) reveals a large activation loop translocation. D. Superimposition of **L2**-bound Erk2 Q103A/C164L (green) with **L4**-bound p38α (magenta, activation loop shown only) (PDB ID: 2BAJ). No pi-stacking is observed between Phe-169 and Tyr-182 in p38α.

Most of the activation loop is well-resolved, including the TEY activation motif. Superimposition of this structure with that of inactive Erk2 in the DFG-in conformation (49) shows a dramatic difference in activation loop configuration (Figure 1-4C), including a translocation of 9.9 Å by the DFG phenylalanine residue. Also of note is the position of the TEY motif: not only are these residues on opposite sides of the active site from those in the DFG-in conformation, but Tyr-185 appears to be involved in a pi-stacking interaction with Phe-166. Interestingly, p38α bound to pyrazolourea **L4** in the DFG-out conformation shows no such interaction (Figure 1-4D), although the similar position of its activation loop with that of Erk2 Q103A/C164L corroborates the hypothesis made by Sullivan et al. that kinases in the DFG-out

conformation cannot be activated by their upstream kinases because the position of their TxY motif renders their activation loops to be inaccessible to MEKs (46).

D. Gatekeeper mutations alter the dynamics of the activation loop.

Having demonstrated that inhibitor-sensitive Erk2 can adopt the DFG-out inactive conformation, we explored how this change affects its dynamic properties. One possibility is that type II inhibitor-sensitized kinases can sample the same conformational space as their wild-type counterparts, and the introduction of gatekeeper and xDFG mutations eliminate unfavorable interactions that prevent inhibitor binding. Alternatively, the introduced mutations could allow p38d, Jnk3, and Erk2 to access new conformational states that are compatible with favorable type II ligand binding. Normally, NMR experiments can be used to test hypotheses about protein dynamics. However, previous reports have shown that kinase activation loops move on an "intermediate" time scale, rendering them unresolvable by NMR due to line broadening (69, 70). Therefore, we used isotope-coded affinity tagging (ICAT) footprinting reagents to probe the active site dynamics of Erk2 Q103T/C164L. This mass spectrometry-based technique measures the alkylation rates of cysteine residues to determine their solvent exposures. ICAT footprinting is complementary to hydrogen-deuterium exchange (HX) footprinting because, while it lacks the ability to measure dynamic changes of the entire protein in a single experiment, it has the advantage of resolution since it follows specific residues rather than peptic fragments. We mutated five individual residues in the active site of Erk2 Q103T/C164L and compared their alkylation rates to those of the single mutant C164L (Figure 1-5A). This mutant was used as a control instead of wild-type Erk2 to allow a direct comparison of the contribution of the gatekeeper residue. Erk2 C164L has no measureable affinity to probe **F**, making it an appropriate wild-type substitute (data not shown).

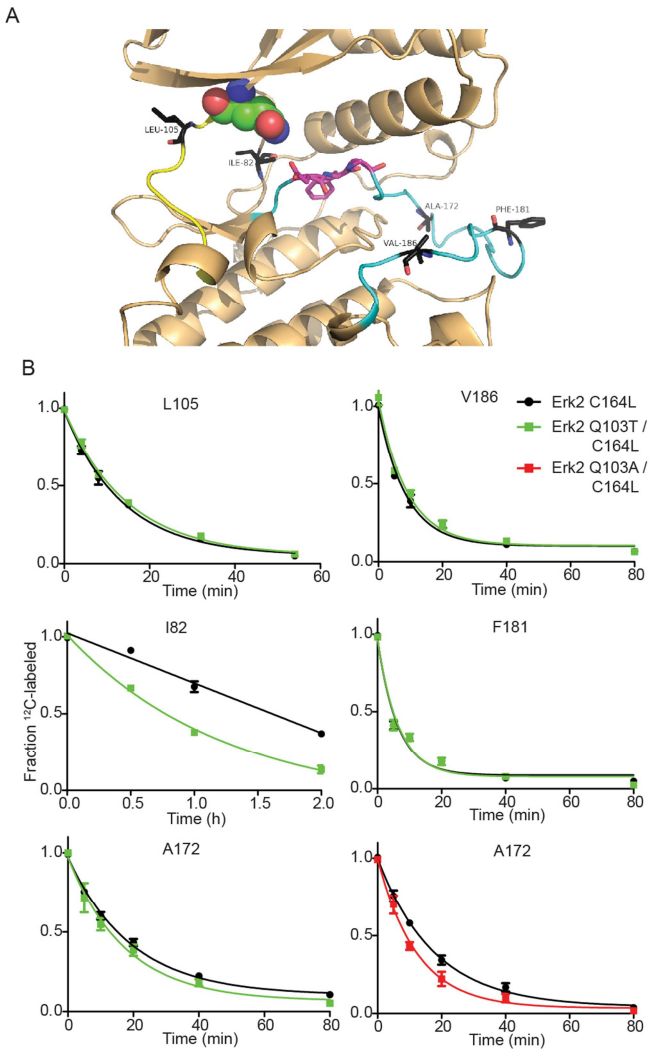

Figure 1-5. A. Residue positions studied (black, sticks). The hinge region (yellow), activation loop (cyan), DFG motif (magenta, sticks), and gatekeeper residue (spheres) are also shown (PDB ID: 1ERK). B. Footprinting timecourses. The proximity of position 82 to the gatekeeper provides the explanation that a smaller gatekeeper residue, as in the case of Erk2 Q103T/C164L, would provide greater solvent accessibility and a faster alkylation rate. Position 172, however, is far from the gatekeeper and still shows altered rates for both Erk Q103T/C164L and Q103A/C164L.

Two of the five positions examined showed altered alkylation rates between Erk2 C164L and Q103T/C164L (Figure 1-5B). Position 82 is located close to the gatekeeper residue, meaning that the observed rate change is likely due to local steric effects of the mutated gatekeeper residue. However, position 172 is on the activation loop of Erk2 and quite distant from the gatekeeper. A rate change at this position suggests the activation loop of the type II ligand-sensitized mutant (Q103T/C164L) can access different states than the wild-type surrogate (C164L). It also appears

that this motion is localized to the region around the DFG motif, since no rate change was observed for positions further along the activation loop. To validate this result, we performed the same experiment on Erk2 Q103A/C164L and found an equivalent effect. These results suggest that the identity of a kinase's gatekeeper residue affects the conformational preference of its activation loop in the *apo* form.

The rate change in position 172 between wild-type surrogate and inhibitor-sensitive Erk2 is apparent but subtle. Molecular dynamics simulations on both short and long time-scales have modeled DFG-out adopting kinases moving fully into the DFG-out conformation within nanoseconds (71, 72); thus, it might be expected that such a large translocation would produce a more significant alkylation rate difference. However, structural analysis shows that despite the large translocation of the activation loop between the DFG-out and –in conformations, the degree of solvent exposure of most of the residues (including position 172) remains the same. Therefore, a vastly different rate difference cannot be expected between residues occupying similar environments.

It is also important to note that while our data suggest that inhibitor-sensitive Erk2 has an altered activation loop conformational preference relative to wild-type Erk2, this does not necessarily mean that the DFG-out conformation of the *apo* form of this enzyme is substantially populated in the absence of ligand. Such would imply that ligands that stabilize the DFG-out conformation bind via a conformational selection mechanism (73, 74) rather than an induced-fit mechanism (75). While kinetics and molecular dynamics calculations provide strong supporting evidence that type II inhibitors bind to the ATP-binding sites of kinases by a conformational selection mechanism (71), we can only conclude from our data that our MAPK mutants have an altered conformational preference that is more conducive to ligand binding than the wild-type.

In a previous study by Emrick et al., several mutations that were predicted to allow increased movement of a hydrophobic core of residues in the active site of Erk2, including the Q103A gatekeeper mutant, result in increased autophosphorylation (63). HX footprinting of one of these Erk2 mutants, I84A, showed that a portion of the activation loop had substantially increased mobility. These observations are consistent with the increased sensitivity of Erk2 Q103A/C164L to type II inhibitors. However, the dynamic difference we observed in position 172 between wild-type surrogate and inhibitor-sensitive Erk2 did not appear in Erk2 I84A from the HX footprinting experiment. Furthermore, LC/MS data revealed that unlike the Q103A and Q103T single mutants, recombinant Erk2 Q103T/C164L and Q103A/C164L expressed in *E. coli* were not phosphorylated at either residue of the TEY activation motif (Figure 1-6). These observations suggest that the dynamic differences observed in our footprinting experiments are independent of any autophosphorylation capability and thus need not be consistent with the HX study by Emrick et al. Furthermore, the I84A mutant, previously shown to undergo a high rate of autophosphorylation (63), showed negligible binding to our fluorescent probe (data not shown), refuting the possibility that autophosphorylation capability and DFG-out conformational accessibility are correlated. Interestingly, the I84A/C164L mutant showed very little autophosphorylation, suggesting that position 164 is a general switch that down-regulates autophosphorylation.

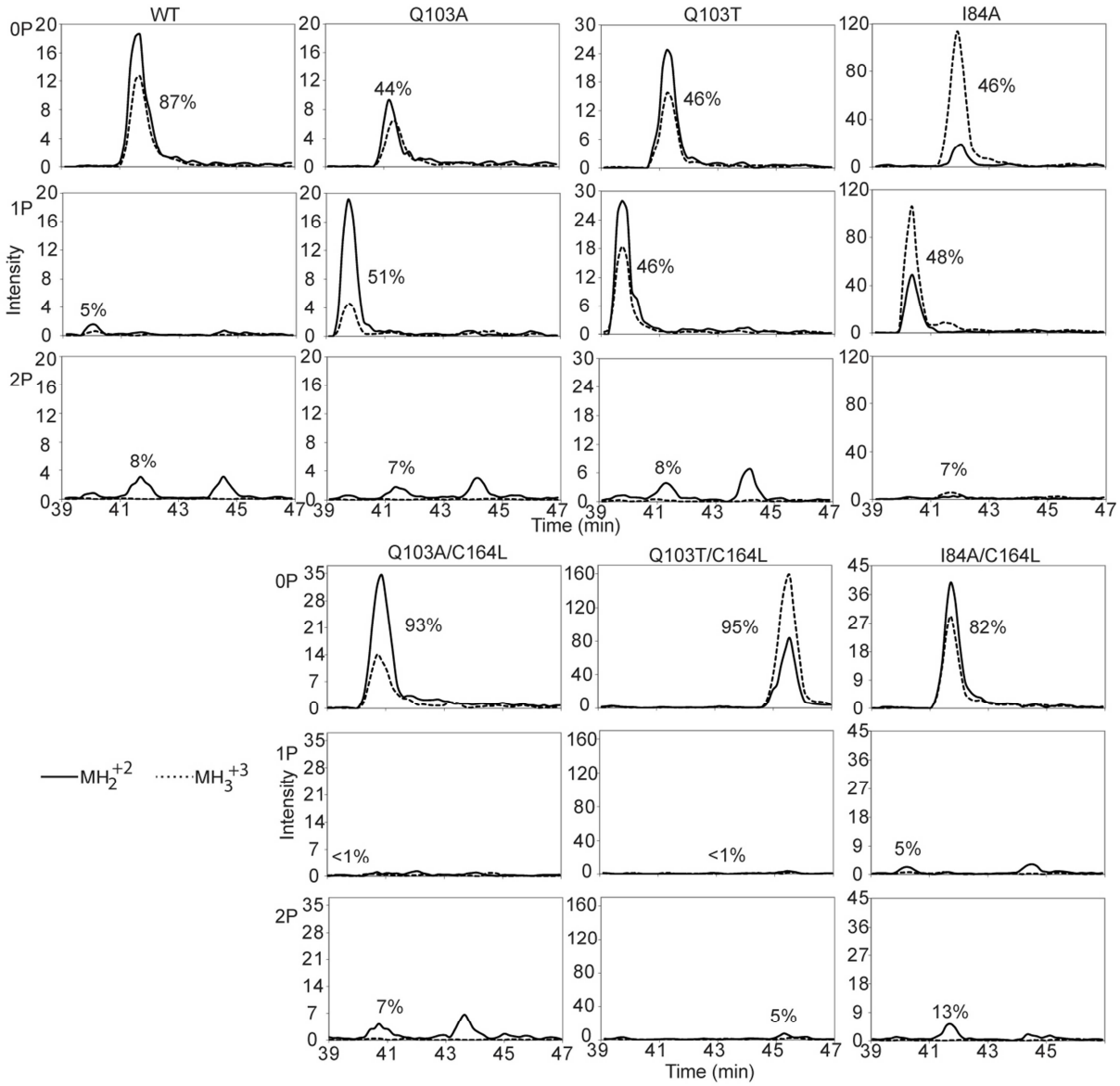

Figure 1-6. Extracted ion chromatographs from LC/MS analyses of un-, mono-, and diphosphorylated peptides of wild-type, gatekeeper, and gatekeeper/xDFG double mutants. The tryptic peptide analyzed was VADPDHDHTGFLTEYVATR (phosphorylated residues underlined) (MW: 2144 Da). Adding the C164L mutation to Erk2 Q103A, Q103T, and I84A significantly reduces the amount of phosphorylation at the TEY activation motif.

To our knowledge, the only study to examine the xDFG position was by Martin et. al, who targeted this residue in the development of new type II inhibitors for Aurora A kinase (76). However, the DFG motif itself has been studied intensely. The catalytic aspartate of this motif makes critical polar contacts with type II inhibitors; thus, it is reasonable that a large adjacent residue may hinder its ability to make these contacts. However, in the case of the Erk2

Q103T/C164L double mutant, leucine is considered to be larger in size (66) and similar in hydrophobicity (77) compared to cysteine. Furthermore, we found that mutating the xDFG position from leucine to cysteine in the inhibitor-sensitive Jnk3 M146I mutant abolishes binding to probe **F** (Figure 1-7A). Therefore, in conjunction with the gatekeeper residue this position appears to play a role in the DFG-out conformational accessibility of protein kinases.

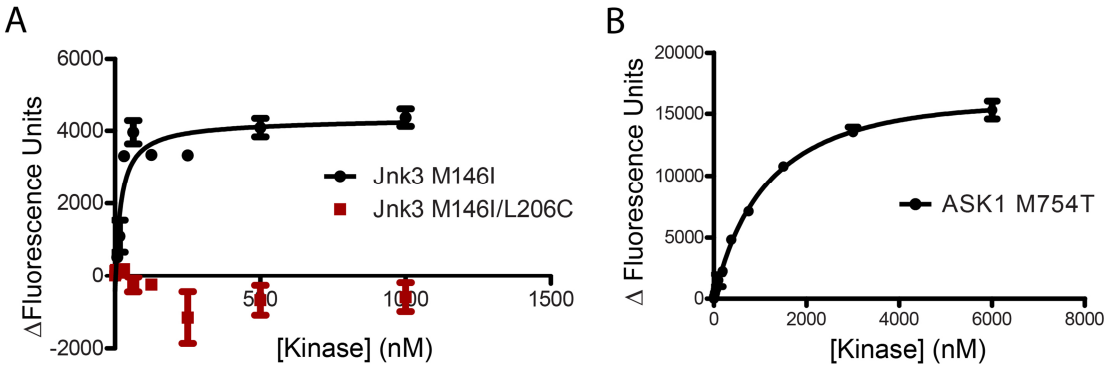

Figure 1-7. A. Binding affinities of two Jnk3 mutants against probe F. Mutating the xDFG residue to cysteine abolishes affinity. B. Binding affinity of ASK1 M754T against probe F (K_d = 1.3 μM).

E. The gatekeeper and xDFG mutations are general.

In a recent proteomic screen using a type II inhibitor to identify kinases that can adopt the DFG-out conformation, we identified the S/T kinase Stk10 (LOK) (54). Stk10 resides in the STE kinase group, whose human members are homologous to yeast Ste20 kinase (78) but share little sequence similarity to MAPKs (Figure 1-8A). Enrichment of Stk10 with resin-coupled **L3** and nanomolar affinity of purified recombinant kinase to BODIPY-conjugated probe **F** corroborated this result. Furthermore, we found that Stk10 was sensitive to the panel of type II inhibitors described above (Figure 1-8C). Finally, a recent joint effort with collaborators resulted in a crystal structure of Stk10 in the DFG-out inactive conformation (79) (Figure 1-8B), making it one of only a handful of S/T kinases outside the MAPK family to be structurally characterized in this form.

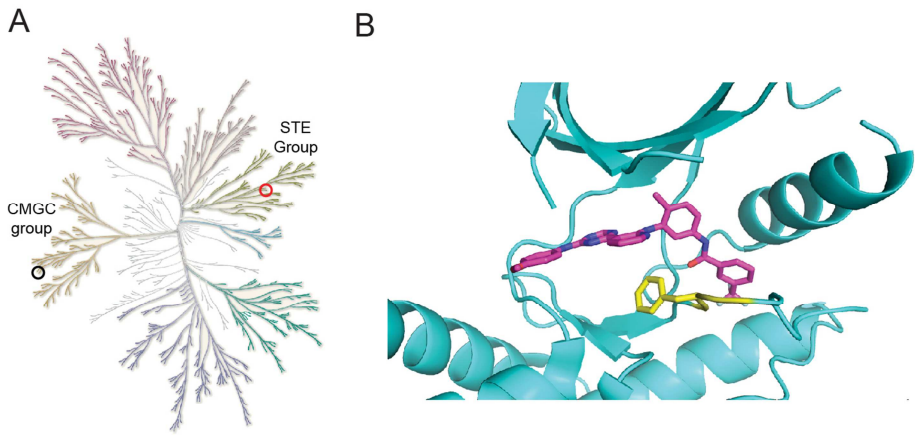

C

	IC_{50} (nM)					
	Ponatinib	GP17	DSA7	Pyrazolourea	Probe K_d (nM)	Diss. $t_{1/2}$ (min)
Stk10	10.0 ± 0.5	22 ± 1	8 ± 1	210 ± 20	30 ± 8	68 ± 1
ASK1 wt	>10000	>10000	>10000	n/d	>2000	n/d
ASK1 M754T/S821C	27 ± 2	7.7 ± 0.4	116 ± 5	n/d	50 ± 10	30 ± 1

Figure 1-8. A. Kinome dendrogram with the S/T kinases p38α (black) and Stk10 (red) circled illustrates the distant relationship between the two kinases. Kinome illustration reproduced courtesy of Cell Signaling Technology, Inc (www.cellsignal.com). B. Stk10 bound to **L3** (magenta) in the DFG-out conformation with activation loop (yellow, F176 in sticks) highlighted (PDB ID: 4EQU). C. Inhibition data of STE group kinases against inhibitors L1-4 and binding and dissociation data of probe F. The ASK1 gatekeeper/xDFG double mutant (M754T/S821C) is inhibited at nanomolar levels for all inhibitors tested and binds to probe F with nanomolar affinity. n/d: not determined.

To test whether our observations for MAPKs are general, we turned to another kinase in the STE group, ASK1. Unlike Stk10, this closely-related kinase showed no measureable binding to our BODIPY-labeled inhibitor or enzymatic inhibition by any of the type II inhibitors in our panel (Figure 1-8C). Therefore, ASK1 provided an ideal candidate to test the generality of using the gatekeeper and xDFG positions to alter DFG-out conformational accessibility. Mutating the gatekeeper position of ASK1 from a methionine to threonine residue, generated an ASK1 mutant (M754T) that has a dissociation constant of 1.3 μM for probe **F** (Figure 1-7B). Encouraged by this result, we also mutated the xDFG position and found that the M754T/S821C double mutant bound to this probe with a K_d of 50 nM (Figure 1-8C). Enzymatic activity assays using this mutant showed that almost all of the small molecules in our type II panel exhibited nanomolar inhibition of this kinase. These data strongly suggest the generality of the gatekeeper and xDFG positions as mediators of the DFG-out inactive conformation.

III. Conclusion

More than ten years after its discovery, the DFG-out inactive conformation has appeared in only a handful of protein kinases. Given the significant pharmacological interest in exploiting the hydrophobic pocket exposed in this conformation to gain a selectivity advantage, it is a worthwhile endeavor to determine if the DFG-out conformation is accessible to all kinases given the proper inhibitor; or the accessibility of this conformation limited by the dynamic properties of the kinase itself. However, such studies are difficult to control due to the often significant sequence disparity between protein kinases.

We have demonstrated that two residue positions in the active site of protein kinases appear to modulate their sensitivity to inhibitors that stabilize the DFG-out inactive conformation. Specifically, we showed that mutations at these positions conferred the ability to adopt the DFG-out conformational state that was disfavored in the wild-type kinase. This effect was demonstrated for the MAPK family as well as the distantly-related STE kinase family, suggesting a general trend across many protein kinases.

Our footprinting experiments suggest that the dynamics of kinases that can adopt the DFG-out conformation are different from those than cannot. However, more research is required to fully discern the dynamic nature of these kinases. Concurrently, our strategy may be used to rapidly sensitize kinases to type II ligands and study conformationally-dependent effects of scaffolding and other noncatalytic functions.

IV. Experimental

A. Small molecule synthesis

i. General information

Unless otherwise noted, all reagents were obtained from commercial suppliers and used without further purification. NMR spectra were obtained on a Bruker AV-300 or -301 instrument at room temperature. Chemical shifts are reported in ppm and coupling constants in Hz. Mass spectra were obtained on a Bruker Esquire Ion Trap instrument.

General HPLC Purification Conditions: Samples were injected on a preparatory reverse-phase C18 column (250 x 21 mm) run over 60 minutes at 8 mL/min (Acetonitrile/Water–0.05% TFA gradient: 1:99 to 100:0). Purified products were detected by UV at the detection frequency of 254 nm detection.

ii. Synthesis of aminoquinazoline inhibitor L2

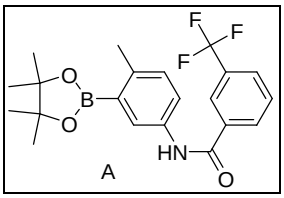

A

[A]*3-(trifluoromethyl)-N-(4-methyl-3-(4,4,5,5-tetramethyl-1,3,2-dioxaborolan-2-yl)phenyl)benzamide:* 5-amino-2-methylphenylboronic acid pinacol ester (0.21 g, 0.86 mmol), 3-(trifluoromethyl)benzoic acid (0.21 g, 1.11 mmol), hydroxybenzotriazole (0.17 g, 1.11 mmol), 1-Ethyl-3-(3-dimethylaminopropyl)carbodiimide (0.21 g, 1.11 mmol) and N,N-Diisopropylethylamine (450 µL, 2.58 mmol) were dissolved in dimethylformamide (2.5 mL) and stirred overnight at room temperature. The crude mixture was diluted in ethyl acetate and washed with NH_4Cl and Na_2CO_3. The organic layer was dried over Na_2SO_4 and concentrated *in vacuo* to afford 0.33 g of compound **A** (96% yield). ^{1}H NMR (300 MHz, $CDCl_3$-d_1) δ 8.14 (s, 1H), 8.07 (d, J = 6.0 Hz, 1H), 7.98 (d, J = 9.0 Hz, 1H), 7.84-7.81 (m, 2H), 7.68 – 7.62 (m, 2H), 7.23 (d, J = 9.0 Hz, 1H), 2.55 (s, 3H), 1.37 (s, 12H). MS *m/z* ($C_{21}H_{23}BF_3NO_3$) calc'd = 405.2, observed: M+1 = 406.4.

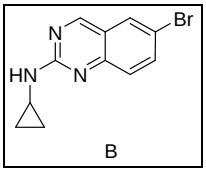

B

[B]*6-Bromo-N-cyclopropylquinazolin-2-amine:* In a resealable Pyrex tube, 6-Bromo-2-iodoquinazoline (made as described (40)) (50.0 mg, 0.15 mmol) and cyclopropylamine (55 µL, 0.75 mmol) were taken up in isopropyl alcohol (1.1 mL). N,N-Diisopropylethylamine (40 µL, 0.22 mmol) was added and the tube was sealed. The suspension was stirred for 2 h at 80 °C. The mixture was cooled to room temperature and concentrated *in vacuo* to afford 33.0 mg of compound **B** (85% yield). The crude compound was used in the next step without further purification. ^{1}H NMR (300 MHz, $CDCl_3$-d_1) δ 8.89 (s, 1H), 7.78 (d, *J* = 2.2 Hz, 1H), 7.69 (dd, *J* = 9.0, 2.3 Hz, 1H), 7.49 (d, *J* = 9.0 Hz, 1H), 5.77 (s, 1H), 2.92 - 2.84 (m, 1H), 0.89 - 0.82 (m, 2H), 0.60 – 0.55 (m, 2H). MS *m/z* ($C_{11}H_{10}BrN_3$) calc'd =263.01, observed: M+1 = 264.1.

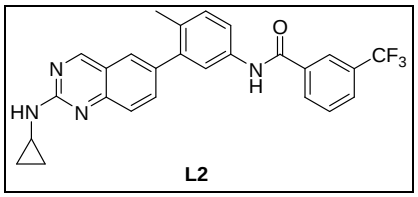

L2

[**L2**]*N-(3-(2-(cyclopropylamino)quinazolin-6-yl)-4-methylphenyl)-3-(trifluoromethyl)benzamide:* A mixture of **A** (71.8 mg, 0.18 mmol), **B** (39.0 mg, 0.15 mmol), tetrakis(triphenylphosphine)palladium (5.2 mg, 4.4 µmol) and sodium carbonate (34.2 mg, 0.32 mmol) was dissolved in a 3:1 mixture of dimethoxyethane/water (0.59 mL). The mixture was heated overnight at 85 °C. The crude mixture was cooled to room temperature, diluted in acetonitrile/water mixture and purified using reverse phase chromatography (HPLC) to obtain 20.0 mg of **L2** (29% yield). ^{1}H NMR (300 MHz, CD_3OD-d_4) δ 9.47 (s, 1H), 8.28 (s, 1H), 8.22 (d, *J* = 9.0 Hz, 1H), 8.13 – 7.99 (m, 1H), 7.91 (d, *J* = 9.0 Hz, 1H), 7.82 – 7.70 (m, 2H), 7.63 – 7.48 (m, 3H), 7.40 – 7.32 (m, 2H), 5.88 (s, 1H), 2.82 – 2.74 (m, 1H), 2.32 – 2.28 (m, 3H), 1.17 –

1.05 (m, 2H), 0.93 – 0.80 (m, 2H). MS *m/z* ($C_{26}H_{21}F_3N_4O$) calc'd = 462.17, observed: M+1 = 463.4.

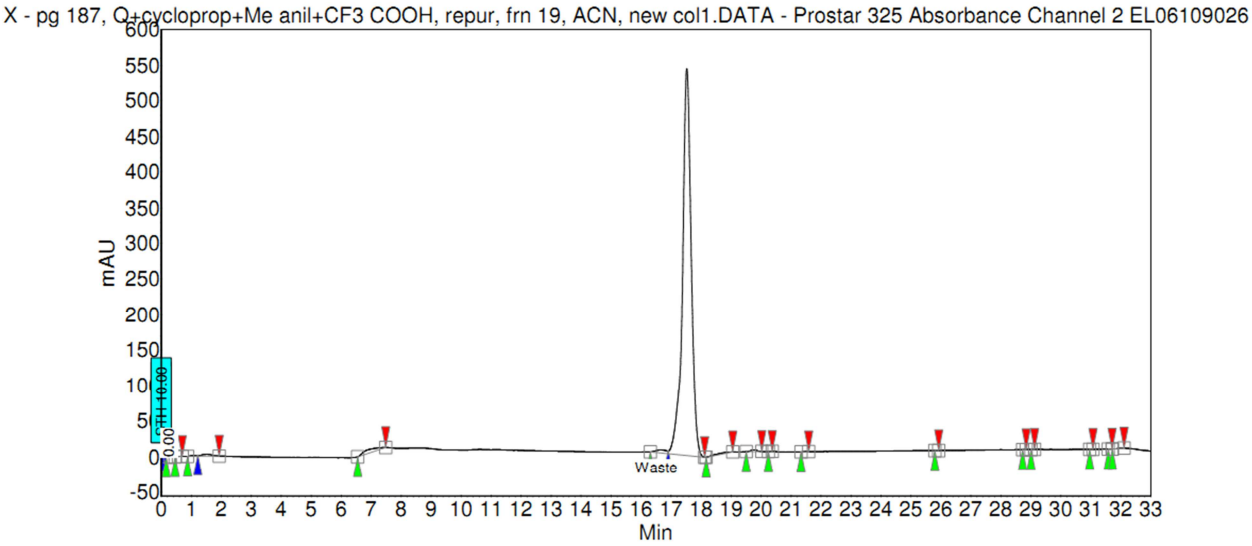

Figure 1-9. Analytical HPLC trace of **L2** (Acetonitrile:water-0.1% CF_3CO_2H gradient)

B. Cloning

Genes for mouse p38α, human ASK1, human Stk10 (S. Knapp) were provided in bacterial expression vectors. Genes for human Jnk3, mouse p38δ (R. Davis), and rat Erk2 (J. Blenis) were cloned into His_6 vector pMCSG7 (M. Donnelly). Genes for human MAPK kinase (MEK) 6, human MEK4, human MEK7 (R. Davis), human MEK2 (P. Khavari), and human Map3k1 (G. Johnson) were cloned into His_6-GST vector pMCSG10 (M. Donnelly). Mutagenesis was performed by Quikchange (Agilent). Plasmids were isolated from cultures grown from single colonies and sequenced. Primers used for cloning and mutagenesis are available upon request.

C. Protein expression and purification

Plasmids were transformed into BL21(DE3) competent cells (Invitrogen). Single colonies were grown at 37 °C in 125 ml lysogeny broth (LB) to 0.4 OD_{600} and then grown at 20 °C until 0.8 OD_{600}. Cultures were then induced with 0.5 mM IPTG and grown overnight at 20 °C. The harvested pellets were resuspended in lysis buffer (50 mM HEPES [pH 7.5], 300 mM NaCl, 20

mM imidazole, protease inhibitor cocktail [Roche]) and sonicated 3 times for 30 s with 2 min rest on ice. Cleared supernatants were then added to 125 µL Ni-NTA slurry (Qiagen) and incubated for 1 h at 4 °C. The resins were washed with lysis buffer, and the proteins were eluted with 500 µL lysis buffer containing 200 mM imidazole. The purified kinases were then exchanged into analysis buffer (50 mM HEPES pH 7.5, 300 mM NaCl, 5 mM DTT) using an Illustra NAP-5 desalting column (GE Healthcare) and quantified by UV_{280} absorbance.

D. Fluorescent probe measurements

These experiments were performed as described (54, 80).

E. Kinase activation and activity assays

ASK1 and Stk10 were catalytically active after purification. MAPKs were activated as follows prior to use in activity assays: kinase was incubated in phosphorylation buffer (50 mM MOPS [pH 7.4], 10 mM $MgCl_2$, 1 mM DTT, 0.001% (v/v) Tween 20) with BSA (0.1 mg/ml), ATP (1.3 mM), and upstream kinase (MEK6 for p38α and -δ, MEK2 for Erk2, and Map3k1+MEK4+MEK7 for Jnk3) for 1 h at room temperature.

Activated kinase was incubated with inhibitor (4% in DMSO, 10 µM starting concentration, then 3-fold dilutions to 0.5 nM) in kinase reaction buffer (50 mM HEPES [pH 7.5], 60 mM $MgCl_2$, 1 mM EGTA) with BSA (50 µg/ml), myelin basic protein (0.2 mg/ml), sodium orthovanadate (2 mM), cold ATP (13 µM), and γ^{32}P ATP (PerkinElmer) (0.2 µCi/well) and spotted onto a phosphocellulose membrane (Whatman). Enzyme concentrations and incubation times varied by kinase based on enzyme linearity. The membrane was washed 4 times with 0.05% phosphoric acid, dried, and exposed overnight to a phosphor screen (GE Healthcare). The screen was then scanned by a phosphor scanner, and spots were quantitated using ImageQuant software. K_i values were determined by non-linear regression using Graphpad Prism software.

F. Kinetics

Erk2 wild-type, Q103T/C164L, and Q103A/C164L were coexpressed with constitutively active GST-MEK2 and purified as above to yield activated, ATP-free kinase. Other kinases were expressed, purified, and activated as above, but then desalted using Zeba spin columns (Pierce) to remove ATP. Activity assays were performed as described above but with different concentrations of ATP (typically 1.6 mM cold ATP with 3.2 μCi γ^{32}P ATP starting concentrations, then 2-fold dilutions to 12.5 μM cold ATP with 25 nCi γ^{32}P ATP). K_m values were determined by non-linear regression using Graphpad Prism software.

G. Mass spectrometry

Kinases (75 pmol) were precipitated with 0.02% sodium deoxycholate and 10% trichloroacetic acid on ice for 10 min. The mixture was centrifuged at 4 °C for 15 min, and the pellet was washed with cold acetone. After centrifugation, the pellet was resuspended in 30 μL 200 mM Tris (pH 8.0), 8 M urea, and 2.4 mM iodoacetamide, and incubated in the dark for 30 min. The solution was then diluted with 210 μL 200 mM Tris (pH 8.0), 5.7 mM $CaCl_2$, and 1 μg/μL porcine trypsin (TPCK treated, Sigma), and incubated at 37 °C overnight. Sample (0.3 pmol) was injected onto a Thermo Scientific Dionex Acclaim Pepmap100 NanoLC capillary column (C_{18}, 150 mm length, I.D. 75 μm, 3 μm particle size) connected inline to a Finnigan LCQ mass spectrometer. Peptides of interest were identified by MS/MS data (Sequest), and corresponding XIC peaks were integrated.

H. ICAT Footprinting

Positions chosen for study were mutated to cysteine using site-directed mutagenesis. Kinases were purified as described above, but desalted into 50 mM Tris pH 8.0, 50 mM KCl, 5 mM $MgCl_2$, and 0.5 mM TCEP. Heavy labeling reagent was added to protein solutions (3 μM), and

aliquots were taken at specified times and quenched with excess DTT. Samples were then prepared and analyzed by mass spectrometry as described above, except light labeling reagent was used instead of iodoacetamide. Alkylation curves were fit using GraphPad Prism software.

I. Crystallography

Erk2 Q103A/C164L was expressed as described above on a 2 L scale and purified as above but then further processed as follows: TEV cleavage was performed overnight at 4 °C, followed by desalting back into lysis buffer (GE Healthcare). The solution was then incubated with 500 µL Ni-NTA slurry for 1 h at 4 °C and loaded onto a polypropylene column (Bio-Rad). The flow-through was concentrated (Pall) and further purified on a Superdex 200 10/300 GL column (GE Healthcare). The eluent in 10 mM HEPES (pH 7.5), 150 mM NaCl, and 5 mM DTT was concentrated to 8 mg/ml, aliquotted, and snap-frozen.

Kinase was incubated with inhibitor **L2** (final 1 mM in 5% DMSO) for 30 min at room temperature and centrifuged before setting up crystallization trials. Sparse-matrix screens (Emerald Biosciences) were used, followed by an additive screen (Hampton Research) to find suitable conditions. Crystals of inhibitor-bound Erk2 Q103A/C164L were grown with 90 mM sodium citrate pH 5.8, 20% (w/v) PEG 6000, 0.7% n-butanol in 96-well sitting-drop plates (Emerald). Prisms appeared at room-temperature overnight. Diffraction images were collected at the University of Washington Biomolecular Structure Center and processed using Mosflm (81) and the CCP4 program suite (82). The initial structural model was found by molecular replacement (83) using PDB entry 3QYW and then subjected to alternating rounds of automated and manual refinement using REFMAC5 (84-86) and Coot (87), respectively. The atomic coordinates and structure factors for inhibitor-bound Erk2 Q103A/C164L have been deposited in the Protein Data Bank under accession code 4I5H.

Chapter 2: Modulation of Signal Transduction in Mitogen-activated Protein Kinases via a Specific Inactive Conformation

I. Introduction

Protein kinases constitute a large portion of intracellular signaling cascades (5). As one of the largest protein families in the human genome, these enzymes play roles in nearly all cellular functions (10). Therefore, careful regulation of kinases is essential for normal cell function.

Protein kinases are known to adopt catalytically active and inactive conformations. Because of the evolutionary pressure to maintain function, active kinase conformations are structurally alike (56). On the other hand, inactive conformations are unconfined by such pressure and are thus more heterogenous. The dynamic nature of proteins makes it difficult to quantify the number of distinct inactive conformations; it is possible that one or many inactive conformations may be sampled over time (37). Nonetheless, a select few inactive conformations have recurred in the literature, being seen in multiple kinases by using small molecule inhibitors that stabilize the active site.

One specific inactive conformation that has been consistently observed in several different kinases is called the DFG-out inactive conformation. This conformation is named for the orientation of the Asp-Phe-Gly (DFG) motif that is conserved in the protein kinase family (88). The DFG motif sits on the activation loop, which often contains phosphorylatable residues that increase the kinase's catalytic activity (4). In its active conformation, the catalytic DFG aspartate residue points towards the active site (DFG-in) to permit catalysis, and the adjacent phenylalanine residue resides in a hydrophobic binding pocket deep within the ATP-binding pocket. The activation loop of the specific inactive form, though, undergoes a marked translocation in which the aspartate moves away from the active site (DFG-out) and the

phenylalanine out of the hydrophobic pocket.

Although the first kinase to be observed in the DFG-out conformation was Insulin Receptor Kinase (IRK) (23), it was not until ten years later upon the discovery that the drug imatinib (Gleevec) stabilized the DFG-out conformation in its target Abl that inactive conformations would generate widespread interest (22). The outstanding selectivity of imatinib for Abl over closely related kinases led to the hypothesis that the DFG-out conformation was rare and only accessible to a small subset of the kinome. However, multiple kinases have since been found to adopt this conformation (89).

The mitogen-activated protein (MAP) kinase p38α was the first serine/threonine (S/T) kinase to be characterized in the DFG-out inactive conformation (Figure 2-1) (43). Subsequently, a wealth of p38α inhibitors that stabilize this conformation (type II) has emerged in pursuit of targeting the kinase's downstream pathways involving inflammation (44, 65). These inhibitors supplanted type I ligands that stabilize the active (DFG-in) conformation such as SB203580, which despite its high potency and selectivity, was abandoned due to acute liver toxicity (90).

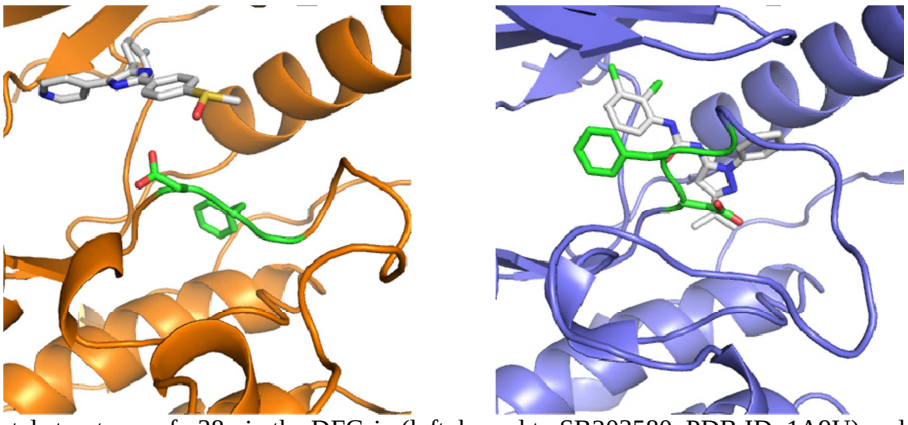

Figure 2-1. Crystal structures of p38α in the DFG-in (left, bound to SB203580, PDB ID: 1A9U) and DFG-out (right, bound to pyrazolourea **1**, PDB ID: 2BAJ) conformations. Inhibitors are shown in white, and the DFG motif in green.

Despite their novel mechanism of binding, type II inhibitors have no inherent selectivity advantage and block kinase activity in a standard, ATP-competitive fashion. However, we

believe the DFG-out conformation itself has some physiological relevance in cell signaling, a hypothesis that has largely been unexplored due to the potential pharmacological benefits of type II inhibitors. Here, we demonstrate that the DFG-out conformation can be used to regulate non-catalytic functions of MAPKs.

II. Results and Discussion

A. Use of the DFG-out conformation to prevent activation of p38α

Literature reports that use the DFG-out conformation in ways other than enzymatic inhibition are scarce. Nonetheless, we did find one study that described the role of this conformation in preventing the activation of p38α (46). Normally this kinase, like other MAPKs, is activated by a specific MAPK kinase (MKK) that phosphorylates the threonine and tyrosine residues on the TxY motif on its activation loop. These phosphorylation events increase the catalytic activity of p38α by several orders of magnitude (16). The authors of the report found that when p38α was stabilized in the DFG-out conformation by type II inhibitors, it was unable to be phosphorylated by its upstream kinase MKK6 (Figure 2-2A). However, when stabilized in the DFG-in conformation by the type I inhibitor SB203580, its phosphorylation was uninhibited.

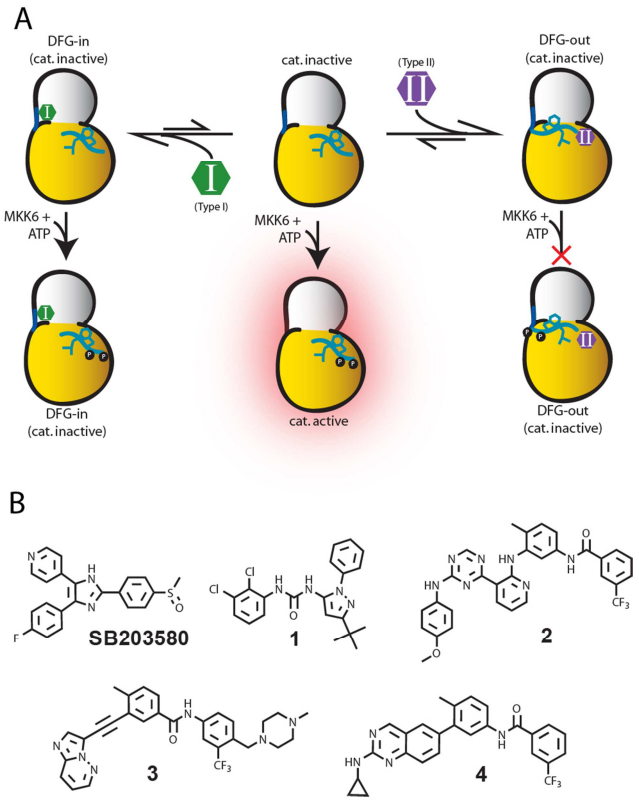

Figure 2-2. A. Schematic for MKK6-dependent phosphorylation of p38α based on which conformation is stabilized. In the DFG-in conformation (unliganded [center] or bound to a type I inhibitor [left]), the kinase can be phosphorylated by MKK6. When stabilized in the DFG-out conformation by a type II ligand (right), phosphorylation is inhibited. B. Inhibitors used in this report. Crystal structures of these ligands stabilizing specific kinase conformations can be found in the Protein Data Bank under accession codes 1A9U (SB203580), 2BAJ (1), 4EQU (2), 3OXZ (3), and 4I5H (4).

We sought to explore the generality of this phenomenon by first testing other type II inhibitors. To this end, we assembled (in addition to SB203580 and the pyrazolourea (**1**) used by Sullivan et al. (46)) three ligands of varied structure that have been shown by crystallography to stabilize the DFG-out inactive conformation (Figure 2-2B): **2**, an equipotent Src/Abl inhibitor (26); **3** (Iclusig), a clinically-approved BCR-Abl inhibitor (64); and **4**, which is based on a series of Lck inhibitors (40); All five of these ligands potently inhibit the activity of p38α (Table 2-1). We then tested the abilities of these ligands to prevent phosphorylation of p38α; like **1**, the type II inhibitors **2-4** did so at nanomolar levels (Table 2-2). Because the type I inhibitor SB203580 did not appear to block phosphorylation to any appreciable extent, we confirmed that this assay could be used to decouple ATP-competitive activity inhibition and DFG-out conformationally-

mediated phosphorylation inhibition.

	K_i (nM)				
	1	**2**	**3**	**4**	**SB203580**
p38α	6.4 ± 1.6	8.0 ± 0.4	8.1 ± 0.2	< 2	28 ± 7
p38δ	>10000	>10000	5800 ± 400	>10000	>10000

Table 2-1. K_is p38α and p38δ against the ligands shown in Figure 2-2B. All data except for those for SB203580 are reproduced from Table 1-2.

	EC_{50} (nM)				
	1	**2**	**3**	**4**	**SB302580**
p38α	<20[a]	49 ± 14	38 ± 7	130 ± 20	>10000
p38δ	1700 ± 300	>10000	350 ± 20	1200 ± 200	>10000

Table 2-2. Activation inhibition of p38α and –δ (EC_{50}) of p38α and pd8δ by the inhibitors shown in Figure 2-2B. The activation of p38α is inhibited by ligands **1-4** but not SB203580. None of these inhibitors affect p38δ.

We then turned to the closely-related MAPK p38δ, which is extensively homologous in sequence and structure to p38α (45); Unlike p38α, though, p38δ is not enzymatically inhibited by any of the type II inhibitors we have tested (Table 2-1). p38α has a threonine "gatekeeper" residue in its active site, but since this residue is methionine in p38δ, the additional steric bulk occludes inhibitor binding (67); However, these two MAPKs are activated by MKK6, and therefore, as Sullivan et al. noted, p38δ could be used as a control to determine if type II inhibitors are enzymatically inhibiting MKK6 or non-enzymatically preventing phosphorylation of p38α by stabilizing the DFG-out conformation. As expected, inhibitors **1**-**5** failed to prevent the phosphorylation of p38δ near the levels of p38α (Table 2-2), further supporting the latter hypothesis.

B. Phospho-site analysis of p38α activation inhibition

The phospho-specific antibodies used for the inhibition assays described above show that type II inhibitors block the dual phosphorylation of the activation loop of p38α. However, these reagents do not provide information on whether inhibitor binding inhibits the phosphorylation of Thr180, Tyr182, or both of these residues. To probe this parameter, we performed similar

activation inhibition experiments using p38α as shown in Table 2-2 and separated phosphorylated isoforms of the kinases by PhosTag-acrylamide PAGE (91); From this analysis, we determined that type II pyrazolourea inhibitor **1** prevented the formation of any bisphosphoryated p38α and allowed very little monophosphorylated product formation, whereas type I inhibitor SB203580 did not inhibit the formation of either mono- or bisphosphorylated protein (Figure 2-3). LC/MS analysis confirmed previous literature reports of other MAPKs (92, 93) that phosphorylation of the tyrosine on the TxY motif constituted the primary monophosphorylated product (Figure 2-4).

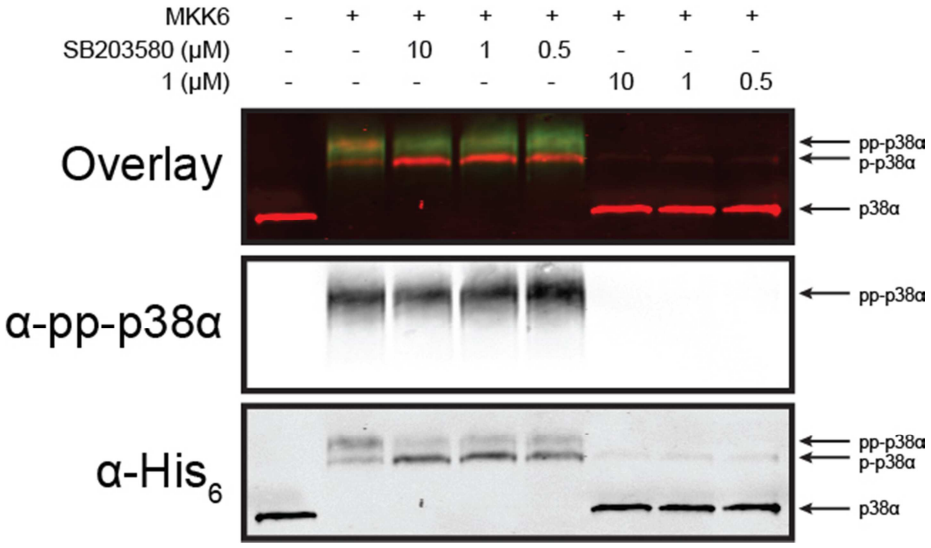

Figure 2-3. Activation inhibition analysis of p38α in the presence of inhibitor **1** or SB203580. The samples were run on a gel cast with 50 μM PhosTag-acrylamide (Wako) and 100 μM $MnCl_2$, and the blot was probed simultaneously with rabbit α-pp-p38α (Cell Signaling) and mouse α-His_6 (Abm).

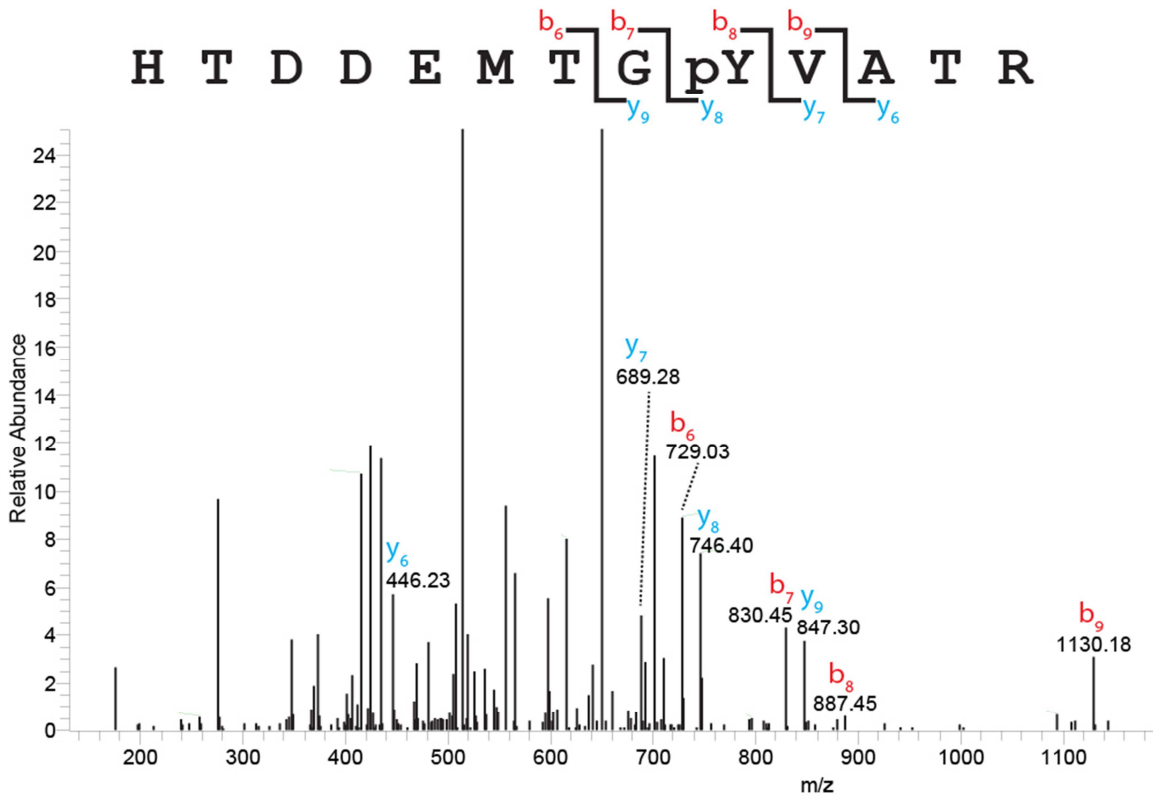

Figure 2-4. MS/MS spectrum of monophosphorylated p38α tryptic peptide. p38α (3 μM) was activated by MKK6 in the presence of inhibitor **1** (10 μM) for 1 h, then digested with trypsin overnight and analyzed by mass spectrometry. Monophosphorylation at Tyr182 was found by Matrix Mascot (www.matrixscience.com) and confirmed manually. No monophosphorylated Thr180 peptide was found.

C. Type II inhibitor-sensitive kinase mutants behave like p38α

Little is known about the physiological importance of discrete inactive conformations. Molecular dynamics simulations on p38α suggest the DFG-out inactive conformation is sampled rarely and transiently (72), yet the k_{cat} of unphosphorylated p38α is less than 1.2×10^{-5} s^{-1} (16), indicating other inactive state(s) dominate the equilibrium. Therefore, it remains unclear why some kinases can adopt the DFG-out inactive conformation naturally and others cannot. Activation inhibition via conformation adoption offers an attractive rationale for maintaining the DFG-out inactive conformation. Kinases that can "lock" themselves into this conformation (via a mechanism yet to be determined) may isolate themselves from an upstream signal, which could be especially useful if that signal has more than one target.

While p38α readily adopts the DFG-out inactive conformation and is sensitive to many type II inhibitors, most MAPKs have very little affinity to conformation-selective pharmacological agents. Erk2 is no exception, which was inconvenient because a number of noncatalytic functions of Erk2 have been discovered (31), and we wished to study these functions using the DFG-out conformation. However, we recently reported the identification of two specific residues that sensitize MAPKs to inhibitors that stabilize the DFG-out inactive conformation (94). Through site-directed mutagenesis, we sensitized the MAPKs Erk2 and p38δ to several diverse type II inhibitors (Figure 2-5A). In addition, by structurally characterizing an inhibitor **4**-Erk2 mutant complex, we showed that the mechanism of binding is through the DFG-out conformation (Figure 2-6).

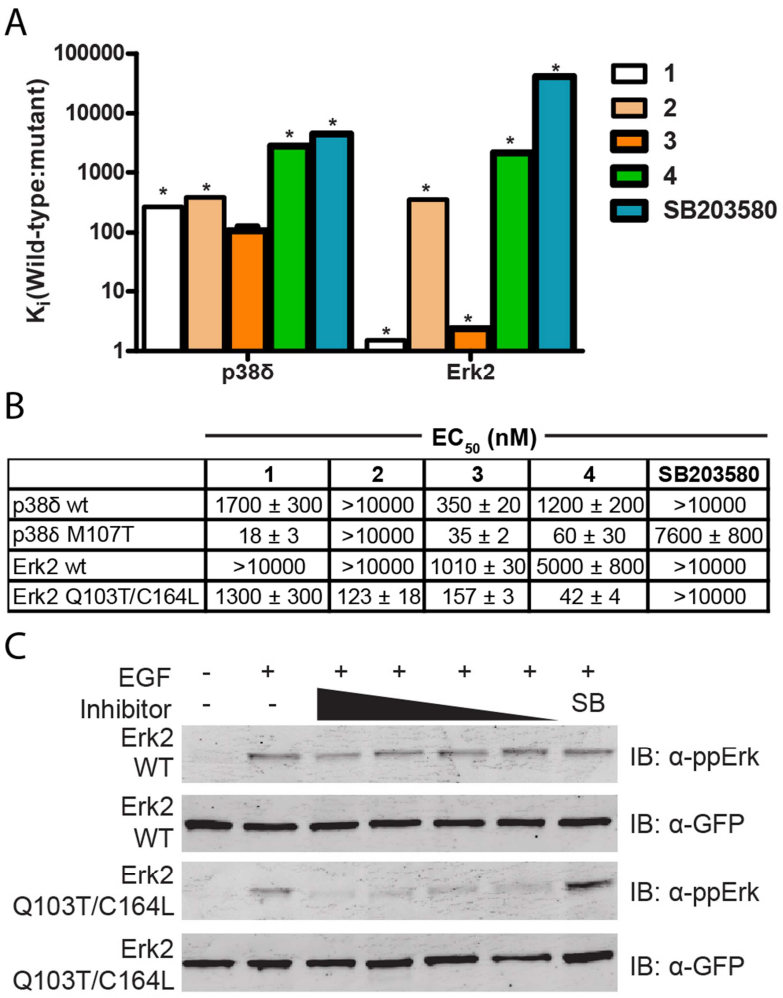

	1	2	3	4	SB203580
p38δ wt	1700 ± 300	>10000	350 ± 20	1200 ± 200	>10000
p38δ M107T	18 ± 3	>10000	35 ± 2	60 ± 30	7600 ± 800
Erk2 wt	>10000	>10000	1010 ± 30	5000 ± 800	>10000
Erk2 Q103T/C164L	1300 ± 300	123 ± 18	157 ± 3	42 ± 4	>10000

Figure 2-5. A. Fold differences in enzymatic inhibition between wild-type p38δ and Erk2 and their respective inhibitor-sensitive mutants M107T and Q103T/C164L by the inhibitors shown in Fig. 1B. Bars with astrices above them indicate the wild-type K_i was not measured accurately beyond 10 μM, and therefore the fold difference may be greater than represented by the bar. These data were reported in Table 1-2. B. Phosphorylation inhibition of p38δ, Erk2, and inhibitor-sensitive mutants. Both mutants show higher levels of inhibition by most of the type II inhibitors (1-4), but not by SB203580. C. Cellular MAPK phosphorylation inhibition. Erk2 wild-type or Q103T/C164L was transiently transfected into HEK293 cells. After serum-starvation, the cells were incubated with DMSO (lanes 1 and 2), ligand **4** (lanes 3-6 [1000, 500, 300, and 100 nM]), or SB203580 (lane 7 [1000 nM]). Epidermal growth factor (EGF) was then added to lanes 2-7 for 5 min, followed by cell lysis, PAGE separation, and immunoblotting. The experiment was performed twice, each with three replicates, and a representative blot is shown.

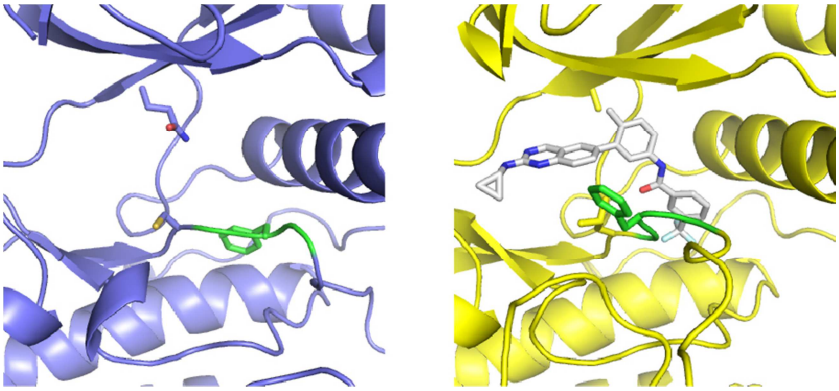

Figure 2-6. Crystal structures of wild-type Erk2 (left, PDB ID: 1ERK) in the DFG-in conformation and (right) Erk2 Q103A/C164L (right, PDB ID: 4I5H) in the DFG-out conformation. The gatekeeper and xDFG residues are shown in stick form. The ligand, if present, is shown in white, and the DFG motif in green.

With these new kinase mutants in hand, we first wondered if they would show the same DFG-out dependent phosphorylation inhibition effect that was observed in p38α. Having wild-type/mutant pairs that differed by only one or two residues provided exquisite control in decoupling enzymatic MKK activity inhibition and *bona fide* DFG-out-mediated phosphorylation inhibition. Testing p38δ, we found that the inhibitor-sensitive M107T mutant behaved similarly to p38α: three out of four type II inhibitors appeared to prevent its phosphorylation, but SB203580 had no effect (Figure 2-5B). Erk2 is activated by a different upstream kinase, MKK2, but the results mimicked those of p38δ: the phosphorylation of inhibitor-sensitive Q103T/C164L was abrogated to a much greater extent than that of the wild-type by inhibitors **1**-**4** but not SB203580.

Having demonstrated the ability of type II inhibitors to block activation loop phosphorylation *in vitro*, we were interested in whether this effect could be observed in a cellular environment. Therefore, we transiently transfected GFP-tagged Erk2 (wild-type or type II inhibitor-sensitive Q103T/C164L) into HEK293 cells and added either a type II (**4**) or type I (SB203580) inhibitor. We then briefly stimulated the cells with EGF to activate the Erk pathway (95). Immunoblot analysis showed that addition of **4** prevented Erk2 Q103T/C164L from being

phosphorylated upon stimulation, whereas SB203580 had no effect (Figure 2-5C). Consistent with the insensitivity of wild-type Erk2 to type II inhibitors, the activation of this kinase was not affected by the presence of either inhibitor.

D. Prevention of dephosphorylation via the DFG-out conformation

Since activation loop phosphorylation of MAPKs could be prevented by stabilizing them in the DFG-out inactive conformation, we hypothesized that their cognate *de*phosphorylation could also be prevented by the same mechanism (Figure 2-7A). MAPKs are selectively dephosphorylated at both residues on their TxY motifs by dual-specificity phosphatases (DUSPs) (96). The specificity of DUSPs vary, but DUSP10 is reported to target p38 and Jnk MAPKs (97). Therefore, we measured the dephosphorylation of p38α by DUSP10 in the presence of the type II inhibitor **1** or the type I inhibitor SB203580 by following the decrease of phosphorylated p38α as determined by ELISA. Similar to its ability to prevent the phosphorylation of p38α, we found that inhibitor **1** also appeared to limit its dephosphorylation, albeit only up to ~75% at saturating concentrations (Figure 2-7B). Perhaps more remarkable, though, is that SB203580 *enhanced* the phosphatase activity of DUSP10, resulting in less phosphorylated p38α compared to DUSP10 alone. To see if this effect applied to other MAPKs, we performed the same experiment with type II inhibitor-sensitive Erk2 Q103T/C164L and its specific phosphatase DUSP6 (98) and observed similar results (Figure 2-7C).

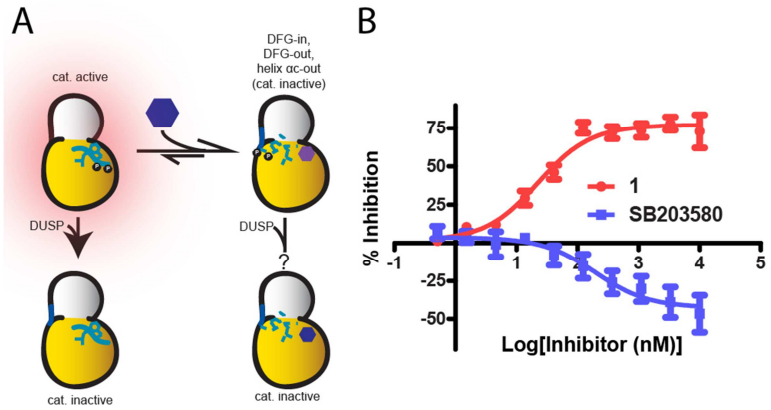

C

	EC_{50} (nM)	
	4	**SB203580**
Erk2 wt	>10000	>10000
Erk2 Q103T/C164L	<20	>-20

Figure 2-7. A. Schematic for MAPK dephosphorylation. B. Effect of ligand **1** (inhibition) or SB203580 (enhancement) on p38α dephosphorylation. EC_{50}s of ligand **1** and SB203580 were determined to be 25 ± 7 and -190 ± 40 (conveying enhancement rather than inhibition), respectively. The average plateau was 78% for ligand **1** and -43% for SB203580. C. Effect of ligand **4** or SB203580 on Erk2 dephosphorylation. The negative symbol for Erk2 Q103T/C164L against SB203580 indicates enhancement rather than inhibition. The average plateau for Erk2 Q103T/C164L was 33% for ligand **4** and -24% for SB203580.

First principles dictate that DUSPs would interact closely with the activation loops of MAPKs. Indeed, hydrogen/deuterium exchange mass spectrometry (HX) experiments show a decrease in exchange on the Erk2 activation loop upon addition of DUSP6 (99). Hence, it is reasonable that stabilizing Erk2 in the DFG-out conformation, which induces an ~10-Å translocation of the activation loop, would hinder the kinase's dephosphorylation by DUSP6. Less clear, though, is how the type I inhibitor SB203580 has the opposite effect, especially considering this ligand does not inhibit phosphorylation.

E. Use of the DFG-out conformation to mediate noncatalytic kinase functions

Having shown that p38α and inhibitor-sensitive Erk2 behave very similarly in functions related to the DFG-out conformation, we directed our efforts towards studying noncatalytic roles of Erk2. One readily-accessible phenomenon also involved DUSP6; Camps et al. demonstrated

that Erk2 increases the catalytic activity of DUSP6 towards small-molecule substrates (Figure 2-8A and Figure 2-9) (34). Selective disruption of this interaction by stabilizing Erk2 in the DFG-out conformation would indicate that binding occurs on or near the activation loop. Accordingly, we titrated either **4** or SB203580 into wild-type and inhibitor-sensitive Erk2 and measured its effect on DUSP6 activation. We found that **4** inhibited the activation of DUSP6 by inhibitor-sensitive Erk2 Q103T/C164L, but not wild-type Erk2 (Figure 2-8B). The type I inhibitor SB203580 had no effect for either the wild-type or mutant kinase. These results suggested that Erk2 is interacting with DUSP6 on or close to the activation loop, and stabilizing the kinase in the DFG-out inactive conformation is sufficient to disrupt this interaction.

A

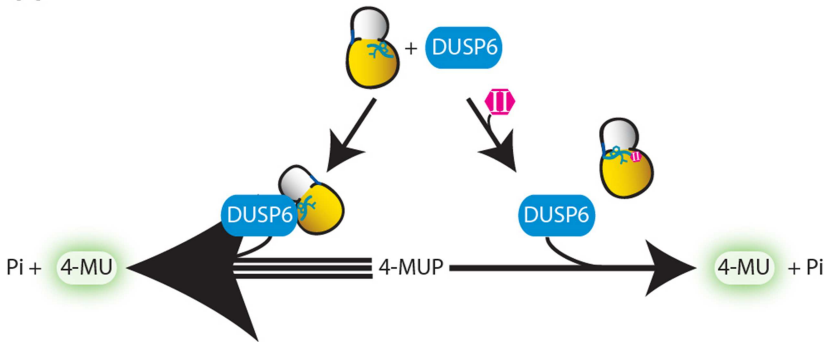

B

	EC_{50} (nM)	
	4	**SB203580**
Erk2 WT	4100 ± 700	>5000
Erk2 Q103T/C164L	<100	>5000

Figure 2-8. A. Schematic of Erk2-mediated enhancement of DUSP6 catalytic activity as reported by Camps et al (34). B. Ligand 4 or SB203580 was titrated into unphosphorylated Erk2 wild-type or inhibitor-sensitive Q103T/C164L. DUSP6 was then added to the reaction, followed by substrate 4-MUP. The phosphatase reaction was followed by fluorescence. The data were then fit to a curve, using zero inhibitor (DMSO) as the minimum possible level of inhibition and no Erk2 as the maximum. The EC_{50} values for ligand 4 were calculated using an average maximum inhibition level of 72% due to incomplete inhibition at saturating inhibitor concentrations.

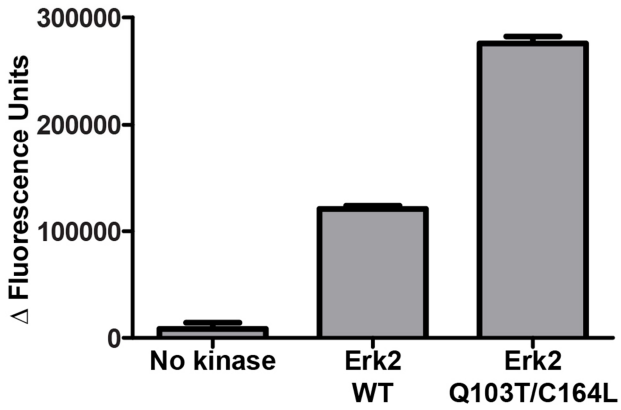

Figure 2-9. Increase in catalytic activity of DUSP6 upon addition of either Erk2 wild-type or Q103T/C164L mutant (both 1 μM). The substrate used was 4-methylumbelliferyl phosphate (4-MUP) (1 mM). Background subtraction was performed using samples without kinase or DUSP6.

To gain mechanistic insight into this effect, we titrated either apo or ligand-bound Erk2 into DUSP6 and followed the consumption of 4-methylumbelliferyl phosphate (4-MUP) by fluorescence (Figure 2-10). We found that both **1** and, to a lesser extent, SB203580 decreased the V_{max} of the reaction relative to unbound Erk2, but neither affected the association of the two proteins (K_d). A model by Zhou et. al. based on HX experiments proposes that the substrate-binding domain of Erk2 is critical for DUSP6 activation. The positions of the residues that form the substrate-binding domain are largely unperturbed when Erk2 is in the DFG-out conformation (Figure 2-11), which explains why ligand **1** does not change the affinity of Erk2 and DUSP6. We then performed a similar experiment but titrated 4-MUP instead of Erk2 (Figure 2-12) and observed that, while neither inhibitor changed the Michaelis constant of the reaction (K_m), ligand **1** drastically lowered the V_{max}, thus revealing its effect on catalytic turnover (k_{cat}).

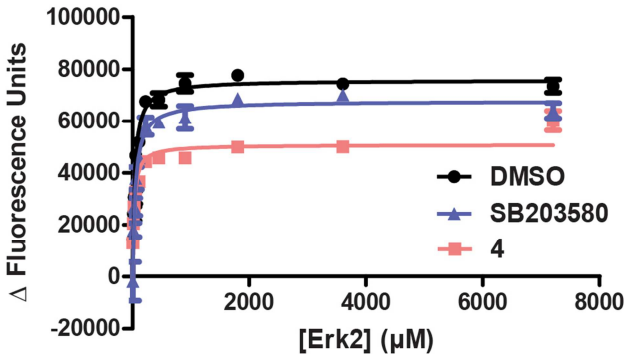

Figure 2-10. Kinetics of the DUSP6/Erk2 Q103T/C164L complex with different inhibitors. K_m[Erk2] values were determined to be 37 ± 3 μM, 49 ± 7 μM, and 27 ± 4 μM for the apo, SB203580-bound, and **4**-bound complexes, respectively.

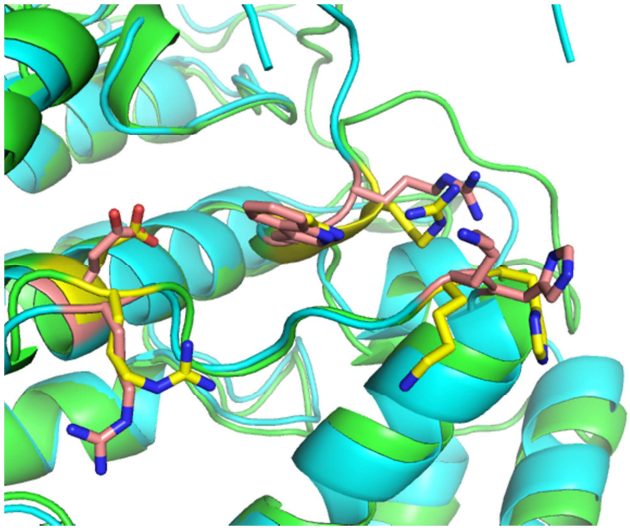

Figure 2-11. Structural alignment of Erk2 in the DFG-in (green, PDB ID: 1ERK) and DFG-out (cyan, PDB ID: 4I5H) conformations with residues forming the substrate binding domain shown as sticks in yellow and salmon, respectively.

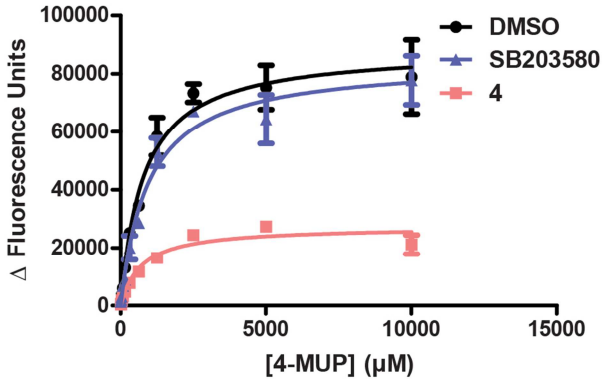

Figure 2-12. Kinetics of the DUSP6/Erk2 Q103T/C164L complex with different inhibitors. K_m[4-MUP] values were determined to be 790 ± 130 μM, 950 ± 160 μM, and 700 ± 130 μM for the apo, SB302580-bound, and 4-bound complexes, respectively.

III. Conclusion

We have found novel uses for the DFG-out inactive conformation in signaling cascades as well as for studying noncatalytic functions. First we extended the observation that the activation of p38α can be prevented through stabilization of the DFG-out conformation by demonstrating this effect in mutant kinases that were sensitized to type II inhibitors both *in vitro* and in a cellular context. We then showed that the *de*phosphorylation of kinases can also be prevented via the same conformation, and more surprisingly, that stabilization of the DFG-in conformation *enhances* dephosphorylation. Finally, we used the DFG-out conformation to perturb the noncovalent interaction between Erk2 and its cognate phosphatase DUSP6. Future work in this area could involve the study of other noncatalytic functions of Erk2 ostensibly any protein kinase.

IV. Experimental

A. General Information

Kinases for *in vitro* experiments were expressed and purified as described (94). Mass spectrometry was performed as described (94). SB203580 was purchased from LC Laboratories. Ligands **1** (65), **2** (26), **3** (64), and **4** (94) were made as described. All other reagents were purchased from commercial suppliers and used without further purification.

B. Cloning and expression

i. eGFP-tagged kinases

The expression vector pcDNA-eGFP (#13031) was obtained through Addgene. A cassette containing an SspI site, linker, and ligation-independent cloning sites was inserted after the eGFP gene using site-directed mutagenesis (100). An SspI site found elsewhere in the vector was removed by site-directed mutagenesis. The final vector was named pcEGFP-LIC. Genes coding

Erk2 wild-type and Erk2 Q103T/C164L were cloned into this vector using the ligation-independent cloning procedure described by Donnelly et al (101).

ii. DUSP6

Human DUSP6 (Addgene) was cloned into pMCSG7 (M. Donnelly) and expressed and purified with the same protocol used for kinases (94).

iii. DUSP10

Human DUSP10 (Open Biosystems) was cloned into pT7CFE1 and expressed using the 1-Step Human *In Vitro* Protein Expression Kit (Pierce) according to the manufacturer's instructions.

C. Activation inhibition assays

These assays were performed based on the work of Sullivan et al.(46) Briefly, kinase was incubated in phosphorylation buffer (50 mM MOPS [pH 7.4], 10 mM $MgCl_2$, 1 mM DTT, 0.001% (v/v) Tween 20) and BSA (0.1 mg/mL) with ATP (5 µM) and titrated inhibitor (2% in DMSO) for 30 min at room temperature. Upstream kinase (MKK2 for Erk2, MKK6 for p38) was then added, and the reactions were incubated at room temperature. Downstream and upstream kinase concentrations as well as incubation times varied by kinase based on substrate linearity. The reactions were then quenched with 20 mM EDTA and bound to polystyrene plates (Costar 96-well EIA/RIA #3590) overnight at 4 °C. Subsequent ELISA was performed using primary antibodies specific for phosphorylated kinase (p38: Cell Signaling #4511; Erk2: Santa Cruz Biotechnology #16982) and α-rabbit HRP-linked secondary antibody (Cell Signaling #7074). EC_{50}s were determined by nonlinear regression using GraphPad Prism software.

D. In-cell activation inhibition

Wild-type or Q103T/C164L mutant kinase genes in pcEGFP-LIC were transfected into low-passage HEK293 cells using Fugene HD transfection reagent (Roche) and split the next day into

a 96-well plate. Cells were serum starved for 24 hours, after which inhibitor was added (final 1% DMSO in culture media) and incubated for 1 h at 37 °C. Human EGF (Cell Signaling, 50 ng/mL) was then added to each well and incubated at 37 °C for 5 min. Cells were lysed by boiling in SDS loading buffer, and cleared lysates were separated by SDS-PAGE. Transferred membranes were immunoblotted with mouse α-GFP and rabbit α-ppErk (Cell Signaling, #2955 and #4370, respectively) and imaged with a Licor Odyssey scanner.

E. Phosphatase inhibition

Phosphorylated kinase (20 nM) was pretitrated with inhibitor for 30 min in buffer (50 mM HEPES [pH 7.4], 300 mM NaCl, 5 mM DTT, 0.1 mg-mL^{-1} BSA) before incubation with DUSP for 1 h. Amount of DUSP added varied by preparation and was tested for linearity before use. Reactions were quenched with 8 mM Na_3VO_4 and bound to polystyrene plates (Costar 96-well EIA/RIA #3590) overnight at 4 °C. Subsequent ELISA was performed using primary antibodies specific for phosphorylated kinase (p38: Cell Signaling #4511; Erk2: Santa Cruz Biotechnology #16982) and α-rabbit HRP-linked secondary antibody (Cell Signaling #7074). EC_{50}s were determined by nonlinear regression using GraphPad Prism software.

F. DUSP6 activation

DUSP6 (140 nM) was incubated with either no kinase, Erk2 wild-type, or Erk2 Q103T/C164L in buffer (50 mM HEPES [pH 7.4], 300 mM NaCl, 5 mM DTT, 0.1 mg-mL^{-1} BSA) for 1 h at room temperature, after which 4-MUP (1 mM) was added. Samples were read at (Ex:355 nm/Em:460 nm) after 2 h at room temperature. Samples without either DUSP6 or Erk2 were used for background correction.

G. DUSP6 activation inhibition

Erk2 (100 nM) was preincubated with titrated inhibitor (1% in DMSO, starting concentration 500 µM) in buffer ((50 mM HEPES [pH 7.4], 300 mM NaCl, 5 mM DTT, 0.1 mg-mL^{-1} BSA) for 30 min. DUSP6 (140 nM) was then added and allowed to incubate for 1 h at room temperature, after which 4-MUP (1 mM) was added. The reaction proceeded for 2 h at room temperature and then read at (Ex:355 nm/Em:460 nm). EC_{50}s were determined by nonlinear regression using GraphPad Prism software.

H. DUSP6 kinetics (4-MUP)

Erk2 (1 µM) was preincubated with inhibitor (10 µM, >99.9% bound) for 30 min in buffer (50 mM HEPES [pH 7.4], 300 mM NaCl, 5 mM DTT, 0.05 mg-mL^{-1} BSA), then incubated with DUSP6 (140 nM) for 1 h before addition of titrated 4-MUP. Samples were read at (Ex:355 nm/Em:460 nm) after 2 h at room temperature. Due to the excessive fluorescence of 4-MUP, separate wells for each concentration of 4-MUP without Erk2 were prepared for background correction. Michaelis constants were determined by nonlinear regression using GraphPad Prism software.

I. DUSP6 kinetics (Erk2)

Titrated amounts of Erk2 (starting at 7.2 µM) were preincubated with inhibitor (10 µM, >99.9% bound) for 30 min in buffer (50 mM HEPES [pH 7.4], 300 mM NaCl, 5 mM DTT, 0.05 mg-mL^{-1} BSA), then incubated with DUSP6 (140 nM) for 1 h before addition of 4-MUP (1 mM). Samples were read at (Ex:355 nm/Em:460 nm) after 2 h at room temperature. Michaelis constants were determined by nonlinear regression using GraphPad Prism software.

Chapter 3: Conformation-selective inhibitors reveal an unexpected correlation between the activation and phosphate-binding loops in the tyrosine kinase Abl

I. Introduction

Protein kinases are one of the largest protein families in the human genome (5). These enzymes play important roles in signal transduction networks that control countless intracellular functions, including immunity, morphogenesis, and cell cycle control (10). Precise control over kinase activity is necessary for proper cellular function. The phosphotransferase activities of protein kinases are mainly regulated on a post-translational level, which is often achieved by modulating the conformation of kinase ATP-binding sites. Due to the necessity of facilitating phosphate transfer, the structural topologies of active kinase ATP-binding sites are highly similar, with key catalytic residues optimally aligned for catalysis (56). However, freed of the necessity to catalyze phosphate transfer, a large number of inactive ATP-binding site conformations are possible (37). Small molecule inhibitors that stabilize specific inactive conformations have greatly aided the biochemical and structural characterization of ATP-binding site conformational accessibility.

A widely observed inactive kinase conformation is exemplified by the interaction of imatinib (Gleevec) with the tyrosine kinase Abl. Like many other kinases, Abl has an activation loop that contains one or more residues that increase catalytic activity upon phosphorylation. At the base of the activation loop is an Asp-Phe-Gly (DFG) motif that is highly conserved across the protein kinase family (56). The aspartate residue of this motif is critical for catalysis due to its role in coordinating magnesium. Imatinib is an example of a type II kinase inhibitor whereby the activation loop must undergo a dramatic conformational change that “flips” the DFG motif

aspartate residue away from the active site, and projects the phenylalanine residue into the ATP-binding site (DFG-out), in order to accommodate drug binding (21, 22). At first, the exceptional selectivity of imatinib for Abl over other closely-related kinases was thought to be due to Abl's rare ability to adopt the DFG-out conformation. However, over the last decade a number of closely related tyrosine kinases have been structurally characterized in the DFG-out conformation using a host of new type II inhibitors (26, 27).

The interaction of imatinib with Abl is also one of the best characterized examples of activation state-selective inhibition (35). Phosphorylation of the activation loop residue Tyr412 (pY412) increases the catalytic activity of Abl by ten-fold (102). Since the DFG motif is only twelve residues upstream from Tyr412, it is believed that this phosphorylation event enhances catalysis by stabilizing the active conformation (DFG-in) of the activation loop. It has been reported that pY412 Abl is more than two orders of magnitude less sensitive to inhibition by imatinib than the unphosphorylated form (npY412) (25). Therefore, it is reasonable to conclude that a kinase stabilized in the active conformation through phosphorylation would pay an additional energetic penalty in adopting the DFG-out inactive conformation. Moreover, imatinib is not the only type II inhibitor of Abl that exhibits this effect; AST 487 is a >30-fold more potent inhibitor of unphosphorylated Abl than the phosphorylated form (35, 103).

However, the mitogen activated protein kinase (MAPK) p38α shows no such relationship between activation loop phosphorylation and type II inhibitor sensitivity. Like Abl, the catalytic activity of p38α is increased when its activation loop is phosphorylated. Indeed, dual phosphorylation of the threonine and tyrosine residues on the TGY motif in the activation loop results in an increase in catalytic activity of several orders of magnitude (16). Also analogous to Abl, p38α is inhibited by a number of potent type II ligands that stabilize the DFG-out

conformation (44, 65, 104). For example, the selective type II inhibitor BIRB-796 (Doramapimod) binds to p38α with sub-nanomolar affinity (43, 89, 105). Yet Sullivan et al. reported nearly identical affinities of unphosphorylated and activation loop-phosphorylated forms of p38α to BIRB-796, as well as several other type II inhibitors (46). Therefore, for p38α it appears that the phosphorylation status of the activation loop does not affect the conformation of the DFG motif.

In this chapter, we further explore the relationship between activation loop phosphorylation and the conformation of the DFG motif in tyrosine kinases. We observe a correlation between phosphorylation state-dependent inhibition of Abl and selectivity for this kinase over the closely-related Src family kinases. We show that small molecule inhibitors that display a preference for non-phosphorylated over phosphorylated Abl also prefer Abl to Src. These same inhibitors are also less potent towards a glycine-rich p-loop mutant of Abl, which forms the basis for our hypotheses that the p-loop is the main source of imatinib selectivity. Our findings shed critical insight into imatinib selectivity and phosphorylation state-dependent inhibition.

II. Results and Discussion

A. Effect of Src Activation Loop Phosphorylation on Type II Inhibitor Potency

We first attempted to determine whether Abl is an exception rather than the rule for the activation state-dependence of type II inhibitor potency in kinases. Stated another way, is the apparent energetic coupling between the conformational preference of the DFG-motif and the phosphorylation status of the activation loop unique to Abl? Since the tyrosine kinase Src (Figure 3-1A), which has been shown to be able to adopt the DFG-out inactive conformation (Figure 3-1B) (26, 27) is closely related to Abl, we asked if this kinase would behave more like Abl or

p38α and show phosphorylation state-dependent or –independent sensitivity, respectively, to type II inhibitors (Figure 3-1C). To this end, we assembled a diverse panel of inhibitors that have been confirmed crystallographically to stabilize the DFG-out inactive conformation of their kinase targets. Figure 3-1D shows the panel of type II ligands that were used in this study: **1** (Rebastinib) and **2** (Iclusig) are potent type II inhibitors of BCR-Abl and imatinib-resistant BCR-Abl mutants (64, 106). **4** and **5** are based on a series of type II inhibitors of Lck (40); the pyridinyl triazine **3** and the pyrazolopyrimidine **6** have been structurally characterized to stabilize the DFG-out conformation of Src (26, 27). Unlike imatinib, all of these type II ligands are potent inhibitors of both Abl and Src.

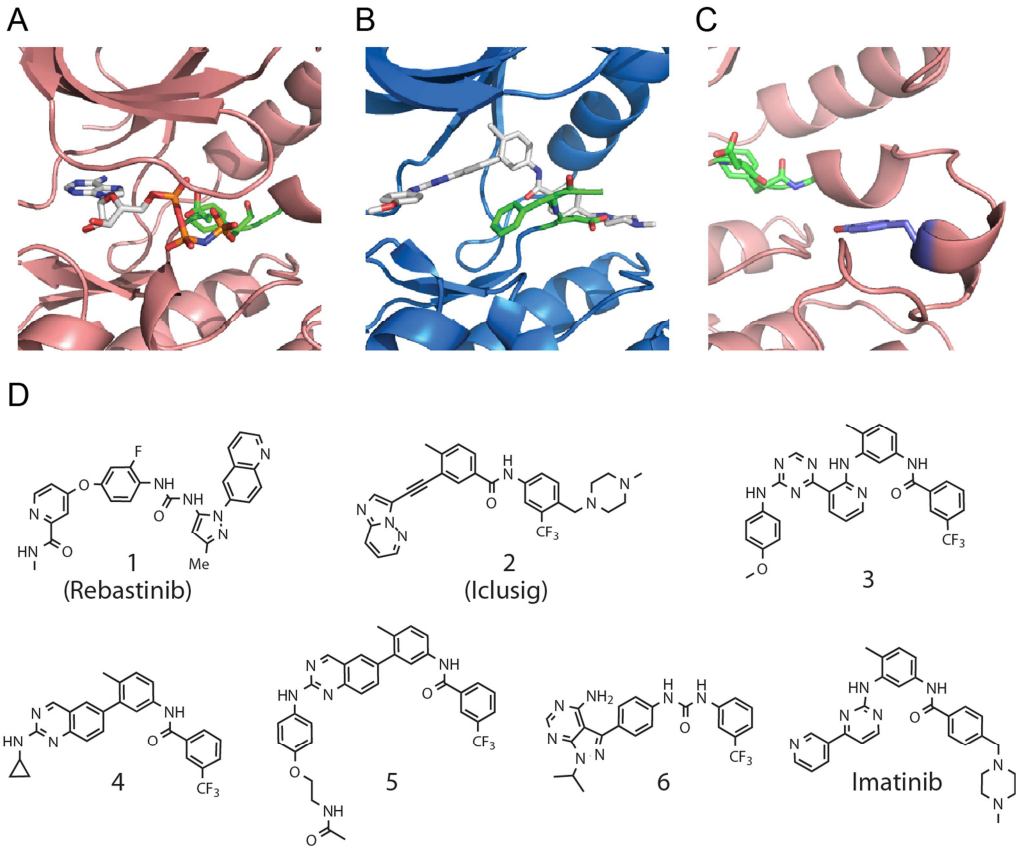

Figure 3-1. A-C. Crystal structure of Src in the (A) DFG-in (bound to an ATP analogue [PDB ID: 2SRC]) and (B) DFG-out (bound to a type II inhibitor [PDB ID: 3G6G]) conformations. (C) Tyr416 (purple) is located ten residues C-terminal to the DFG motif, which is shown in green for all structures. D. Type II inhibitors known to stabilize the DFG-out conformation despite varied structures.

For biochemical studies with Src, we utilized a recombinant construct that contains a kinase domain and the regulatory SH2 and SH3 domains. To prevent any inhibitory auto-phosphorylation that could arise during our biochemical studies, the regulatory tyrosine in Src's C-terminal tail (Tyr527) (107, 108) was mutated to a non-phosphorylatable phenylalanine (Figure 3-2). Co-expression of this Src construct (Src Y527F) with the tyrosine phosphatase YopH in *E. coli*, followed by purification, yields homogenous kinase that is completely dephosphorylated (npY416-Src) (109). In order to generate Src that is phosphorylated at Tyr416 in the activation loop (pY416-Src), the ability of high concentrations of Src-family kinases to undergo efficient activation loop auto-phosphorylation was exploited (2, 110, 111). Quanatitative activation loop phosphorylation was confirmed by immunoblot analysis and LC/MS of tryptic peptides (Figure 3-3).

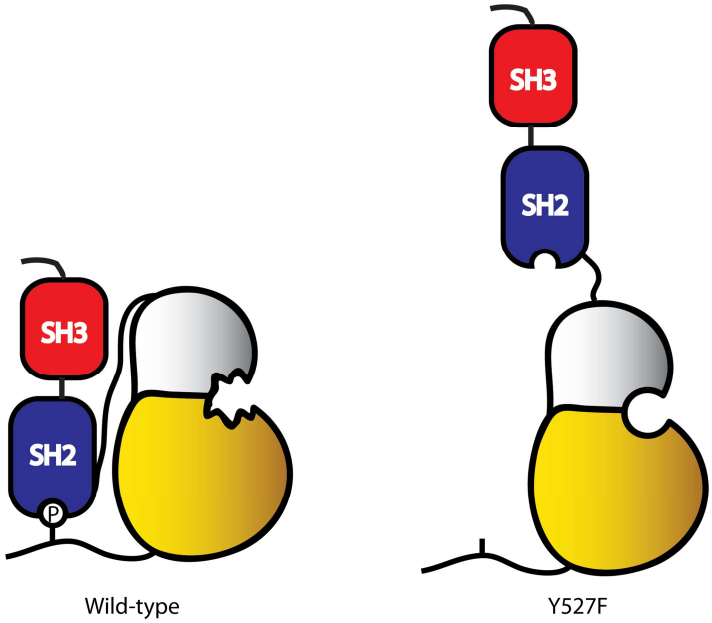

Figure 3-2. Phosphorylation of Src at position Tyr527 facilitates a binding interaction between the tail of the catalytic domain and the SH2 domain, causing a decrease in catalytic activity (left). Mutating this position to Phe releases this interaction and restores activity (right).

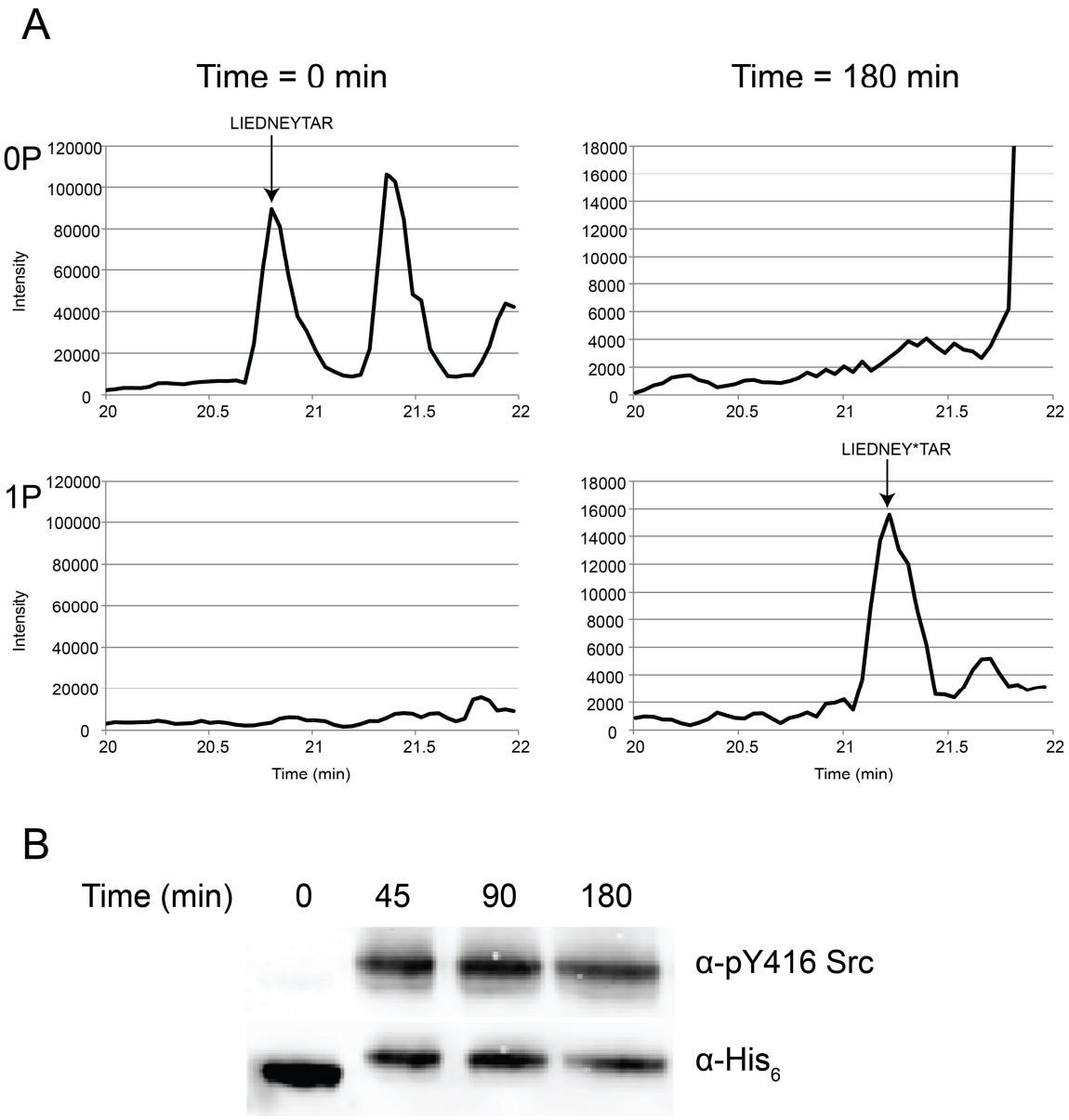

Figure 3-3. A. Extracted ion chromatographs from LC/MS analyses of tryptic digests of Src either alone (left) or after incubation with ATP for 3 h (right). Only the monophosphorylated peak is obseved after 3 h, indicating quanititative phosphorylation. B. Timecourse analysis by immunoblot of Src autophosphorylation.

Next, we tested the potencies of the type II inhibitors shown in Figure 3-1B for the npY416-Src and pY416-Src constructs in *in vitro* activity assays. In stark contrast to the reported preference of imatinib for non-phosphorylated Abl over the activation loop-phosphorylated form, most of the type II inhibitors tested demonstrated a minimal preference (< 3-fold) for npY416-Src. Indeed, only ligand **1** showed notable selectivity (~11-fold) between the two Src phospho-

isoforms (Figure 3-4A). To confirm that the observed lack of selectivity is not due to the presence of the Y527F mutation in the C-terminal tail of npY416, we tested a subset of the type II inhibitors against unphosphorylated, wild-type (wt) Src (Table 3-1). As expected, the K_is of all of the inhibitors tested are the same for non-phosphorylated wt and Y527F Src. Additionally, to rule out the possibility that the lack of observed phosphorylation state-dependent inhibition is due to autophosphorylation of npY416-Src during the activity assay, we verified by immunoblot that no pY416-Src is formed under the assay conditions used (Figure 3-5). Finally, to determine whether the observed lack of preference is specific to Src or more general to the Src-family kinases (SFKs), we performed equivalent assays with Hck (Table 3-2). Similar to Src, none of the three inhibitors tested showed a >4-fold preference for unphosphorylated Hck. Thus, it seems that SFKs are more similar to the MAPK p38α than to Abl in their sensitivities to type II inhibitors.

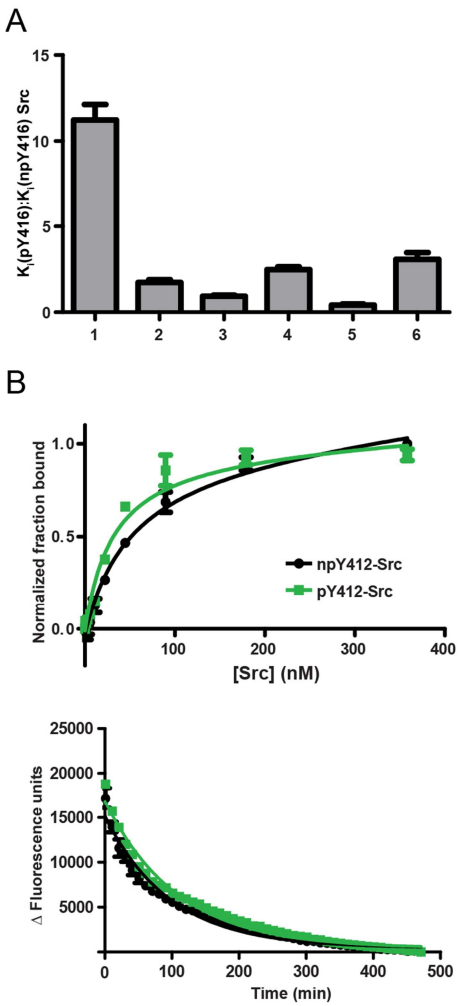

Figure 3-4. A. Comparison of K_is of pY416-Src::npY416-Src for the inhibitors shown in Fig. 1B (excluding imatinib). With the exception of **1**, the inhibition difference between the two phosphoforms is three-fold or less. B. Direct binding (top) and dissociation (bottom) measurements of pY416-Src (green) and npY416-Src (black) to a BODIPY-conjugated type II inhibitor show no appreciable difference between the two phosphoforms.

	K_i (nM)		
	2	**3**	**6**
npY416-Src (Y527F)	5.2 ± 0.1	2.8 ± 0.1	13 ± 1
npY416-Src (wt)	29.8 ± 0.9	3.1 ± 0.1	12.5 ± 1.3

Table 3-1. K_is of npY416-Src (Y527F) and npY416-Src (wt) against type II inhibitors shows that the two constructs have similar inhibition profiles.

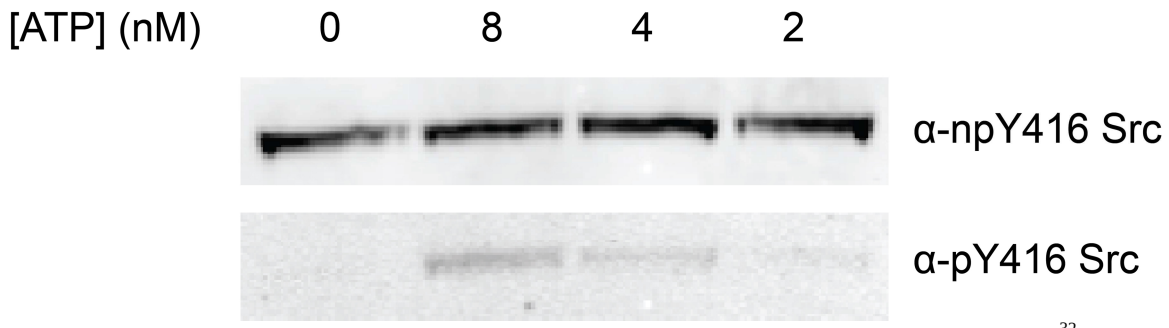

Figure 3-5. Autophosphorylation of Src (10 nM) at low concentrations of ATP. The concentration of γ^{32}P ATP used in the activity assays was ~2 nM, and the concentration of Src was at least ten-fold less than what was used for the immunoblot analysis.

	K_i (nM)		
	2	**3**	**4**
npY416-Hck	1.5 ± 0.1	4.2 ± 0.3	10 ± 1
pY416-Hck	4.8 ± 0.3	7.7 ± 0.2	20 ± 0.3

Table 3-2. K_is of npY416-Hck and pY416-Hck against three ligands shows little difference between phosphoforms, similar to that observed for Src.

To confirm that npY416-Src and pY416-Src have the same affinities for DFG-out stabilizing ligands without using an activity assay, their dissociation constants (K_ds) for a BODIPY-labeled version of inhibitor **3** were determined. This probe has been used previously to assess DFG-out conformational accessibility for a number of kinases, including Src (54). We found the K_d of this probe for npY416- and pY416-Src to be almost identical (Figure 3-4B). Further, a binding dissociation experiment demonstrated that both phospho-isoforms of Src have similar binding kinetics (k_{off}) for this type II probe. This information is significant because type II inhibitors are known to have slow binding kinetics, primarily due to the large conformational change of the activation loop required to accommodate a type II ligand (43). That this rate is both slow and very similar for npY416- and pY416-Src indicates that these phospho-isoforms undergo similar conformational changes in order to accommodate type II inhibitors.

B. Type II inhibitor sensitivity to the phosphorylation status of the activation loop of Abl

Having determined that most type II inhibitors show little preference for either phospho-form of Src, we returned to Abl in order to investigate whether activation state selectivity is specific to

the kinase or the inhibitor imatinib. First, the compounds described above were tested for their abilities to inhibit Abl. Unlike imatinib, all of the inhibitors tested have similar potencies for non-phosphorylated Abl and Src (Figure 3-6A). Five other type II inhibitors were also tested against Abl: **7** (AST-487), a predicted type II inhibitor of the kinase FLT3 (112); and four analogs of **3** that have variable hinge region contacts (Figure 3-6B). Interestingly, these five additional inhibitors are highly selective for Abl over Src (Figure 3-6C), as much as 600-fold in the case of AST-487. Next, the phosphorylation state-dependence of Abl inhibition by this assembled compound panel was determined using activation loop phosphorylated Abl (pY412-Abl) that was generated using a previously described procedure (25, 102). Consistent with previous reports, imatinib and **7** are much more potent against npY412-Abl than pY412-Abl (Figure 3-6D). In addition, compounds **8**-**11** are all >50-fold selective for the non-phosphorylated form of Abl. In contrast, **2**, **3**, **5**, and **6** show minimal (≤5-fold) activation state-dependent inhibition. One interesting trend that becomes apparent from analyzing these data is that inhibitors that are selective for Abl over Src show activation state-dependent inhibition of Abl, while non-selective compounds show little or no phospho-dependence. Plotting the inhibitory constants (K_is) of the inhibitors tested for npY416-Src and pY412-Abl shows a correlation in potencies (Figure 3-6E). In essence, phosphorylated Abl behaves like non-phosphorylated Src in the presence of type II inhibitors.

A

K_i (nM)

	1	2	3	4	5	6
npY412-Abl	0.42 ± 0.01	0.13 ± 0.01	0.76 ± 0.04	0.12 ± 0.01	0.18 ± 0.02	2.2 ± 0.1
npY416-Src	5.1 ± 0.2	1.0 ± 0.1	1.6 ± 0.1	0.68 ± 0.03	0.11 ± 0.01	8.2 ± 0.8

B

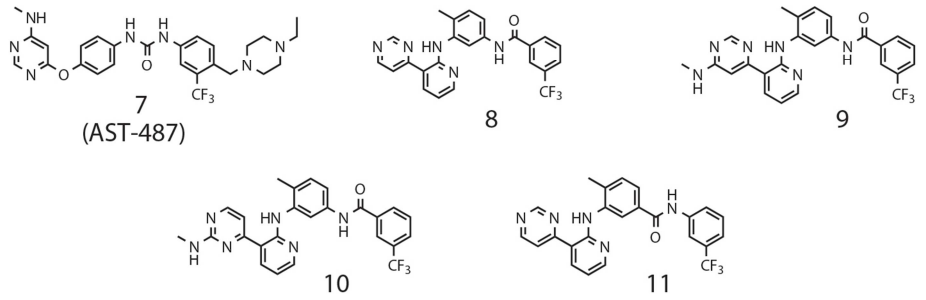

C

K_i (nM)

	7	8	9	10	11	Imatinib
npY412-Abl	0.41 ± 0.03	0.28 ± 0.02	2.8 ± 0.1	0.39 ± 0.02	0.5 ± 0.1	0.81 ± 0.03
npY416-Src	87 ± 1	8.9 ± 0.5	530 ± 30	19 ± 1	23 ± 1	> 3300

D

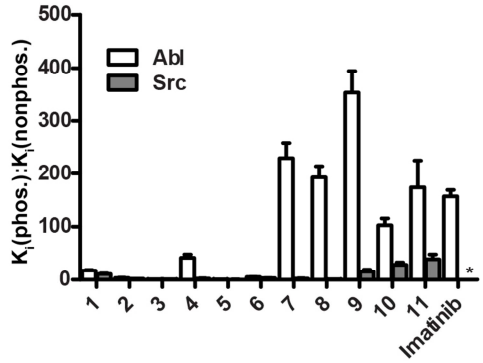

E

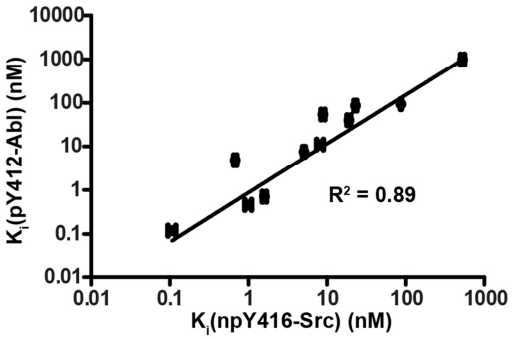

Figure 3-6. A. K_is of inhibitors shown in Figure 3-1D against npY412-Abl and npY416-Src. Since Abl was being compared directly to Src, only the catalytic domains of both kinases were used. B. Structures of **7** (AST-487) and analogues of **3**. C. K_is of inhibitors shown in B against npY412-Abl and npY416-Src (catalytic domains only). D. Comparison of phosporylated:unphosphorylated forms of Abl and Src. Most of the inhibitors shown in Figure 3-1D do not appear to discriminate between phospho-isoforms of either kinase, but those shown in B greatly favor npY412-Abl over pY412-Abl. The asterisk indicates that the K_i for imatinib for Src could not be measured accurately. E. Comparison of inhibition profiles of pY412-Abl and npY416-Src (catalytic domains only) indicates correlation.

C. Src is as Capable of Adopting the DFG-out conformation as Abl

Based on the correlation between pY412-Abl and npY416-Src, we hypothesized that the mechanism by which certain inhibitors can discriminate between Abl activation states is linked

to their selectivity for Abl over Src. Therefore, we further investigated differences in type II inhibitor sensitivity between these two kinases. Despite the overall active site similarities between Src and Abl, it has been proposed that Src pays a significant energetic penalty to adopt the DFG-out inactive conformation relative to Abl (24, 113). Recent molecular dynamics (MD) simulations have indicated that dissimilarities in the overall active site flexibilities of Src and Abl result in different relative stabilities of their DFG-out conformations. In particular, these MD simulations suggest that one residue difference in Src, Leu317, appears to alter the conformational preference of the DFG motif in this kinase (114). However, the fact that several of the type II inhibitors in our panel (**1** – **6**) are nearly equipotent against Src and Abl indicates that Src does not likely pay a substantial energetic penalty for adopting the DFG-out inactive form. Furthermore, Abl-selective type II inhibitors differ from their non-selective analogs in regions that interact with the adenosine pocket and not the hydrophobic pocket created by movement of the DFG motif. Finally, a Src mutant that that contains the equivalent Abl residue (Src L317I) (Figure 3-7) does not show increased sensitivity to imatanib or any of the other type II inhibitors that were tested (Table 3-3). Therefore, a simple DFG motif conformational preference between Src and Abl cannot account for the selectivities of imatinib and **7 – 11.**

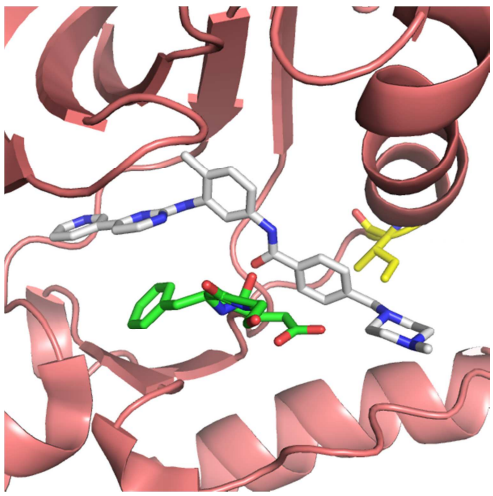

Figure 3-7. Crystal structure of Src L317I (PDB ID: 3OEZ) bound to imatinib (white). The DFG motif is shown in green and Ile317 in yellow.

	K_i (nM)				
	2	**7**	**8**	**9**	**Imatinib**
Src	1.0 ± 0.1	87 ± 1	8.9 ± 0.5	530 ± 30	> 3300
Src L317I	0.56 ± 0.3	135 ± 5	72 ± 18	1400 ± 100	> 3300

Table 3-3. K_is of five inhibitors against Src kinase domain (KD) and Src KD L317I demonstrate that this mutation has little or no effect on inhibitor potency.

D. P-loop Interactions Modulate Potencies of Some Type II inhibitors

Another distinguishing feature of Abl's interaction with imatinib is the kinked conformation of its phosphate-binding loop (also referred to as the glycine-rich loop) when bound to this drug. This highly conserved and flexible loop, which makes critical contacts with the phosphates of ATP, is located between strands β1 and β2 of the N-terminal lobe. The kinked orientation of the p-loop of Abl in the Abl-imatinib complex allows extensive van der Waals contacts and hydrophobic interactions between the kinase and drug. A co-crystal structure of Src bound to imatinib shows that the p-loop of this kinase does not make similar contacts (22). Imatinib's interactions with Abl's flexible p-loop have been shown to be a major determinant of this drug's selectivity for Abl over Src (25). Furthermore, some of the most common clinically-observed imatinib-resistant mutants occur in the p-loop (36). The most notable differences between activation state-dependent and –independent inhibitors occur in regions that would be expected to project towards the p-loop. Therefore, we further explored the interactions of this region with our type II inhibitor panel by determining their abilities to inhibit the catalytic activity of Abl Y253H, which is an imatinib-resistant p-loop mutant of Abl that is frequently observed in the clinic (Figure 3-8A and B). Consistent with previous reports, imatinib is a much less potent inhibitor of the npY412-Abl Y253H than npY412-Abl (Figure 3-8C). Like imatinib, the potencies of activation state-dependent inhibitors **7 – 11** are greatly diminished for npY412-Abl

Y253H. However, activation state-independent inhibitors **1** – **6** are nearly equipotent against npY412-Abl and npY412-Abl Y253H. Therefore, there appears to be a strong correlation between activation state-dependent inhibition and sensitivity to p-loop mutations.

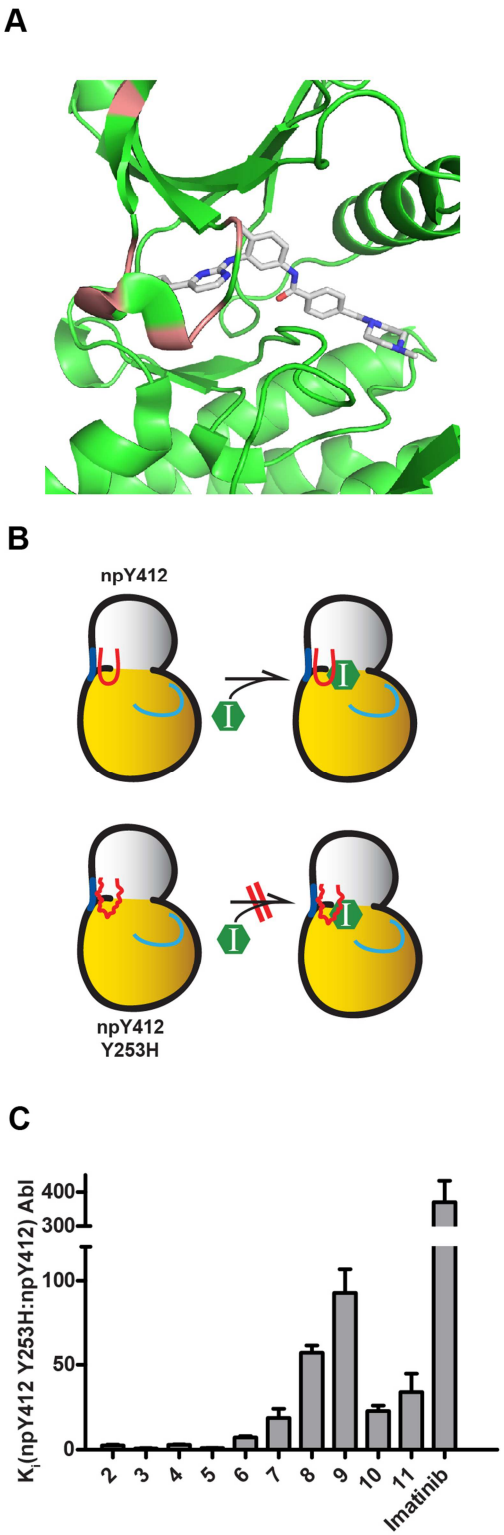

Figure 3-8. A. Crystal structure of Abl bound to imatinib (PDB ID: 1IEP). P-loop mutations found in the clinic are shown in salmon. B. A model for p-loop-mediated knockback of inhibition. The p-loop is shown in red, and the activation loop is shown in cyan. C. K_is of inhibitors against Abl wild-type and Y253H demonstrate that only ligands **7** – **11** and imatinib interact with the p-loop.

E. Activation Loop Phosphorylation Affects Type II Inhibitor Potency Independent of the P-loop

Knowing that both activation loop phosphorylation and a p-loop mutation affect the potencies of compounds **7** – **11**, we asked if these two kinase features were directly linked; that is, does activation loop phosphorylation abrogate inhibitor binding differently than the p-loop, or does it directly affect the conformation of the p-loop (Figure 3-9A)? Given that the p-loop residue Tyr253 is more than 20 Å away from the activation loop residue Tyr527 (Figure 3-9B), the hypothesis that a long-range interaction exists between these two residues seemed implausible. However, plotting our inhibitor data for pY412-Abl and npY412-Abl Y253H suggested that these two features were at least correlated (Figure 3-9C). To further investigate this matter, we tested pY412-Abl Y253H against several inhibitors described above. If the activation loop and p-loop are linked, then the inhibition of pY412-Abl Y253H by these ligands should be no more potent than those of either pY412-Abl or npY412-Abl Y253H individually. However, we observed that the potencies of **2**, **3**, **7**, and imatinib for pY412-Abl Y253H were greater than both of the individual variants (Figure 3-9D), suggesting that the activation loop and p-loop are independent. We then compared the pY412 forms of Abl wild-type and Y253H with their npY412 counterparts to assess the specific effect of activation loop phosphorylation (Figure 3-9E). From this analysis, we found that inhibitors **2** and **3** are at most 10-fold less potent towards the pY412 forms, supporting the notion that these ligands are insensitive to activation loop phosphorylation. In contrast, **7** and imatinib are up to 200-fold less potent towards pY412-Abl, further indicating that the potencies of these ligands are highly influenced by phosphorylation, and that this effect is independent of the Y253H p-loop mutation.

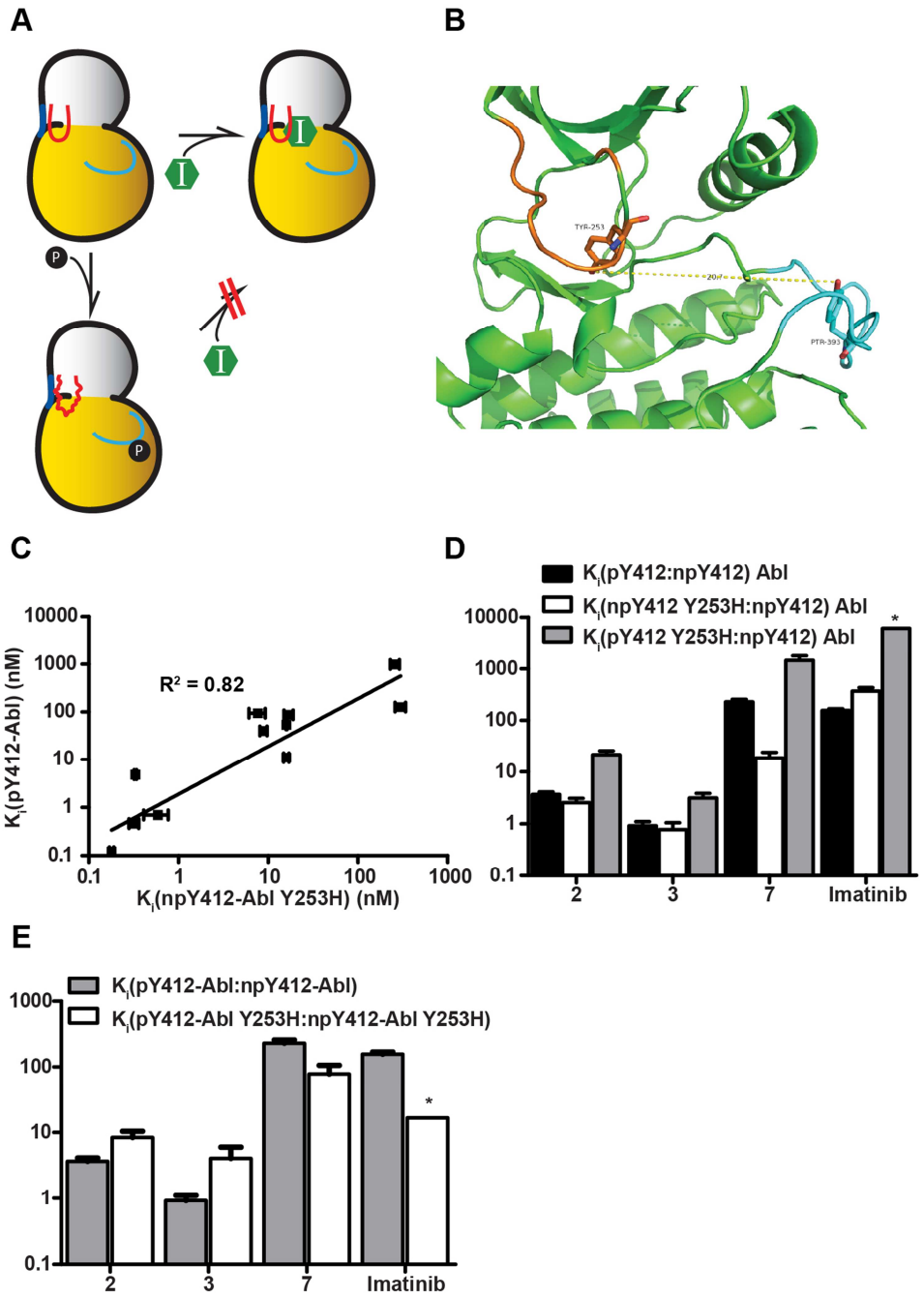

Figure 3-9. A. A model for the hypothesis that activation loop phosphorylation disrupts the conformation of the p-loop, which in turn abrogates ligand inhibition. The p-loop is shown in red, and the activation-loop is shown in cyan. B. Crystal structure of Abl (PDB ID: 2GQG) with the distance between Tyr253 and Tyr412 (Tyr393 in the structure) measured to be >20 Å. The p-loop is shown in orange, and the activation loop is shown in cyan. C. Comparison of K_is for npY412-Abl Y253H and pY412-Abl. D. Fold differences between pY412-Abl, npY412-Abl Y253H, and pY412-Abl Y253H; and npY412 Abl. E. Fold differences between phosphorylated and unphosphorylated forms of Abl and Abl Y253H. The asterices in D and E indicate that no inhibition was observed for pY412-Abl Y253H against imatinib up to 5000 nM, so although 5000 nM was used as the K_i, the actual value is higher.

Although long-range interactions are known to occur in protein kinases (63), it is logical from a first-principles standpoint that the activation and p-loops act independently to abrogate inhibitor potency. Nonetheless, it cannot be ignored that a correlation exists between inhibitors that are sensitive to activation loop phosphorylation and the Y253H p-loop mutation (Figure 3-9C), and there is evidence in the literature of interplay between these two regulatory motifs. For example, Kwarcinski et. al. used the Abl Q252C p-loop mutant in conjunction with an irreversible inhibitor to imply that the activation and p-loops are connected (115). Furthermore, we found that the rate of activation loop phosphorylation of Abl Y253H by Hck is much slower than for Abl wild-type (Figure 3-10), meaning that either the p-loop is a critical recognition element for Hck or that the Y253H mutation is altering the conformation of the activation loop. More work must be done to generate a model that incorporates all available experimental data.

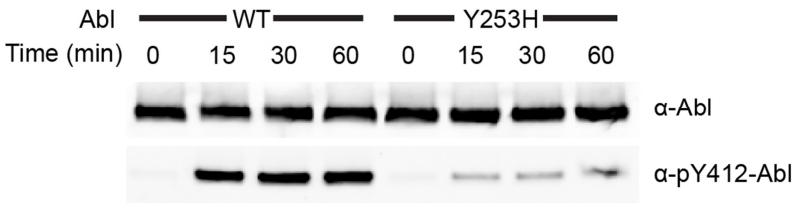

Figure 3-10. Activation loop phosphorylation of Abl wt and Abl Y253H (both at 15 µM) by Hck (700 nM) and ATP (500 µM) at 37 °C. The top and bottom immunoblots were performed separately using the same samples at the same volumes.

F. The P-loop of Abl displays altered dynamics in the presence of different DFG-out ligands

Having demonstrated that p-loop interactions contribute substantially to the potencies of certain inhibitors to Abl, we were interested in knowing specifically how these inhibitors affected the conformation of the p-loop. For example, imatinib and **2** are sensitive and resistant, respectively, to p-loop mutations. However, superimposition of Abl in complex with imatinib and **2** indicates no conformational differences in the p-loop region (Figure 3-11). On the other

hand, line broadening in this region has been observed in NMR experiments (116), implying plasticity that cannot be observed by crystallographic studies.

Figure 3-11. P-loops of two superimposed structures of Abl bound to imatinib (PDB ID: 1IEP, salmon) and **2** (PDB ID: 3OXZ, yellow).

We used a mass spectrometry-based footprinting technique to study the dynamics of Abl's p-loop when bound to different inhibitors. This method uses isotope-coded affinity tagging reagents to ratiometrically determine the alkylation rate of cysteine residues over time (117) and has been used before to study the dynamics of other protein kinases (94, 118). Since the p-loop of Abl has no cysteines, we performed our studies using a p-loop mutant (Q252C) that has been characterized previously (Figure 3-12A) (115). Alkylation at this position proceeded at the same rate for *apo* and **7**-bound Abl, but slower for **3**-bound Abl (Figure 3-12B). We performed the same experiment with **2**, which, like **3**, does not interact with the p-loop, and observed the same effect (Figure 3-12C). Therefore, it appears that only inhibitors which do *not* interact with the p-loop are able to somehow limit the chemical exposure of Cys252.

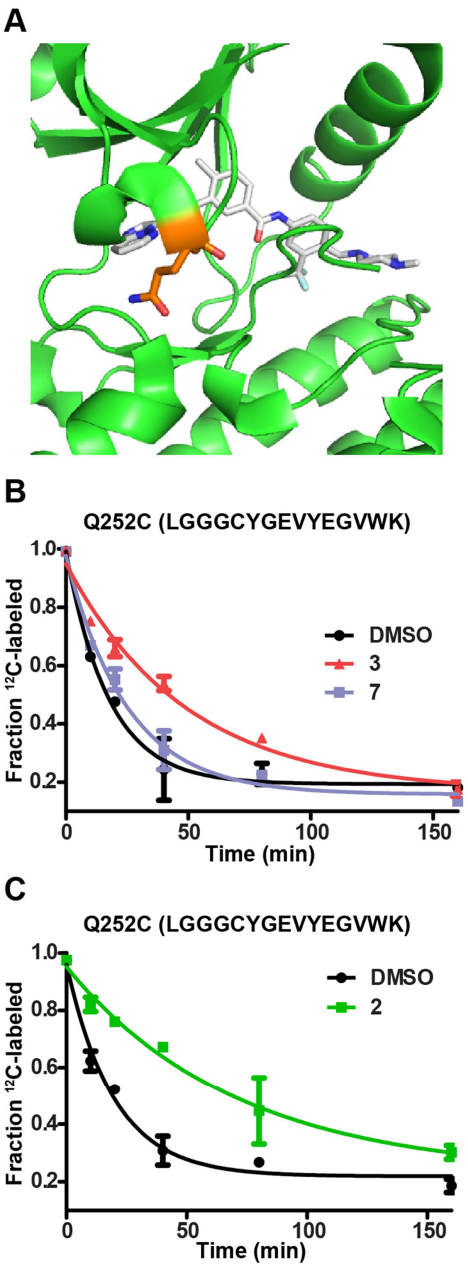

Figure 3-12. A. Crystal structure of Abl in complex with **2** (PDB ID: 3OXZ) (white) with and Gln252 shown in orange. B. ICAT-based alkylation timecourse of Abl alone (black) or bound to **3** (red) or **7** (blue) at engineered position Cys252. C. Same as B but with ligand **2** (green).

In an effort to explain these results, we analyzed thirty crystals structures of Abl in the Protein Data Bank (Table 3-4) and found only modest diversity in p-loop conformation. The majority of these structures, including those bound to imatinib, **2**, and **3**, show a "kinked" conformation that blankets the adenosine pocket. A small subset, though, displays an extended

conformation which is commonly observed in Src-family kinases (119, 120). Furthermore, these few structures are bound to widely disparate ligands that promote different inactive conformations such as helix αc-out, DFG-out, and DFG-in. In light of this information and our ICAT data, we hypothesize that the conformation of Abl's p-loop in crystal structures is not indicative of its true flexibility, even when bound to small-molecule inhibitors. If so, then ligands **2** and **3** could be promoting p-loop conformations that offer greater shielding of Cys252.

PDB ID	P-loop conformation
3OXZ	Kinked
2QOH	Kinked
3CS9	Kinked
1OPK	Kinked
3K5V	Kinked
1OPJ	Kinked
2G2F	**Extended/Disordered**
2G2I	Extended
2G2H	Kinked
3DK3	Kinked
3DK6	Kinked
2G1T	**Extended**
2GQG	Kinked
2F4J	Kinked
1M52	Kinked
2V7A	**Extended**
2E2B	Kinked
3MS9	Kinked
1IEP	Kinked
3KF4	Kinked
3KFA	Kinked
3UE4	Kinked
1OPL	Kinked
2HZ0	**Extended/Disordered**
2HZN	**Disordered**
2HZ4	**Disordered**
2HZI	Kinked
2HIW	Kinked

2FO0	Kinked
3QRK	Kinked
3QRI	Kinked

Table 3-4. Thirty-one crystal structures of Abl in the Protein Data Bank classified by p-loop conformation.

III. Conclusion

In this work, we have examined how architectural motifs in tyrosine kinases affect small molecule-inhibitor potency. Based on recent literature reports demonstrating that activation loop phosphorylation of Abl decreases its potency to imatinib, we asked if the closely-related kinase Src would show the same effect. However, type II ligands that were equipotent towards Abl and Src showed no difference in inhibition between unphosphorylated and activation loop-phosphorylated forms of Src. We then expanded our scope to a larger group of inhibitors and found that those which were selective for Abl over Src were also sensitive to activation loop phosphorylation of Abl. In contrast, inhibitors which were equipotent for Abl and Src showed no phospho-dependence for Abl.

Interestingly, the inhibitors that were sensitive to activation loop phosphorylation of Abl were also sensitive to a clinically relevant mutation in the p-loop. However, despite this correlation, it appears that the activation and p-loops act independently to abrogate inhibitor potency. Our results delineate the correlation between the activation and p-loops and help explain the fundamental basis of imatinib selectivity.

It is curious that inhibitors which are not sensitive to mutations in the p-loop still manage to alter its conformation, as demonstrated by our ICAT footprinting experiments. The dynamics of this motif and its specific role in inhibitor recognition remain elusive. Further research in this area is critical for improved kinase therapeutic development.

IV. Experimental

A. Cloning and mutagenesis

Bacterial expression plasmids containing genes encoding Src 3D, Hck 3D, and Abl KD were kindly provided by J. Kuriyan. All mutagenesis was performed by Quikchange (Agilent).

B. Protein purification

Recombinant proteins were expressed and purified as described (109, 121).

C. Fluorescence measurements

These experiments were performed as described (54, 80).

D. Synthetic methods

i. General information

Imatinib was purchased from ChemieTek (Indianapolis, IN). **1** (106), **2** (64), **3** (25), **4** (94), **6** (27), **7** (112), and **11** (122) were made as described. Unless otherwise noted, all reagents were obtained from commercial suppliers and used without further purification. NMR spectra were obtained on a Bruker AV-300 or -301 instrument at room temperature. Chemical shifts are reported in ppm and coupling constants in Hz. Mass spectra were obtained on a Bruker Esquire Ion Trap instrument.

General analytical condition A - CH_3CN/H_2O–0.1% CF_3CO_2H.

General analytical condition B - CH_3OH/H_2O–0.1% CF_3CO_2H.

General HPLC Purification Conditions: Samples were injected on a preparatory reverse-phase C18 column (250 x 21 mm) run over 60 minutes at 8 mL/min (Acetonitrile/Water–0.05% TFA gradient: 1:99 to 100:0). Purified products were detected by UV at the detection frequency of 254 nm detection.

ii. Synthesis of compounds 5 and 8 – 10

N-(3-(2-(4-(2-aminoethoxy)phenylamino)quinazolin-6-yl)-4-methylphenyl)-3-(trifluoromethyl)benzamide (123), 4-(2-chloropyridin-3-yl)pyrimidine (122), (E)-1-(2-chloropyridin-3-yl)-3-(dimethylamino)prop-2-en-1-one (122), and N-(3-amino-4-methylphenyl)-3-(trifluoromethyl)benzamide (26), were made as described.

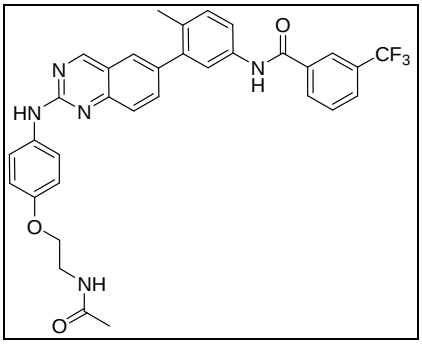

[5] N-(3-(2-(4-(2-aminoethoxy)phenylamino)quinazolin-6-yl)-4-methylphenyl)-3-(trifluoromethyl)benzamide (11.6 mg, 0.02 mmol) was stirred in a mixture of Ac_2O (416 µL) and NEt_3 (11.6 µL) for 2.5 h at room temperature. The reaction mixture was concentrated *in vacuo*, diluted with a mixture of acetonitrile/water and purified by reverse phase chromatography (HPLC) to obtain 10.2 mg of the desired product **5** (82% yield). ^{1}H NMR (300 MHz, Chloroform-d) δ 9.43 (s, 1H), 8.27 (s, 1H), 8.21 (d, *J* = 9.0 Hz, 1H), 8.03 – 7.90 (m, 2H), 7.81 – 7.71 (m, 2H), 7.64 – 7.48 (m, 4H), 7.37 – 7.29 (m, 3H), 7.16 – 7.08 (m, 2H), 5.80 (s, 1H), 4.13 (t, *J* = 6.0 Hz, 2H), 3.60 (t, *J* = 3.0 Hz, 2H), 2.34 – 2.28 (m, 3H), 2.00 - 1.99 (m, 3H). MS *m/z* ($C_{33}H_{28}F_3N_5O_3$) calc'd = 599.21, observed: M+1 = 600.5

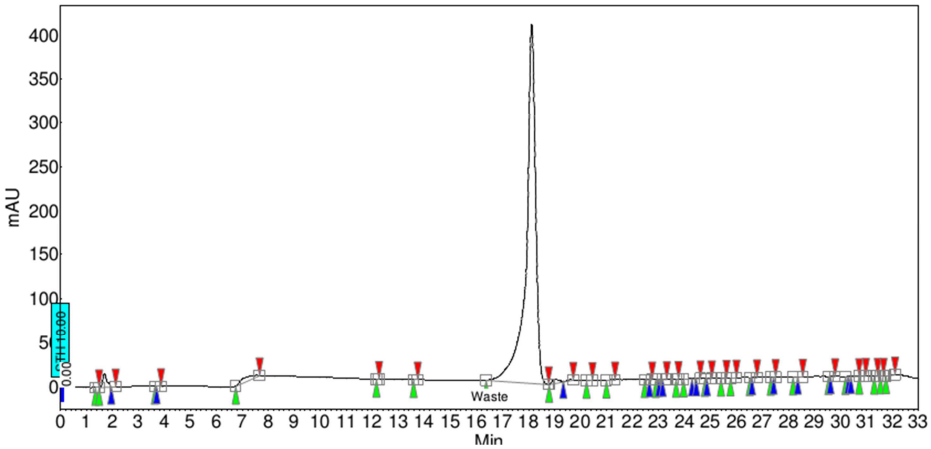

Figure 3-13. Analytical condition A of ligand **5**

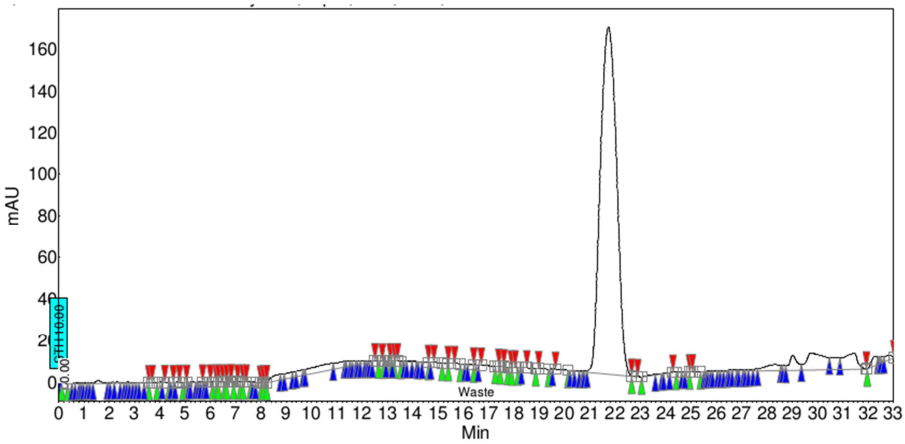

Figure 3-14. Analytical condition B of ligand **5**

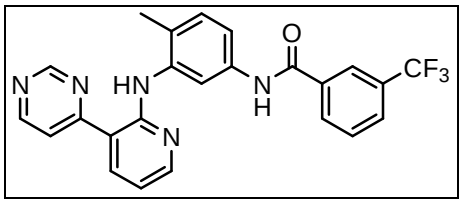

[8] 4-(2-chloropyridin-3-yl)pyrimidine (14 mg, 0.073 mmol) and N-(3-amino-4-methylphenyl)-3-(trifluoromethyl)benzamide (50 mg, 0.17 mmol) were dissolved in DMSO (30 µL) and a drop of NEt_3-TFA salt was added to the reaction mixture. The reaction was stirred for 4 d at 95°C. The crude material was purified using reverse phase liquid chromatography to obtain 6.3 mg of the desired product **8** (20% yield). ^{1}H NMR (300 MHz, $CDCl_3$-d_1) δ 9.37 (s, 1H), 9.06 (s, 1H), 9.02 (d, J = 3 Hz, 1H), 8.51 (d, J = 6 Hz, 1H), 8.28 (s, 1H), 8.20-8.16 (m, 2H), 7.95 (d, J = 6 Hz,

1H), 7.80-7.75 (m, 3H), 7.64-7.59 (m, 1H), 7.37 (d, *J* = 6 Hz, 1H), 7.09-7.04 (m, 1H), 2.37 (s, 3H). MS *m/z* ($C_{24}H_{18}F_3N_5O$) calc'd = 449.15, observed: ($M+H^+$) = 450.5

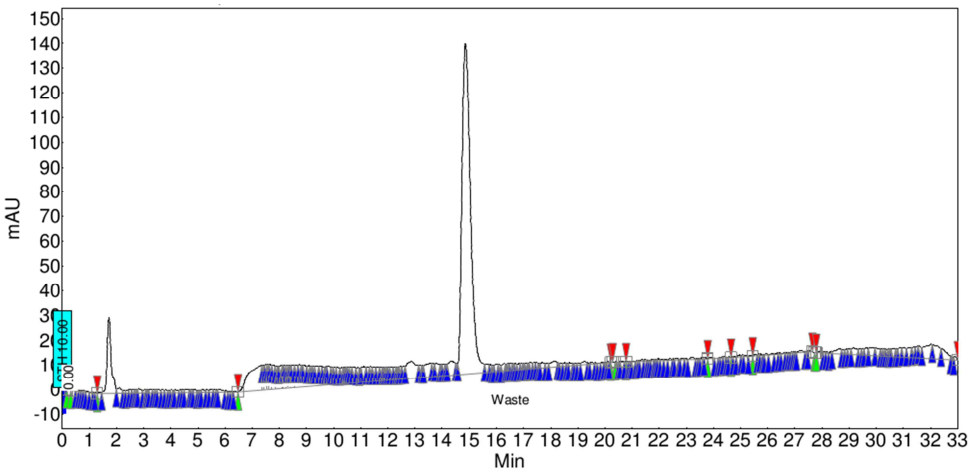

Figure 3-15. Analytical condition A of ligand **8**

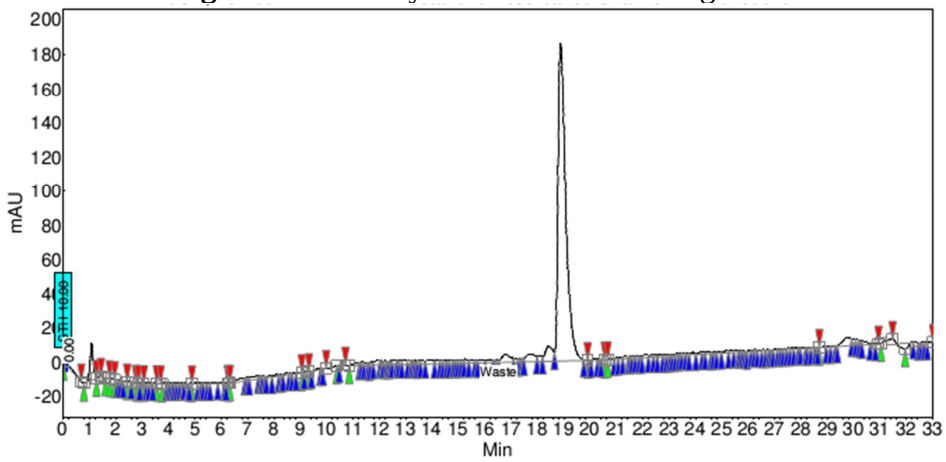

Figure 3-16. Analytical condition B of ligand **8**

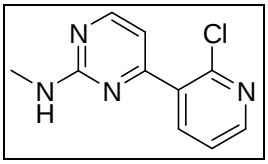

[4-(2-chloropyridin-3-yl)-N-methylpyrimidin-2-amine] N-methylguanidine (126 mg, 1.15 mmol) and sodium methoxide (50 mg, 0.93 mmol) were suspended in methanol (0.2 mL) at room temperature for 30 min. Then (E)-1-(2-chloropyridin-3-yl)-3-(dimethylamino)prop-2-en-1-one (76 mg, 0.36 mmol) in methanol (1 mL) was added to the reaction dropwise. The reaction was refluxed at 50 °C for 23 h. The crude material was purified by column chromatography

(50% ethyl acetate in hexanes) to obtain 51 mg of the desired product (64% yield). ^{1}H NMR (300 MHz, DMSO-d_6) δ 8.32 (dd, J = 3 Hz, J = 6 Hz, 1H), 8.23 (d, J = 6 Hz, 1H), 7.84 (broad s, 1H), 7.39-7.35 (m, 1H), 7.10-7.09 (m, 1H), 6.68 (d, J = 6 Hz, 1H), 2.63 (d, J = 6 Hz, 3H).

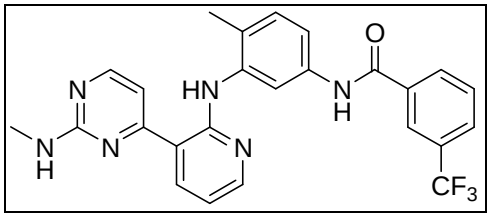

[9] 4-(2-chloropyridin-3-yl)-N-methylpyrimidin-2-amine (20 mg, 0.09 mmol) and N-(3-amino-4-methylphenyl)-3-(trifluoromethyl)benzamide (63 mg, 0.21 mmol) were dissolved in DMSO (75 µL), and a drop of NEt_3-TFA salt was added to the reaction mixture. The reaction was stirred for 4 d at 95 °C. The crude material was purified using reverse phase liquid chromatography to obtain 16 mg of the desired product **9** (37% yield). ^{1}H NMR (300 MHz, CD_3OD-d_4) δ 8.82 (d, J = 6 Hz, 1H), 8.50 (d, J = 6 Hz, 1H), 8.27 (s, 1H), 8.23 (d, J = 6 Hz, 1H), 7.98-7.91 (m, 3H), 7.78-7.73 (m, 1H), 7.65 (d, J = 9 Hz, 1H), 7.53 (d, J = 6 Hz, 1H), 7.39 (d, J = 6 Hz, 1H), 7.15 (t, J = 9 Hz, 1H), 2.98 (s, 3H), 2.34 (s, 3H). MS m/z ($C_{25}H_{21}F_3N_6O$) calc'd = 478.17, observed: ($M+H^+$) = 479.4

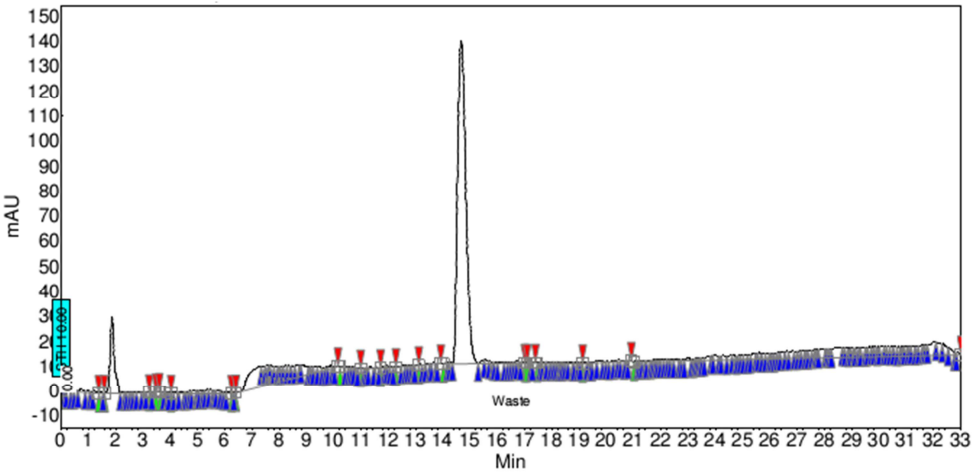

Figure 3-17. Analytical condition A of ligand **9**

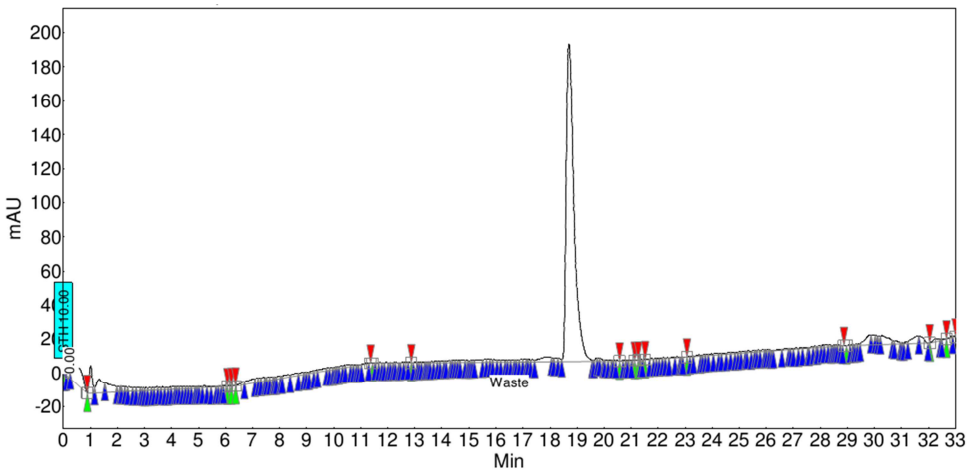

Figure 3-18. Analytical condition B of ligand **9**

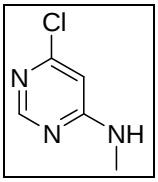

[6-chloro-N-methylpyrimidin-4-amine] 4,6-dichloropyrimide (600 mg, 4 mmol), methylamine-HCl salt (570 mg, 8.4 mmol) and NEt_3 (480 mg, 4.8 mmol) were suspended in 2-propanol (4 mL) and refluxed at 80 °C for 5 h. The reaction was taken up in ethyl acetate, and the organic layer was washed with saturated K_2CO_3. The organic layer was collected, dried over Na_2SO_4 and concentrated *in vacuo*. The crude material was purified by column chromatography (30-50% ethyl acetate in hexanes) to obtain 390 mg of the desired product (68% yield). ^{1}H NMR (300 MHz, $CDCl_3$-d_1) δ 8.37 (s, 1H), 6.37 (S, 1H), 2.98 (d, J = 6 Hz, 3H). MS *m/z* ($C_5H_6ClN_3$) calc'd = 143.03, observed: ($M+H^+$) = 144.0

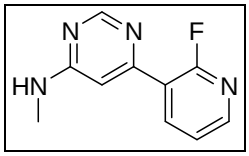

[6-(2-fluoropyridin-3-yl)-N-methylpyrimidin-4-amine] 6-chloro-N-methylpyrimidin-4-amine (170 mg, 1.2 mmol), 2-fluorophenylboronic acid (84 mg, 0.62 mmol),

tetrakis(triphenylphosphine)palladium (36 mg, 0.031 mmol) and K_2CO_3 (170 mg, 1.2 mmol) were dissolved in 1:1 acetonitrile:H_2O (1.2 mL) in a round bottom flask. The flask was saturated with N_2 for 10 minutes, and the reaction was refluxed for 2 h at 80 °C. The reaction was then diluted with ethyl acetate, and the organic layer washed with H_2O (3X). The ethyl acetate layer was collected, dried over Na_2SO_4 and concentrated *in vacuo*. The crude material was purified by column chromatography (60-80% ethyl acetate in hexanes) to obtain 52 mg of the desired product (41% yield). ^{1}H NMR (300 MHz, CD_3OD-d_4) δ 8.53 -8.46 (m, 2H), 8.30 (s, 1H), 7.51-7.46 (m, 1H), 6.97 (s, 1H), 2.98 (s, 3H). MS *m/z* ($C_{10}H_9FN_4$) calc'd = 204.08, observed: ($M+H^+$) = 205.1

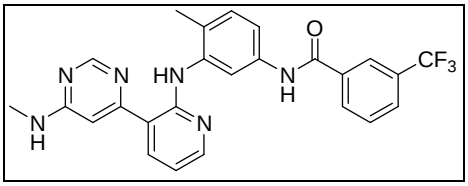

[10] 6-(2-fluoropyridin-3-yl)-N-methylpyrimidin-4-amine (20 mg, 0.099 mmol) and N-(3-amino-4-methylphenyl)-3-(trifluoromethyl)benzamide (70 mg, 0.24 mmol) were dissolved in DMSO (80 µL), and a drop of NEt_3-TFA salt was added to the reaction mixture. The reaction was stirred for 3 d at 95 °C. The crude material was purified using reverse phase liquid chromatography to obtain 7 mg of the desired product **10** (14% yield). ^{1}H NMR (300 MHz, CD_3OD-d_4) δ 8.84 (broad s, 1H), 8.40 (broad s, 1H), 8.27 (s, 1H), 8.22 (d, J = 6 Hz, 1H), 8.03 (m, 1H), 7.94-7.91 (m, 2H), 7.78 -7.73 (m, 1H), 7.65-7.51 (m, 3H), 7.46-7.43 (m, 1H), 7.12-7.06 (m, 2H), 3.05 (s, 3H), 2.34 (s, 3H). MS *m/z* ($C_{25}H_{21}F_3N_6O$) calc'd = 478.17, observed: ($M+H^+$) = 479.3

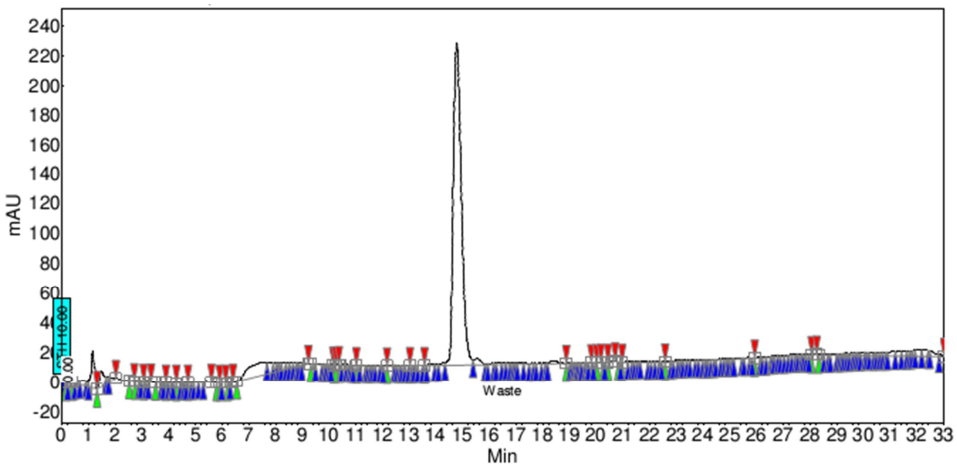

Figure 3-19. Analytical condition A of ligand **10**

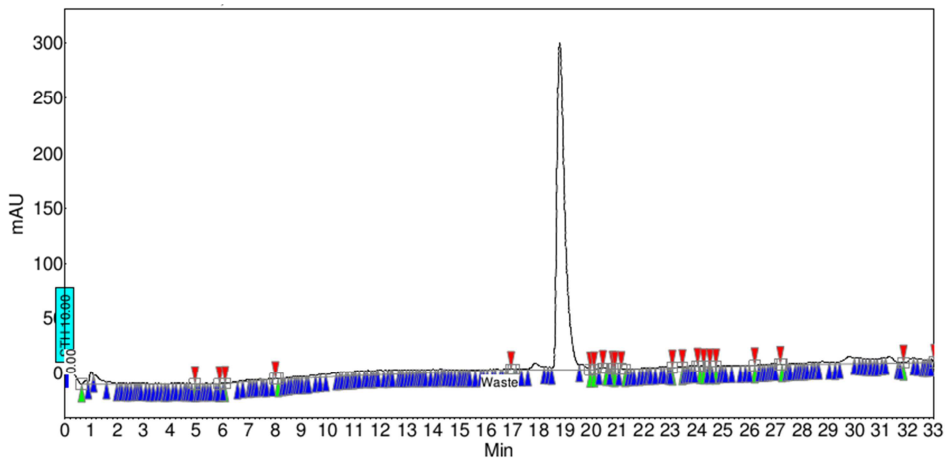

Figure 3-20. Analytical condition B of ligand **10**

E. Activation of Src

Src Y527F (250 nM) was incubated in buffer (50 mM MOPS [pH 7.4], 67 mM NaCl, 10 mM $MgCl_2$, 0.001% (v/v) Tween 20) with ATP (1 mM) at 25 °C or 37 °C for 3 h. Quantitative phosphorylation was determined by immunoblot using antibodies specific for phospho- and non-phospho-Src Tyr416 (Cell Signaling) and LC/MS of tryptic digests (performed as described (94)).

F. Activation of Abl

Abl wild-type was activated as described (25). Abl Y253H (15 µM) was incubated with Hck Y527F (7.4 µM) in buffer (50 mM HEPES [pH 7.5], 67 mM NaCl, 60 mM $MgCl_2$, 1 mM

EGTA) with ATP (500 µM) for 6 h at 30 °C and used at 80 pM in activity assays. Due to the high concentration of Hck, a negative control with no Abl was incubated simultaneously and used as the background correction factor in the activity assays. However, since the dilution factor was so large (>5 orders of magnitude) and the substrate used was Abl-specific, the background was no higher than that observed in other assays.

G. Activity assays

These assays were performed as described (25, 26, 79). Since the amount of γ^{32}P ATP in the reactions was equivalent to ~2 nM, $IC_{50} \approx K_i$. In cases where cold ATP was used to activate the kinase prior to the assay, the activation mixture was diluted sufficiently to contribute at most 2 µM to the final reaction.

F. ICAT footprinting

Labeling reagents were made as described (117), and experiments were performed generally as described (118). Briefly, one 3-µM stock of protein in 50 mM Tris (pH 8.0), 50 mM KCl, 5 mM $MgCl_2$, and 0.5 TCEP-HCl was divided into aliquots, and inhibitor (10 µM) was added to yield final solutions containing 1% (v/v) DMSO. Heavy labeling reagent was was added to the protein solutions, and aliquots were taken at specified times and quenched with excess DTT. Samples were precipitated with 0.02% (w/v) sodium deoxycholate and 10% (w/v) trichloroacetic acid on ice for 30 min. The precipitated protein was pelleted and washed with cold acetone, then resuspended in 8 M urea with light labeling reagent. After incubation in the dark for 30 min, the solutions were diluted with 210 µL Tris pH 8.0, 5.7 mM $CaCl_2$, and 1 µg porcine trypsin, and incubated at 37 °C overnight. Samples were analyzed on a Thermo Finnigan LTQ mass spectrometer.

References

1. Skamnaki VT, *et al.* (1999) Catalytic mechanism of phosphorylase kinase probed by mutational studies. *Biochemistry* 38(44):14718-14730.

2. Osusky M, Taylor SJ, & Shalloway D (1995) Autophosphorylation of purified c-Src at its primary negative regulation site. *J. Biol. Chem.* 270(43):25729-25732.

3. Roberts PJ & Der CJ (2007) Targeting the Raf-MEK-ERK mitogen-activated protein kinase cascade for the treatment of cancer. *Oncogene* 26(22):3291-3310.

4. Adams JA, McGlone ML, Gibson R, & Taylor SS (1995) Phosphorylation modulates catalytic function and regulation in the cAMP-dependent protein kinase. *Biochemistry* 34(8):2447-2454.

5. Manning G, Whyte DB, Martinez R, Hunter T, & Sudarsanam S (2002) The protein kinase complement of the human genome. *Science* 298(5600):1912-1934.

6. Fabbro D, *et al.* (2002) Protein kinases as targets for anticancer agents: from inhibitors to useful drugs. *Pharmacol. Ther.* 93(2-3):79-98.

7. Kumar S, Boehm J, & Lee JC (2003) p38 MAP kinases: key signalling molecules as therapeutic targets for inflammatory diseases. *Nat. Rev. Drug. Discov.* 2(9):717-726.

8. Long YC & Zierath JR (2006) AMP-activated protein kinase signaling in metabolic regulation. *J. Clin. Invest.* 116(7):1776-1783.

9. Workman P, Clarke PA, Raynaud FI, & van Montfort RL (2010) Drugging the PI3 kinome: from chemical tools to drugs in the clinic. *Cancer Res.* 70(6):2146-2157.

10. Manning G, Plowman GD, Hunter T, & Sudarsanam S (2002) Evolution of protein kinase signaling from yeast to man. *Trends Biochem. Sci.* 27(10):514-520.

11. Plowman GD, Sudarsanam S, Bingham J, Whyte D, & Hunter T (1999) The protein kinases of Caenorhabditis elegans: a model for signal transduction in multicellular organisms. *Proc. Natl. Acad. Sci. U.S.A.* 96(24):13603-13610.

12. Noble ME, Endicott JA, & Johnson LN (2004) Protein kinase inhibitors: insights into drug design from structure. *Science* 303(5665):1800-1805.

13. Zhang J, Yang PL, & Gray NS (2009) Targeting cancer with small molecule kinase inhibitors. *Nat. Rev. Cancer* 9(1):28-39.

14. Cohen P & Alessi DR (2013) Kinase drug discovery--what's next in the field? *ACS Chem. Biol.* 8(1):96-104.

15. Canagarajah BJ, Khokhlatchev A, Cobb MH, & Goldsmith EJ (1997) Activation mechanism of the MAP kinase ERK2 by dual phosphorylation. *Cell* 90(5):859-869.

16. Zhang YY, Mei ZQ, Wu JW, & Wang ZX (2008) Enzymatic activity and substrate specificity of mitogen-activated protein kinase p38alpha in different phosphorylation states. *J. Biol. Chem.* 283(39):26591-26601.

17. Zhou B & Zhang ZY (2002) The activity of the extracellular signal-regulated kinase 2 is regulated by differential phosphorylation in the activation loop. *J. Biol. Chem.* 277(16):13889-13899.

18. Cohen P (2002) Protein kinases--the major drug targets of the twenty-first century? *Nat. Rev. Drug Discov.* 1(4):309-315.

19. Zuccotto F, Ardini E, Casale E, & Angiolini M (2010) Through the "gatekeeper door": exploiting the active kinase conformation. *J. Med. Chem.* 53(7):2681-2694.

20. Goldman JM & Melo JV (2003) Chronic myeloid leukemia--advances in biology and new approaches to treatment. *N. Engl. J. Med.* 349(15):1451-1464.

21. Zimmermann J, Buchdunger E, Mett H, Meyer T, & Lydon NB (1997) Potent and selective inhibitors of the Abl-kinase: phenylamino-pyrimidine (PAP) derivatives. *Bioorg. Med. Chem. Lett.* 7(2):187-192.

22. Schindler T, *et al.* (2000) Structural mechanism for STI-571 inhibition of abelson tyrosine kinase. *Science* 289(5486):1938-1942.

23. Hubbard SR, Wei L, Ellis L, & Hendrickson WA (1994) Crystal structure of the tyrosine kinase domain of the human insulin receptor. *Nature* 372(6508):746-754.

24. Lin YL, Meng Y, Jiang W, & Roux B (2013) Explaining why Gleevec is a specific and potent inhibitor of Abl kinase. *Proc. Natl. Acad. Sci. U.S.A.* 110(5):1664-1669.

25. Seeliger MA, *et al.* (2007) c-Src binds to the cancer drug imatinib with an inactive Abl/c-Kit conformation and a distributed thermodynamic penalty. *Structure* 15(3):299-311.

26. Seeliger MA, *et al.* (2009) Equally potent inhibition of c-Src and Abl by compounds that recognize inactive kinase conformations. *Cancer Res.* 69(6):2384-2392.

27. Dar AC, Lopez MS, & Shokat KM (2008) Small molecule recognition of c-Src via the Imatinib-binding conformation. *Chem. Biol.* 15(10):1015-1022.

28. Davis MI, *et al.* (2011) Comprehensive analysis of kinase inhibitor selectivity. *Nat. Biotechnol.* 29(11):1046-1051.

29. Bishop AC, *et al.* (1999) Generation of monospecific nanomolar tyrosine kinase inhibitors via a chemical genetic approach. *J. Am. Chem. Soc.* 121(4):627-631.

30. Bishop AC, *et al.* (2000) A chemical switch for inhibitor-sensitive alleles of any protein kinase. *Nature* 407(6802):395-401.

31. Rodriguez J & Crespo P (2011) Working without kinase activity: phosphotransfer-independent functions of extracellular signal-regulated kinases. *Sci. Signal.* 4(196):re3.

32. Therrien M, Michaud NR, Rubin GM, & Morrison DK (1996) KSR modulates signal propagation within the MAPK cascade. *Genes Dev.* 10(21):2684-2695.

33. Hu S, *et al.* (2009) Profiling the human protein-DNA interactome reveals ERK2 as a transcriptional repressor of interferon signaling. *Cell* 139(3):610-622.

34. Camps M, *et al.* (1998) Catalytic activation of the phosphatase MKP-3 by ERK2 mitogen-activated protein kinase. *Science* 280(5367):1262-1265.

35. Wodicka LM, *et al.* (2010) Activation state-dependent binding of small molecule kinase inhibitors: structural insights from biochemistry. *Chem. Biol.* 17(11):1241-1249.

36. Deininger M, Buchdunger E, & Druker BJ (2005) The development of imatinib as a therapeutic agent for chronic myeloid leukemia. *Blood* 105(7):2640-2653.

37. Jura N, *et al.* (2011) Catalytic control in the EGF receptor and its connection to general kinase regulatory mechanisms. *Mol. Cell* 42(1):9-22.

38. Liu Y & Gray NS (2006) Rational design of inhibitors that bind to inactive kinase conformations. *Nat. Chem. Biol.* 2(7):358-364.

39. Mol CD, *et al.* (2004) Structural basis for the autoinhibition and STI-571 inhibition of c-Kit tyrosine kinase. *J. Biol. Chem.* 279(30):31655-31663.

40. DiMauro EF, *et al.* (2006) Discovery of aminoquinazolines as potent, orally bioavailable inhibitors of Lck: synthesis, SAR, and in vivo anti-inflammatory activity. *J. Med. Chem.* 49(19):5671-5686.

41. Hodous BL, *et al.* (2007) Synthesis, structural analysis, and SAR studies of triazine derivatives as potent, selective Tie-2 inhibitors. *Bioorg. Med. Chem. Lett.* 17(10):2886-2889.

42. Wan PT, *et al.* (2004) Mechanism of activation of the RAF-ERK signaling pathway by oncogenic mutations of B-RAF. *Cell* 116(6):855-867.

43. Pargellis C, *et al.* (2002) Inhibition of p38 MAP kinase by utilizing a novel allosteric binding site. *Nat. Struct. Biol.* 9(4):268-272.

44. Angell RM, *et al.* (2008) Biphenyl amide p38 kinase inhibitors 4: DFG-in and DFG-out binding modes. *Bioorg. Med. Chem. Lett.* 18(15):4433-4437.

45. Remy G, *et al.* (2010) Differential activation of p38MAPK isoforms by MKK6 and MKK3. *Cell. Signal.* 22(4):660-667.

46. Sullivan JE, *et al.* (2005) Prevention of MKK6-Dependent Activation by Binding to p38α MAP Kinase. *Biochemistry* 44(50):16475-16490.

47. Fox T, *et al.* (1998) A single amino acid substitution makes ERK2 susceptible to pyridinyl imidazole inhibitors of p38 MAP kinase. *Protein Sci.* 7(11):2249-2255.

48. Xie X, *et al.* (1998) Crystal structure of JNK3: a kinase implicated in neuronal apoptosis. *Structure* 6(8):983-991.

49. Zhang F, Strand A, Robbins D, Cobb MH, & Goldsmith EJ (1994) Atomic structure of the MAP kinase ERK2 at 2.3 A resolution. *Nature* 367(6465):704-711.

50. Wang Z, *et al.* (1997) The structure of mitogen-activated protein kinase p38 at 2.1-A resolution. *Proc. Natl. Acad. Sci. U.S.A.* 94(6):2327-2332.

51. Griffith J, *et al.* (2004) The structural basis for autoinhibition of FLT3 by the juxtamembrane domain. *Mol. Cell* 13(2):169-178.

52. Wood ER, *et al.* (2004) A unique structure for epidermal growth factor receptor bound to GW572016 (Lapatinib): relationships among protein conformation, inhibitor off-rate, and receptor activity in tumor cells. *Cancer Res.* 64(18):6652-6659.

53. Krishnamurty R, *et al.* (2013) Active site profiling reveals coupling between domains in SRC-family kinases. *Nat. Chem. Biol.* 9(1):43-50.

54. Ranjitkar P, Brock AM, & Maly DJ (2010) Affinity reagents that target a specific inactive form of protein kinases. *Chem. Biol.* 17(2):195-206.

55. Gruenbaum LM, *et al.* (2009) Inhibition of pro-inflammatory cytokine production by the dual p38/JNK2 inhibitor BIRB796 correlates with the inhibition of p38 signaling. *Biochem. Pharmacol.* 77(3):422-432.

56. Kornev AP, Haste NM, Taylor SS, & Eyck LF (2006) Surface comparison of active and inactive protein kinases identifies a conserved activation mechanism. *Proc. Natl. Acad. Sci. U.S.A.* 103(47):17783-17788.

57. Kornev AP & Taylor SS (2010) Defining the conserved internal architecture of a protein kinase. *Biochim. Biophys. Acta, Proteins Proteomics* 1804(3):440-444.

58. Kornev AP, Taylor SS, & Ten Eyck LF (2008) A helix scaffold for the assembly of active protein kinases. *Proc. Natl. Acad. Sci. U.S.A.* 105(38):14377-14382.

59. Quintás-Cardama A & Cortes J (2008) Therapeutic Options Against BCR-ABL1 T315I-Positive Chronic Myelogenous Leukemia. *Clin. Cancer. Res.* 14(14):4392-4399.

60. Kobayashi S, *et al.* (2005) EGFR mutation and resistance of non-small-cell lung cancer to gefitinib. *N. Engl. J. Med.* 352(8):786-792.

61. Tamborini E, *et al.* (2004) A new mutation in the KIT ATP pocket causes acquired resistance to imatinib in a gastrointestinal stromal tumor patient. *Gastroenterology* 127(1):294-299.

62. Azam M, Seeliger MA, Gray NS, Kuriyan J, & Daley GQ (2008) Activation of tyrosine kinases by mutation of the gatekeeper threonine. *Nat. Struct. Mol. Biol.* 15(10):1109-1118.

63. Emrick MA, *et al.* (2006) The gatekeeper residue controls autoactivation of ERK2 via a pathway of intramolecular connectivity. *Proc. Natl. Acad. Sci. U.S.A.* 103(48):18101-18106.

64. Huang WS, *et al.* (2010) Discovery of 3-[2-(imidazo[1,2-b]pyridazin-3-yl)ethynyl]-4-methyl-N-{4-[(4-methylpiperazin-1-y l)methyl]-3-(trifluoromethyl)phenyl}benzamide (AP24534), a potent, orally active pan-inhibitor of breakpoint cluster region-abelson (BCR-ABL) kinase including the T315I gatekeeper mutant. *J. Med. Chem.* 53(12):4701-4719.

65. Dumas J, *et al.* (2000) 1-Phenyl-5-pyrazolyl ureas: potent and selective p38 kinase inhibitors. *Bioorg. Med. Chem. Lett.* 10(18):2051-2054.

66. Esque J, Oguey C, & de Brevern AG (2010) A novel evaluation of residue and protein volumes by means of Laguerre tessellation. *J. Chem. Inf. Model.* 50(5):947-960.

67. Zhang C, *et al.* (2005) A second-site suppressor strategy for chemical genetic analysis of diverse protein kinases. *Nat. Methods* 2(6):435-441.

68. Laskowski RA & Swindells MB (2011) LigPlot+: multiple ligand-protein interaction diagrams for drug discovery. *J. Chem. Inf. Model.* 51(10):2778-2786.

69. Langer T, *et al.* (2004) NMR backbone assignment of a protein kinase catalytic domain by a combination of several approaches: application to the catalytic subunit of cAMP-dependent protein kinase. *Chembiochem* 5(11):1508-1516.

70. Vogtherr M, *et al.* (2006) NMR characterization of kinase p38 dynamics in free and ligand-bound forms. *Angew. Chem., Int. Ed.* 45(6):993-997.

71. Shan Y, *et al.* (2009) A conserved protonation-dependent switch controls drug binding in the Abl kinase. *Proc. Natl. Acad. Sci. U.S.A.* 106(1):139-144.

72. Frembgen-Kesner T & Elcock AH (2006) Computational sampling of a cryptic drug binding site in a protein receptor: explicit solvent molecular dynamics and inhibitor docking to p38 MAP kinase. *J. Mol. Biol.* 359(1):202-214.

73. Tsai CJ, Kumar S, Ma B, & Nussinov R (1999) Folding funnels, binding funnels, and protein function. *Protein Sci.* 8(6):1181-1190.

74. Boehr DD, McElheny D, Dyson HJ, & Wright PE (2006) The dynamic energy landscape of dihydrofolate reductase catalysis. *Science* 313(5793):1638-1642.

75. Koshland DE (1958) Application of a Theory of Enzyme Specificity to Protein Synthesis. *Proc. Natl. Acad. Sci. U.S.A.* 44(2):98-104.

76. Martin MP, *et al.* (2012) A novel mechanism by which small molecule inhibitors induce the DFG flip in Aurora A. *ACS Chem. Biol.* 7(4):698-706.

77. Kyte J & Doolittle RF (1982) A simple method for displaying the hydropathic character of a protein. *J. Mol. Biol.* 157(1):105-132.

78. Record CJ, *et al.* (2010) Structural comparison of human mammalian ste20-like kinases. *PLoS One* 5(8):e11905.

79. Ranjitkar P, *et al.* (2012) Affinity-Based Probes Based on Type II Kinase Inhibitors. *J. Am. Chem. Soc.* 134(46):19017-19025.

80. Hari SB, Ranjitkar P, & Maly DJ (2012) Determination of the kinetics and thermodynamics of ligand binding to a specific inactive conformation in protein kinases. *Methods Mol. Biol.* 928:153-159.

81. Leslie AGW (1992) Recent changes to the MOSFLM package for processing film and image plate data. *Joint CCP4 + ESF-EAMCB Newsletter on Protein Crystallography* 26.

82. Winn MD, *et al.* (2011) Overview of the CCP4 suite and current developments. *Acta Crystallogr., Sect. D: Biol. Crystallogr.* 67(Pt 4):235-242.

83. McCoy AJ, *et al.* (2007) Phaser crystallographic software. *J. Appl. Crystallogr.* 40(Pt 4):658-674.

84. Murshudov GN, Vagin AA, & Dodson EJ (1997) Refinement of macromolecular structures by the maximum-likelihood method. *Acta Crystallogr., Sect. D: Biol. Crystallogr.* 53(Pt 3):240-255.

85. Murshudov GN, *et al.* (2011) REFMAC5 for the refinement of macromolecular crystal structures. *Acta Crystallogr., Sect. D: Biol. Crystallogr.* 67(Pt 4):355-367.

86. Vagin AA, *et al.* (2004) REFMAC5 dictionary: organization of prior chemical knowledge and guidelines for its use. *Acta Crystallogr., Sect. D: Biol. Crystallogr.* 60(Pt 12 Pt 1):2184-2195.

87. Emsley P & Cowtan K (2004) Coot: model-building tools for molecular graphics. *Acta Crystallogr., Sect. D: Biol. Crystallogr.* 60(Pt 12 Pt 1):2126-2132.

88. Huse M & Kuriyan J (2002) The Conformational Plasticity of Protein Kinases. *Cell* 109(3):275-282.

89. Fabian MA, *et al.* (2005) A small molecule-kinase interaction map for clinical kinase inhibitors. *Nat. Biotechnol.* 23(3):329-336.

90. Dominguez C, Powers DA, & Tamayo N (2005) p38 MAP kinase inhibitors: many are made, but few are chosen. *Curr. Opin. Drug Discov. Devel.* 8(4):421-430.

91. Kinoshita E, Takahashi M, Takeda H, Shiro M, & Koike T (2004) Recognition of phosphate monoester dianion by an alkoxide-bridged dinuclear zinc(II) complex. *Dalton Trans.* (8):1189-1193.

92. Scott A, Haystead CM, & Haystead TA (1995) Purification of a 12,020-dalton protein that enhances the activation of mitogen-activated protein (MAP) kinase by MAP kinase kinase. *J. Biol. Chem.* 270(41):24540-24547.

93. Robbins DJ & Cobb MH (1992) Extracellular signal-regulated kinases 2 autophosphorylates on a subset of peptides phosphorylated in intact cells in response to insulin and nerve growth factor: analysis by peptide mapping. *Mol. Biol. Cell* 3(3):299-308.

94. Hari SB, Merritt EA, & Maly DJ (2013) Sequence determinants of a specific inactive protein kinase conformation. *Chem. Biol.* 20(6):806-815.

95. Robinson FL, Whitehurst AW, Raman M, & Cobb MH (2002) Identification of novel point mutations in ERK2 that selectively disrupt binding to MEK1. *J. Biol. Chem.* 277(17):14844-14852.

96. Sun H, Charles CH, Lau LF, & Tonks NK (1993) MKP-1 (3CH134), an immediate early gene product, is a dual specificity phosphatase that dephosphorylates MAP kinase in vivo. *Cell* 75(3):487-493.

97. Tanoue T, Moriguchi T, & Nishida E (1999) Molecular cloning and characterization of a novel dual specificity phosphatase, MKP-5. *J. Biol. Chem.* 274(28):19949-19956.

98. Muda M, *et al.* (1996) The dual specificity phosphatases M3/6 and MKP-3 are highly selective for inactivation of distinct mitogen-activated protein kinases. *J. Biol. Chem.* 271(44):27205-27208.

99. Zhou B, *et al.* (2006) Mapping ERK2-MKP3 binding interfaces by hydrogen/deuterium exchange mass spectrometry. *J. Biol. Chem.* 281(50):38834-38844.

100. Bryksin AV & Matsumura I (2010) Overlap extension PCR cloning: a simple and reliable way to create recombinant plasmids. *Biotechniques* 48(6):463-465.

101. Stols L, *et al.* (2002) A New Vector for High-Throughput, Ligation-Independent Cloning Encoding a Tobacco Etch Virus Protease Cleavage Site. *Protein Expres. Purif.* 25(1):8-15.

102. Tanis KQ, Veach D, Duewel HS, Bornmann WG, & Koleske AJ (2003) Two distinct phosphorylation pathways have additive effects on Abl family kinase activation. *Mol. Cell. Biol.* 23(11):3884-3896.

103. Manley PW, Cowan-Jacob SW, Fendrich G, Jahnke W, & Fabbro D (2011) Nilotinib, in Comparison to Both Dasatinib and Imatinib, Possesses a Greatly Prolonged Residence

Time When Bound to the BCR-ABL Kinase SH1 Domain. *ASH Annual Meeting Abstracts* 118(21):1674-.

104. Cumming JG, *et al.* (2004) Novel, potent and selective anilinoquinazoline and anilinopyrimidine inhibitors of p38 MAP kinase. *Bioorg. Med. Chem. Lett.* 14(21):5389-5394.

105. Regan J, *et al.* (2003) The kinetics of binding to p38MAP kinase by analogues of BIRB 796. *Bioorg. Med. Chem. Lett.* 13(18):3101-3104.

106. Flynn DL, Petillo PA, & Kaufman MD (2010) US7790756B2.

107. MacAuley A & Cooper JA (1989) Structural differences between repressed and derepressed forms of p60c-src. *Mol. Cell. Biol.* 9(6):2648-2656.

108. Cartwright CA, Eckhart W, Simon S, & Kaplan PL (1987) Cell transformation by pp60c-src mutated in the carboxy-terminal regulatory domain. *Cell* 49(1):83-91.

109. Seeliger MA, *et al.* (2005) High yield bacterial expression of active c-Abl and c-Src tyrosine kinases. *Protein Sci.* 14(12):3135-3139.

110. Patschinsky T, Hunter T, Esch FS, Cooper JA, & Sefton BM (1982) Analysis of the sequence of amino acids surrounding sites of tyrosine phosphorylation. *Proc. Natl. Acad. Sci. U.S.A.* 79(4):973-977.

111. Johnson LN, Noble ME, & Owen DJ (1996) Active and inactive protein kinases: structural basis for regulation. *Cell* 85(2):149-158.

112. Shieh W-C, *et al.* (2008) Syntheses of a Triad of Flt3 Kinase Inhibitors: From Bench to Pilot Plant†. *Organic Process Res. Dev.* 12(6):1146-1155.

113. Lovera S, *et al.* (2012) The different flexibility of c-Src and c-Abl kinases regulates the accessibility of a druggable inactive conformation. *J. Am. Chem. Soc.* 134(5):2496-2499.

114. Boubeva R, Pernot, L., Cristiani, A., Moretti, L., Berteotti, A., Perozzo, R., Gervasio, F., Scapozza, L. (2011) A single amino-acid dictates the dynamics of the switch between active and inactive C-Src conformation. *PDB ID: 3OEZ.*

115. Kwarcinski FE, Fox CC, Steffey ME, & Soellner MB (2012) Irreversible inhibitors of c-Src kinase that target a nonconserved cysteine. *ACS Chem. Biol.* 7(11):1910-1917.

116. Vajpai N, *et al.* (2008) Solution conformations and dynamics of ABL kinase-inhibitor complexes determined by NMR substantiate the different binding modes of imatinib/nilotinib and dasatinib. *J. Biol. Chem.* 283(26):18292-18302.

117. Underbakke ES, Zhu Y, & Kiessling LL (2008) Isotope-coded affinity tags with tunable reactivities for protein footprinting. *Angew. Chem., Int. Ed.* 47(50):9677-9680.

118. Wang L, *et al.* (2012) Divergent allosteric control of the IRE1alpha endoribonuclease using kinase inhibitors. *Nat. Chem. Biol.* 8(12):982-989.

119. Xu W, Doshi A, Lei M, Eck MJ, & Harrison SC (1999) Crystal structures of c-Src reveal features of its autoinhibitory mechanism. *Mol. Cell* 3(5):629-638.

120. Sicheri F, Moarefi I, & Kuriyan J (1997) Crystal structure of the Src family tyrosine kinase Hck. *Nature* 385(6617):602-609.

121. Piserchio A, Cowburn D, & Ghose R (2012) Expression and purification of Src-family kinases for solution NMR studies. *Methods Mol. Biol.* 831:111-131.

122. Hodous BL, *et al.* (2007) Evolution of a highly selective and potent 2-(pyridin-2-yl)-1,3,5-triazine Tie-2 kinase inhibitor. *J. Med. Chem.* 50(4):611-626.

123. Brigham JL, Perera BG, & Maly DJ (2013) A Hexylchloride-Based Catch-and-Release System for Chemical Proteomic Applications. *ACS Chem. Biol.* 8(4):691-699.